Karlsruhe Institute of Technology

Development of Pattern Recognition Algorithms for the Central Drift Chamber of the Belle II Detector

Zur Erlangung des akademischen Grades eines

DOKTORS DER NATURWISSENSCHAFTEN

von der Fakultät für Physik
des Karlsruher Institut für Technologie (KIT)

genehmigte

DISSERTATION

von

M.S.-Phys. Viktor Trusov

aus Poltava, Ukraine

Datum der mündlichen Prüfung:	4. November, 2016
Referent:	Prof. Dr. Michael Feindt
Korreferent:	PD Dr. Andreas Meyer

Contents

1. Introduction

In 1973 Kobayashi and Maskawa proposed a mechanism which describes CP violation by introducing an irreducible complex phase in the quark mixing matrix. They predicted three families of quarks that was confirmed by the later discovery of the b quark. The problem of CP violation can shed light on the problem of matter-antimatter asymmetry, which is one of the mysteries of modern cosmology. Also, B physics and CP violation studies have a potential to measure parameters of the electroweak interaction and to test the Standard Model. The studies of CP violation may lead to physics beyond the Standard Model and to New Physics Phenomena. This brings B physics studies to the level of the most important objectives in modern high energy physics.

Experiments which are focused on the studies of B physics are called B factories. They are designed to generate a unprecedentedly high amount of B mesons and to study their properties. The process $e^+e^- \rightarrow \Upsilon(4S) \rightarrow B\bar{B}$ is responsible for generation of B mesons at B factories, and it brings clean physics environment in which only final state particles from B decays are registered by the detector.

The Belle II experiment will be one of B factories with the highest luminosity ever achieved. It was developed as an upgrade of its predecessor, the Belle experiment, but with redesigned components and currently being under construction. The experiment is intended to analyze generated B mesons by combining measured parameters of the decay products, such as the type of particles in the final state and their kinematic parameters. The Belle II detector itself can only provide response signal, generated by the decay products. The task of event reconstruction is entrusted to the reconstruction software, which processes the signals from the detector.

Pattern recognition (which is also called tracking in scope of high energy physics experiments) plays a substantial role in the event reconstruction. It is intended to provide a sufficient amount of information about charged particles, created in studied processes, for further physics analyses. As it is a crucial part of the reconstruction, it should operate with high efficiency. Inefficiency in tracking leads to losses in the event information, and as a result physics processes would be wrongly reconstructed or discarded. In scope of the Belle II experiment, pattern recognition should correctly reconstruct as much as possible events to preserve collected data, and withing limited computational time since a large amount of data should be processed.

An overview of the Belle II experiment is given in chapter 2. Still, the detector is not deployed, and the first physics run is expected to take place in 2018. Thus, the Belle II software framework is developed and tested using Monte Carlo simulated data. The description of the software framework is presented in chapter 3. Most of its features were used to develop the pattern recognition algorithm, which is discussed in present work.

In chapter 4 a general overview of tracking techniques is given. Chapter 5 contains discussion of one of the tracking detectors of the Belle II , the Central Drift Chamber, and algorithms which have been chosen to perform pattern recognition using its output.

The main matter of the current work is given in chapters 6 and 7, where the essential features of the developed tracking algorithm and its performance are presented. The algorithm is based on the track segment recognition technique introduced by the ATLAS experiment [1], where Legendre transformation is used to find patterns of hits which are sharing the common tangent. The feasibility of the method for purposes of the Belle II tracking has been tested in work [2] and proved that Legendre based tracking is capable to efficiently reconstruct tracks with low execution time. The current work is a continuation of the former development, aimed to improve the capability of the algorithm to reconstruct generic $B\bar{B}$ decays. Variuos features have been introduced to cover a wide range of the kimematic parameters of tracks of different types. The performance of the method was studied in comparison to the Belle tracking. Also, the stability of the pattern recognition was tested in conditions of high beam induced backround levels.

2. The Belle II Experiment

The Belle II experiment will be a successor of the Belle experiment, with reworked hardware and software. It was developed to fulfill challenging physics goals, which are setting high requirements on its components performance.

One of the features of the experiment is that it operates at the electron-positron acceleration ring with asymmetric beam energies. The asymmetric energy beams and detector configuration has been chosen to enhance CP violation studies. Due to momentum conservation in e^+e^- interaction, the rest frame of created B-mesons is boosted toward direction of the high energy ring. This configuration gives an opportunity to measure decay length of boosted B mesons. Thus, the Belle II detector will be equipped with a high-end vertexing detector, which will allow to perform accurate measurements of the decay position. On the other hand, the whole tracking system of the detector will bring a possibility to reconstruct particles trajectories precisely and, as result, restore the information about the physics events.

In this chapter an overview of physics goals and experimental setup will be given.

2.1. Physics Goals at Belle II

The Belle II experiment is designed to study rare processes, many of which were detected at the predecessor experiment, namely Belle, but with much higher sensitivity. The physics program of the experiment also includes the yet not observed processes, but which may be detected with the Belle II sensitivity. Various New Physics phenomena are expected to be studied, such as lepton flavor violation, as well as the precise measurements of the SM processes.

Physics Achievements at Belle experiment

Among the various achievements of the Belle experiment there are following important scientific results [3]:

- The observation of mixing induced time-dependent CP-violation in the system of neutral B mesons and a measurement of the standard model CP violation parameter $\sin 2\phi_1$ through the analysis of the $B^0 \to J/\psi K^0$ decay [4].

- The evidence of time-dependent CP-violation in $B^0 \to \pi^+\pi^-$ decays and the measurement of the ϕ_2 angle [5].
- Measurement of time-dependent CP-violation in the penguin-dominated modes $B^0 \to \phi K_S$, $K^+K^-K_S$ and ηK_S and determination of the deviation of $\sin 2\phi_1$ from the measurement in tree-dominated $B^0 \to J/\psi K^0$ decays [6]. The discrepancy is statistically limited, so larger dataset of the Belle II experiment will allow to distinguish the presence of NP effects.
- The discovery of the $X(3872)$ resonance [7].
- The detection of direct CP-violations in B decays to $\pi^+\pi^-$ and $K^+\pi^-$ [8, 9], and prove of difference of DCPV in $B^+ \to K^+\pi^-$ and $B^0 \to K^+\pi^-$ decays [10].
- The determination of the ϕ_3 angle using time independent measurement of the Dalitz distribution in $B \to D^{(*)}K$ decays [11].
- The measurement of time-dependent CP-violation in $B^0 \to K^0_s\pi^0\gamma$ [12].
- The first observation of pure leptonic decay $B^- \to \tau^-\bar{\nu}_\tau$ [13].
- Evidence for the phenomenon of mixing in the system of neutral charmed meson D^0 [14].
- The measurement of the rare $B \to K^*\ell^+\ell^-$ penguin decays [15].

Examples of the Belle II Physics Program

Belle II has a broad range of physical processes to study. Expected physical performance would be complementary to other HEP experiments, providing valuable amount of information to build a complete picture of nature. In the following part of the section, short overview of the main physics reach at Belle II is given [16, 3, 17].

$b \to s\bar{s}s$ decays

The measured value of $\sin 2\phi_1$ slightly differs for $B \to \phi K_S$ and $B \to J/\psi K^0$ decays, $\Delta S = \sin 2\phi_1^{\phi K_S} - \sin 2\phi_1^{J/\psi K^0} = 0.22 \pm 0.17$. The SM and possible New Physics (NP) loop process of $b \to s\bar{s}s$ is shown in Fig. 2.1 (left diagram). The decay time distribution of both decays is sensitive to the $\sin 2\phi_1$ and can explain ΔS corrections at the lower scale. NP particles can contribute in the $B \to \phi K_S$ as shown in Fig. 2.1 (right diagram) and change ΔS expectations.

$B \to K^{(*)}\nu\overline{\nu}$ decays

In the Standard Model $b \to s\nu\overline{\nu}$ decay proceeds at the one-loop level through penguin and box diagrams. The theoretical predictions for this decay are accurate due to the presence of the leptons without charge in the final state. The

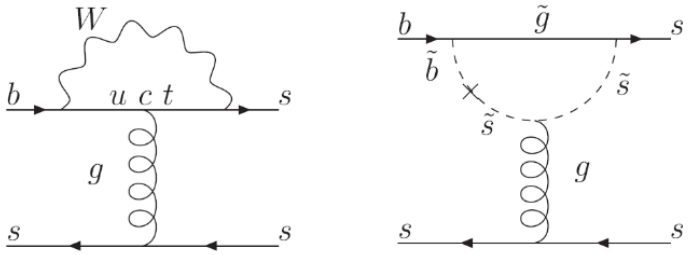

Figure 2.1.: The SM contribution (left) and the gluino-down squark contribution (right) to the $b \to s\bar{s}s$ decay [3]

inclusive branching fraction is estimated to be 4×10^5 for the sum of three neutrino flavors, whereas the exclusive branching fractions are predicted to be $Br\,(B^- \to K^-\nu\overline{\nu}) \approx 4 \times 10^6$. However, it's a challenging task to reconstruct this decay since neutrinos are undetectable particles for the Belle II detector.

$B \to \tau\nu$ decay

First evidence of the $B \to \tau\nu$ decay was found at Belle. $Br(B \to \tau\nu)$ can be suppressed or enhanced by the physics beyond the SM. This mode is challenging to measure due to the presence of ν in final state. Precise determination of $Br(B \to \tau\nu)$ can help to measure $|V_{ub}|$ precisely and lead to NP effects.

$b \to s\gamma$ decays

Radiative $B \to s\gamma$ decays can be used for search for the non-SM right-handed photons. If the photon helicity is mixed, the photon has an elliptical polarization. In NP models the right-handed currents are not suppressed and can show significant CP-asymmetry.

$B \to K\pi$ decays

The main processes underlying $B \to K\pi$ decays are the same for charged and neutral B mesons, resulting in the equal expected asymmetries $A_{CP}^{K^+\pi^0}$ and $A_{CP}^{K^+\pi^-}$. However, a precise measurement by Belle showed difference $\Delta A = A_{CP}^{K^+\pi^0} - A_{CP}^{K^+\pi^-} = 0.164 \pm 0.035 \pm 0.013$. The difference could be due to the neglected contributions to charged B meson decays or to NP effect which violates isospin.

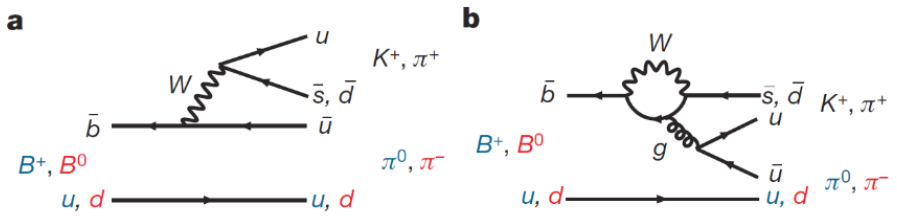

Figure 2.2.: Tree (a) and penguin (b) diagrams contributing to the $B \to K\pi$ decay [10]

	LER (positron beam)	HER (electron beam)
Beam energy (GeV)	4.0	7.007
Beam Current (mA)	3.60	2.60
Number of bunches	2500	
Half crossing angle (mrad)	41.5	

Table 2.1.: Characteristics of the electron and positron beams.

$\tau \to \mu\gamma$ decays

Lepton flavor violation detection in τ decays is the one of the most important goals of the Belle II experiment. Lepton flavor conservation in the SM is associated with the massless neutrinos. Observation of the neutrino oscillations imply the mixing of the lepton flavors, which is violating the lepton flavor conservation. Some extensions of the Standard Model predict enhanced lepton-flavor-violating decays with the $Br\,(\tau \to \mu\gamma) \approx 10^{-8}$ [18, 19]. Belle II sensitivity should allow to observe or to provide evidence of this effect, even with the high physics background levels.

2.2. SuperKEKB Accelerator Facility

SuperKEKB is a two-ring, asymmetric energy electron-positron collider, with the center-of-mass energy corresponding to the mass of the $\Upsilon(4S)$ resonance, which most likely decays into pair of B-mesons. The positron low energy ring (LER) and the electron high energy ring (HER) cross at one point, called the interaction point (IP), where electrons and positrons collide. The Belle II detector surrounds the interaction region, detecting products of the e^-e^+ interaction. The main characteristics of the HER and LER are provided in Table 2.1.

2.2.1. Luminosity

To achieve the desired precision of the measurements and to achieve the physics goals described in Sec. 2.1, more data should be collected compared to the Belle experiment. The Belle II experiment is designed to operate at an instant luminosity of $8 \times 10^{35}\ \mathrm{cm}^{-2}\mathrm{s}^{-1}$, which is 40 times higher compared to the luminosity of the Belle experiment.

The luminosity of the accelerator can be written as [20]

$$\mathcal{L} = \frac{1}{2er_e}\left(\frac{\gamma_\pm I \xi_y}{\beta_y^*}\right)_\pm \left(\frac{R_\mathcal{L}}{R_y}\right), \tag{2.1}$$

where r_e is the classical electron radius, $\gamma_\pm$ is the Lorenz factor, I is the beam current, β_y^* is the vertical beta function at the IP, $R_\mathcal{L},\ R_y$ are the geometrical reduction factors, determined by bunch length, beta functions at the IP and the crossing angle, ξ_y is the vertical beam-beam tune shift parameter [20], which characterizes the magnitude of the beam-beam interaction.

The SuperKEKB accelerator facility is an upgrade of its predecessor, namely KEKB accelerator. Main difference is the implementation of the "Nano-Beam" scheme [21] which leads to increasing in luminosity due to the minimizing the longitudinal overlapping of the beams by shortening β_y^*. Schematic view of the beams collision can be found in Fig. 2.3

2.2.2. Beam Induced Background

Due to the high current of the beams and the small interaction region, beam-induced background of the Belle II experiment will be 10 times larger than in the Belle experiment. Tracking performance and, as result, physics performance are strongly depend on the beam background level and on the occupancy of the detector. Possible sources of the beam-induced background include upstream synchrotron radiation (SR), backscattering of SR from downstream, scattering of the beam on residual gas, Touschek scattering, radiative Bhabha scattering, electron-positron pair production.

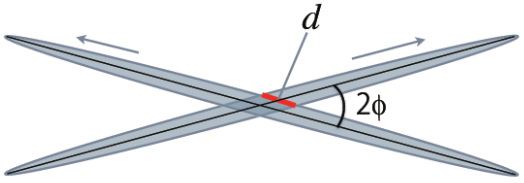

Figure 2.3.: Schematic view of the beam crossing in the nanobeam scheme.

Synchrotron Radiation (Upstream and Downstream)

Synchrotron radiation from the HER depends on the current of the beam, beam optics configuration, and geometry of the interaction region. For SR from upstream there are no direct hits expected. SR from downstream appears when outgoing beams pass beam focusing magnet, called quadrupole. In the case of SuperKEKB, each ingoing and outgoing beam has its own quadrupole and beam orbits are on center in the magnets. Therefore SR level is much lower than in KEKB case.

Beam-Gas Scattering

Beam-gas scattering (bremsstrahlung and Coulomb scattering) leads to changes in the momentum of beam particles, which then interact with the beam pipe or magnets, producing secondary particles. This is one of the major source of the beam-induced background, and it depends on the beam current, the vacuum level in the beam-pipe, and strength of the magnetic field in the focusing magnets.

Touschek Scattering

Touschek scattering is an intra-bunch scattering, which changes the momenta of the beam particles. This effect also leads to interaction of scattered particles with the beam-pipe and production of secondary particles. This source of the beam-induced background is proportional to the beam current, number of bunches, and the inverse of the beam size. Taking into account parameters of the beams, Touschek scattering brings major contribution to the beam-induced background. The main source of the Touschek scattering is the low energy ring.

Radiative Bhabha Scattering

The radiative Bhabha scattering rate is proportional to the luminosity. Photons, produced in this process, interact with the magnets and produce neutrons, which are the main background source of the K_L and μ detector. Compared to KEKB, the contribution of this process to the beam-induced background is significantly decreased.

Electron-Positron Pair Production via Two Photon Process

Electron-positron pairs, which are produced via the two-photon process $e^+e^- \rightarrow e^+e^-e^+e^-$, have very low momentum and cause high occupancy in the innermost PXD layer. It has been estimated [3] that there are 900 to 14000 e^+e^- pairs

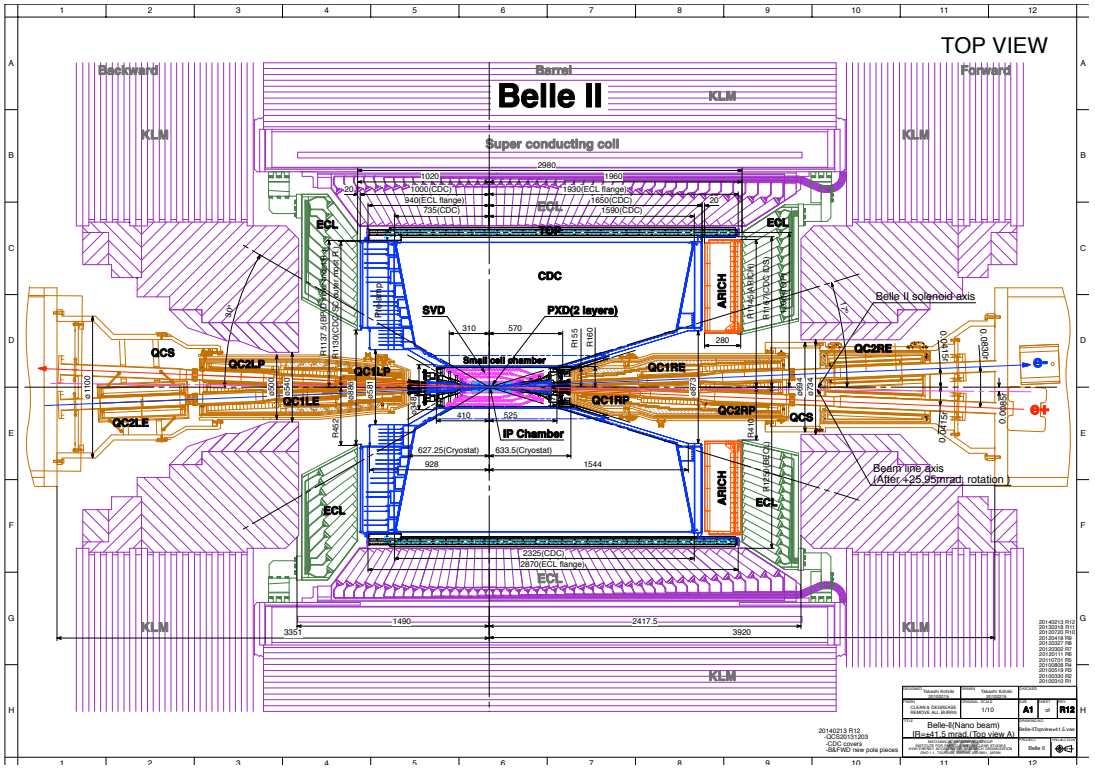

Figure 2.4.: The Belle II spectrometer design ($y - z$ cross section)

in each event will affect the first layer of PXD, resulting in an occupancy up to 1.5%.

2.3. The Belle II Spectrometer

The Belle II detector is a general purpose symmetric spectrometer, which is designed to operate at SuperKEKB and will be an upgrade of the Belle spectrometer. Fig. 2.4 shows configuration and components of the Belle II detector. To handle the increased luminosity and beam background level many components of the Belle detector will be replaced.

The Belle II coordinate system has been chosen in the following way [22]: the z axis corresponds to the Belle II solenoid axis, and the reference point corresponds to the interaction region. The x axis is horizontal outward of the accelerator ring. The y axis is vertical upward.

The detector consists of the following subdetector:

- Pixel Detector (PXD)
- Silicon Vertex Detector (SVD)

- Central Drift Chamber (CDC)
- Particle Identification Detector (PID)
- Electromagnetic calorimeter (ECL)
- K_L and μ Detector (KLM)
- Superconducting magnet

Description of the individual detector components is presented in the next sections. Detailed information about Belle II detector and its subsystems can be found in [3].

2.3.1. Tracking System

The tracking system consists of PXD, SVD and CDC subsystems. It designed in the way to provide sufficient amount of information about detected physical event, namely information about charged particles. It includes momentum estimation, energy losses and production vertex.

The Belle II spectrometer is placed inside of the superconducting solenoid, which generates magnetic field of $B = 1.5$ T. Charged particles with the velocity $\mathbf{v}$ in the magnetic field $\mathbf{B}$ experience the Lorenz force, which transforms its straight propagation trajectory into helical one with a radius

$$r = \frac{m}{|q|}\frac{v \sin\theta}{B}, \tag{2.2}$$

where m and q are the mass and the charge of the particle respectively, θ is the angle between $\mathbf{B}$ and $\mathbf{v}$.

Pixel Detector

The PXD system is developed for the precise vertex reconstruction of B-meson decays, as well as for handling high beam background rates. The pixel detector based on DEPFET (Depleted Field Effect Transistor) technology, which allows for thin sensors of 50 µm thickness. The DEPFET is a semiconductor detector concept which combines detection and amplification components in one device. The readout electronics is placed outside of the acceptance region so this leads to a decreased material budget.

The PXD consists of two layers of sensors (Fig. 2.5), with radii of 14 mm and 22 mm. The inner layer consists of 8 sensors, and outer layer of 12 sensors. Sensitive areas of each of the layer depends on the required angular acceptance of the tracker.

The high background occupancy of the detector results in a high amount of output. The information from the outer tracking systems is used to reduce the volume of the transfered and stored PXD data.

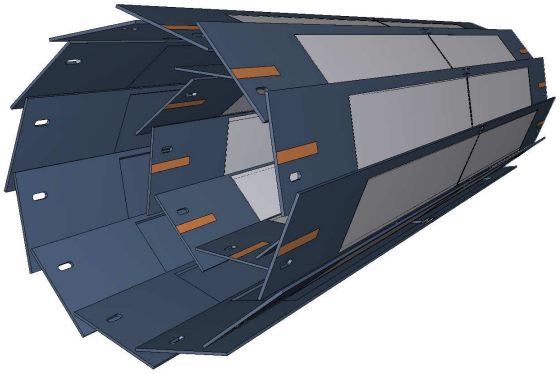

Figure 2.5.: The layout of the PXD sensors [3]

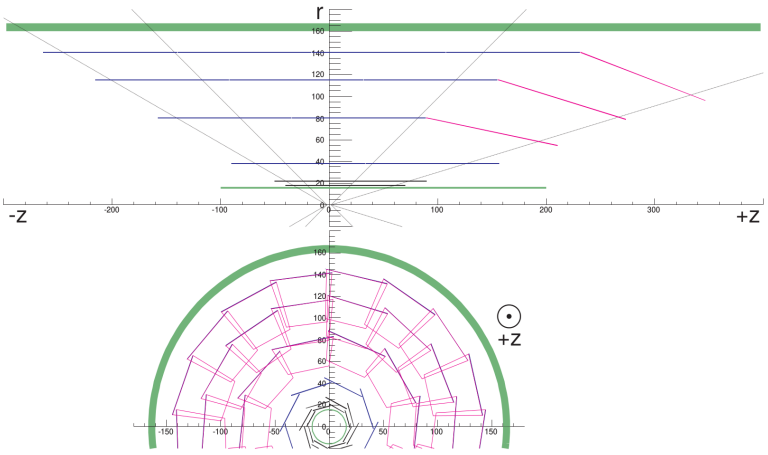

Figure 2.6.: The layout of the SVD detector [3]

Silicon Vertex Detector

The main purpose of the SVD is to provide information for the vertex reconstruction. It covers the full Belle II tracking acceptance region ($17° < \theta < 150°$), with the inner radius of 38 mm and the outer radius of 140 mm. In combination with the PXD, it is able to reconstruct low $-$ p_t tracks, which are important for the efficient reconstruction of the D^* daughters.

The SVD consists of four layers of a double-sided silicon strip detectors. Principal scheme of the detector is shown in Fig. 2.6.

Central Drift Chamber

The CDC detector is used for a detection of the charged particles by the reconstruction of hits patterns, which the particle left in the detector. It plays three important roles:

- determination of the particle trajectory and its momentum

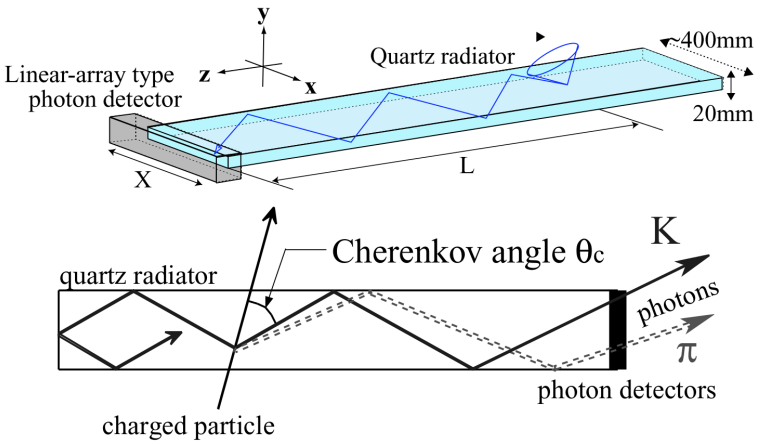

Figure 2.7.: Overview of TOP counter [3]

- measurement of the energy losses in the gas volume as part of particle identification process
- providing the trigger information on the charged particles

More detailed description of the CDC is given is Sec. 5.1.

2.3.2. Particle Identification

Particle Identification system (PID) is developed to fulfill needs of particle type identification. It consists of two parts:

- Time-of-Propagation counter (TOP) in the barel region.
- Aerogel Ring-Imaging Cherenkov detector (ARICH) in the forward end-cap region.

TOP Counter

Overview of TOP counter is shown in Fig. 2.7. The radiator consists of a long quartz bar for radiation of the photons and for propagation them to the bar end, a spherical mirror on the forward end to focus the light, and a prism at the backward end to allow Cherenkov ring image to expand before the detection. The Cherenkov image is reconstructed using two coordinates $(x;\ y)$ and precise timing provided by photomultipliers. The array of radiators consists of 16 modules and surrounds outer wall of the CDC.

ARICH detector

ARCIH detector (Fig. 2.8) is developed to provide a separation between K and π particles at the whole p_t scpectrum, and for π, μ and e below 1 GeV/c. The

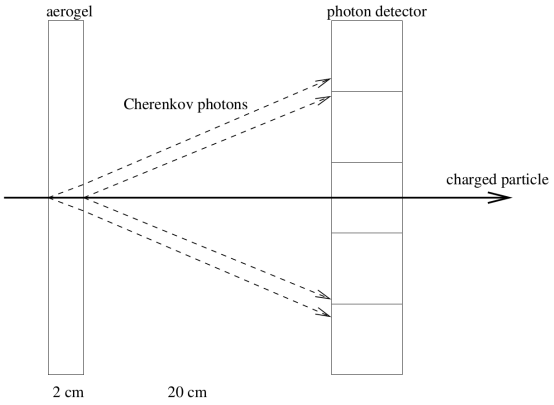

Figure 2.8.: Overview of ARICH detector [3]

ARCIH consists of the following elements: an aerogel radiator, which produces Cherenkov photons; an expansion volume which allows to form light rings; an array of position sensitive photon detectors, which are able to detect single photons with a good resolution.

2.3.3. Electromagnetic Calorimeter

The ECL is a high resolution electromagnetic calorimeter, which is able to detect neutral particles in a wide energy range from 20 MeV up to 4 GeV. It is build of CsI(Tl) scintilation crystals, which have a high light output, a short radiation length and a good mechanical properties. The ECL consists of a barrel and encap sections and covers the polar angle region of $12^\circ < \theta < 155^\circ$. The barrel part consists of 6624 crystals (with an average cross section of 6×6 cm^2) and the endcap consists of 2112 crystals.

2.3.4. K_L and μ detector

The K_L and μ (KLM) detector is the outermost part of the Belle II spectrometer, placed outside of the superconducting solenoid. It consists of the alternating sandwich of iron plates and active detector elements, based on a glass-electrode resistive plate chambers. The KLM (barrel and endcap parts) covers polar angle region of $20^\circ < \theta < 155^\circ$.

Muons and charged hadrons, that decay in flight or do not interact hadronically, with p_t higher 0.6 GeV/c travel through the detector until they escape. K_L mesons interact with ECL or KLM systems and produce a hadronic shower which can be registered in either one of the subsystems or both.

2.3.5. Triggers System

The trigger system consists of sub-trigger systems and final decision logic. Sub-trigger systems summarize information from its components and provide it to the final decision logic which makes decision on the processed event. The total latency in the trigger system is about 5 µs. Each component is developed on Field Programmable Gates Array (FPGA), wich allows to easily re-configure trigger logic [3].

The following trigger sub-systems are present in Belle II:

- CDC sub-trigger - provides information about charged particles trajectories
- ECL sub-trigger - gives energy deposit information and Bhabha process identification (for the luminosity measurement)
- Barrel and Endcap PID sub-triggers - provide precise timing and hit topology information
- KLM sub-trigger - gives muon track information

2.3.6. Data Aquisition System

The main task of the Data Aquisition System (DAQ) is to read out signals from the detector upon trigger signal is received from the trigger system. The system processes read out data and provides it to the storage system. The DAQ system is challenged to operate at high event rates, and as result to have low processing time. Fig. 2.9 shows the global design of the Belle II DAQ system.

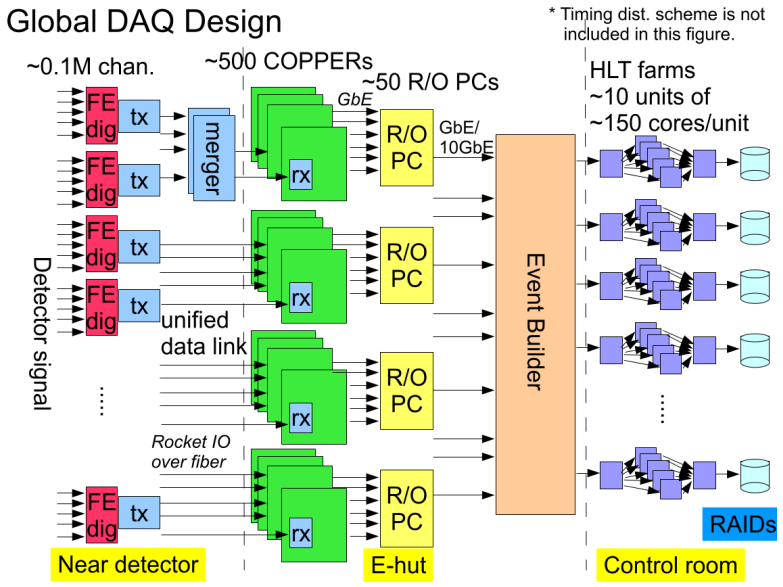

Figure 2.9.: Overview of DAQ concept [3]

3. The Software Framework

Modern high energy physics experiments are fully operated by automated software. To preserve and process large amounts of data, experiment-specific frameworks are developed. These include tools to operate the trigger system, to collect data from the detector and store it for the further processing, data processing such as reconstruction of physical events, tools for data analysis and Monte Carlo simulation. In this chapter, the organization of the Belle II software framework will be discussed.

3.1. Belle II Analysis Software Framework

The Belle II experiment inherits the best software development experiences from its predecessor, the Belle experiment, as well as concepts of software frameworks of other HEP experiments, such as CDF, ALICE, LHCb [23, 24]. It has been decided to develop an independent framework, called Belle II Analysis Software Framework (BASF2), rather than adopt the Belle Analysis Framework (BASF) to the needs of the Belle II . The BASF2 framework is organized in a modular way, which brings the possibility to reuse parts of the code at the different stages of data flow, such as high-level triggers, offline reconstruction and data analyses.

BASF2 uses external libraries to extend the functionality of the framework, e.g.:

ROOT ROOT [25] is the software framework being developed for data processing, statistical analyses and data storage, and it is widely used in HEP experiments. The latest version (ROOT ver. 6) is used in BASF2.

Geant4 Geant4 [26] is a toolkit for the simulation of particle interaction with matter.

Boost Boost is a set of C++ libraries (e.g algorithms, containers, iterators, concurrent programming etc), providing functionality to solve various programming tasks.

Google Test For the code testing purposes, the Google Test framework [27] is integrated into BASF2.

Generators EvtGen [28], Pythia [29], Photos [30], Tauola [31] and Phokhara [32]

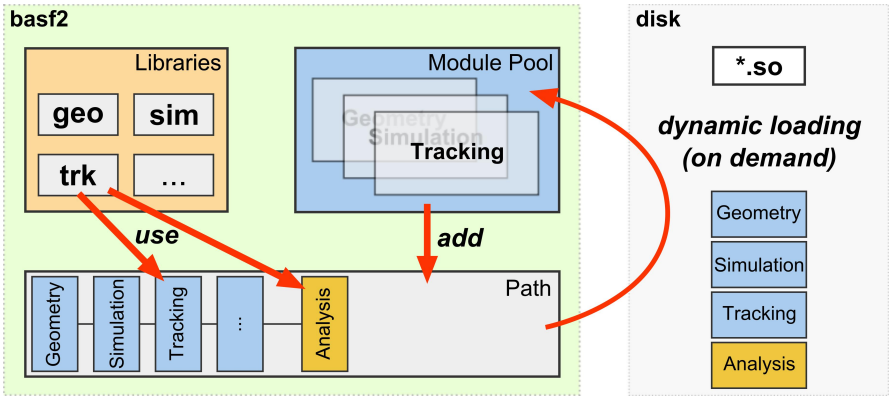

Figure 3.1.: BASF2 subsystem organization [24]

are packages to performe simulation of particles decay processes.

Eigen Eigen is used to perform linear algebra calculations.

NeuroBayes NeuroBayes [33] is an neural network package to perform multivariate analysis of correlated data.

RAVE RAVE [34] is a toolkit for reconstruction and fitting of the interaction vertices.

Millepede II Millepede II [35] is a package for linear least squares fits with a large number of parameters.

The code basis (libraries and modules) of BASF2 is written in C++, with the standard C++11 [36]. To compile the environment, the SCons [37] software construction tool is used. In general, the build is configured via configuration scripts, written in Python, and performed using the GCC compiler. The compilation results in libraries, that provide functionality, and modules, which use libraries to fulfill specific tasks [24]. With such organization of the framework it is possible to reuse the same algorithms to solve different tasks during the whole data processing chain.

Fig. 3.1 shows the organization of BASF2 framework. The execution is performed and configured with a steering file, written in Python, in which the execution order, the so-called path, is specified. It is possible to define the list of modules to execute, their configuration and the order of the defined modules. Each module can be configured via a module-specific set of parameters to carry out the assigned task. Data exchange between separate modules is performed via a DataStore interface, which plays the role of a common storage and can be accessed within each module. Collections of entries in DataStore have unique names for identification, and are being created by the modules. Also, it is possible to associate the objects among various collections by relations interfaces, which allow to store and retrieve connections between objects (e.g `CDCHit` → `RecoTrack`).

The Code Management

The whole code basis of BASF2 framework is managed by the Subversion (SVN) [38] revision control system. The main advantages of using SVN consist in its client-server architecture, the storage of the full history of changes in the central repository (located on KEK Computing Center servers), the possibility to create branches and the 2-dimensional organization of the repository filesystem (beside of the folder structure, it is possible to trace back modification of files). Files from the central repository can be duplicated as local copies and modified. Modifications on the client side can be fixed and transfered back to the repository as commits and distributed among other users. On the user side it is possible to use the `git svn` interface to use Git [39] as a client of SVN server. This tool allows to benefit from all features of the Git revision control system throughout the code development process.

Proving of the Code Quality

In order to ensure the quality and performance of the BASF2 code, regression tests with the validation framework, unit tests and integration tests are established within the framework; also, to keep the same coding convention for the whole framework, cppcheck and checkstyle utilities are available. These tools can be launched within the local installation of BASF2 to check the performance before committing the code to the official repository. Beside of that, nightly integration tests on the KEK computing servers are performed to show the status of the official code in the central SVN repository. Development (nightly) builds can point out compilation failures on various systems, failed unit tests, missing documentation, memory leaks in the software and changes in algorithms' performance.

The validation framework has been developed to reveal changes in the performance of the code. This is done by comparison of quantities, that characterize the functionality or the output itself of the algorithms, across various versions (revisions) of the code with the reference value. To check for deviations from the reference, χ^2 and p-value tests are performed. If significant deviation is present, the validation system notifies about it by producing warning or error messages, depending on the significance. To perform libraries and modules testing, validation-compatible Python and C scripts are created for each part of the BASF2 framework. The general validation flow is shown in Fig. 3.2. The execution of the validation scripts results in plots, which are being compared. Comparison is done via a web interface, which has two modes: static HTML, and Interactive Web Server. Also, to isolate the revision, in which changes in the validation results appear, the application of the `git bisect` utility has been adopted to the validation framework. It simplifies searches for commits, which introduce degradation of the code performance.

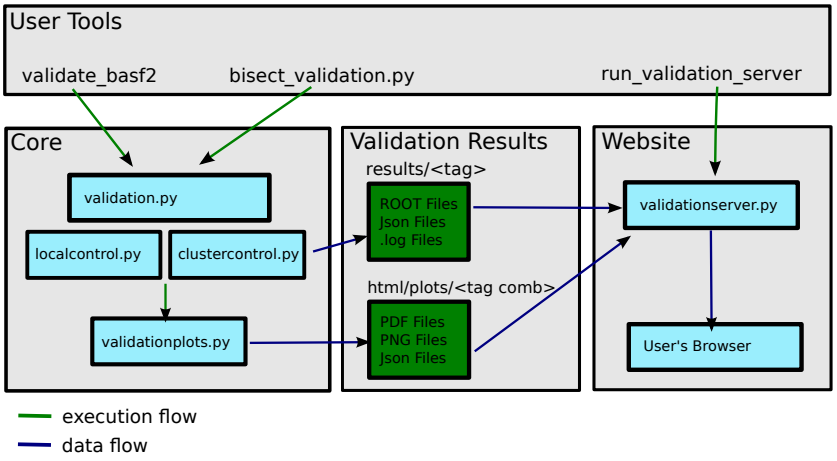

Figure 3.2.: Validation system structure, taken from the BASF2 software portal [40]

Unit tests are developed to verify the behavior of the algorithms and to check that it works as expected. Testing cases imply standard conditions of the algorithm execution as well as limitary cases. Execution of the unit tests results in succeeded or failed test.

3.2. Computing Model

The Belle II computing system has to handle an amount of raw data in the order of 10^{10} events per year. This requires to process data without any delay and store it with the data acquisition system. The Belle II computing model is established to fulfill such high demanding computing tasks as raw data collection, reconstruction of physical events for the analyses, Monte-Carlo production, and data preservation. Each of the tasks relies on the performance of different computing systems, such as data acquisition systems, computational power and data transfer bandwidth.

To meet all requirements of the Belle II computing model, distributed computing is adopted [41], based on gLite [42]. It allows to sufficiently increase computing resources by using of computational power of facilities of the members of the Belle II collaboration. Moreover, processed data will be distributed among members of the collaboration for ease access and as backup.

To store data, there are three data formats defined: **DST files**, which contains all output information after the event reconstruction; **mini-DST** (mDST) files, in which analysis-relevant information is stored (e.g. tracks, particles identification, vertexes, calorimeter clusters); **micro-DST** (µDST) files, which are reduced mDST files, containing only ntuples for specific analyses. All data are stored in ROOT files.

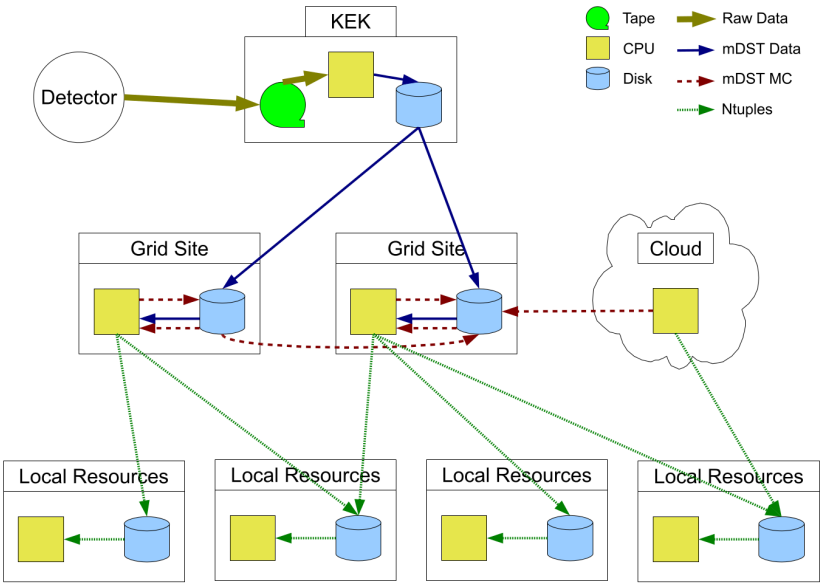

Figure 3.3.: The Belle II computing model [3]

The Belle II computing model has a tiered structure (Fig. 3.3). It includes data centers to store raw data, regional data centers to store processed data, sites which provide computational resources for Monte-Carlo production, and local resources. In the raw data centers, the data from the detector is stored and processed. The KEK Data Center plays the role of the main raw data center, storing all raw data and producing DST and mDST files. A copy of the raw data will be transferred to the Pacific Northwest National Laboratory (PNNL) and will be partially processed to produce mDST files. Afterwards, the produced mDST files will be distributed to regional data centers. Also, Monte Carlo data samples, with simulated events of e^+e^- collisions, are produced at regional data centers and Monte Carlo production sites. It's volume should be in the order of 6 times higher than the data collected by the detector to decrease systematic uncertainties. The data analysis will be performed on local facilities, clusters, using grid and cloud computing.

3.2.1. Cloud and Grid Computing

Grid computing is a large-scale distributed system, which provides computational resources for high performance computing. It consists of a system of heterogeneous clusters, linked together with a network, each of them performing a part of the task, given to the whole system. Thus, grid computing provides users with a significant computational power. To fulfill requirements for a demanded computational power, cloud computing has been integrated into the Belle II computing model. It allows to increase computational resources, in case

grid and on-site computing are not able to completely fulfill the requirements, by buying computing time from commercial vendors. Integration of grid, cloud computing and local resources are done basing on the DIRAC framework, allowing to use all three possibilities simultaneously [43].

3.3. Reconstruction

After the data are stored, the reconstruction is performed by the offline software (namely the BASF2 framework) which store it in the mDST format, preparing it for the further analyses. Reconstruction starts with the gathering of low-level information about the events being reconstructed, and ends up with the physics-related information (such as particles being created in the physical process, decay vertexes and kinematics of the event). The reconstruction chain involves a lot of BASF2 modules, each of them performing subset of reconstruction tasks. In most cases, the output of the reconstruction modules is used as input for the next modules in the chain, and/or stored to the mDST files.

There are several major steps in the reconstruction chain:

- finding of track candidates;
- track fitting and vertex reconstruction;
- dE/dx and particle type hypothesis determination;
- reconstruction of the ECL clusters;
- K_0 and μ reconstruction;
- preparation of mDST output.

Track candidates are reconstructed using hits' information.Track finding is performed separately in CDC and VXD subdetectors, with merging of matching tracks afterwards. A discussion on the CDC track finding will be given in Sec. 5.2. The VXD track finder searches for tracks by combining PXD and SVD hits produced in the event. It uses a SectorMap and a Cellular Automaton to define track candidates, with further candidate fitting and application of a neural network of Hopfield type to ensure the quality of the candidates [44]. CDC and VXD track candidates are fitted with GENFIT 4.2, which calculates the kinematic parameters. Merging of the candidates proceeds with extrapolation of trajectories (i.e, CDC track candidates are extrapolated into the VXD volume and vice versa) and finding of complementary tracks. Matched tracks are combined into a single candidate and fitted again. Afterwards, pairs of positive and negative tracks are fitted to determine decay vertexes of neutral particles.

After the track reconstruction, modules to determine dE/dx and the particle type are inserted into the reconstruction chain. The dE/dx information is extracted out of the fit results, and corrected by the individual interactions (hits) of the track with the material [45]. It is possible to build likelihood function

for particle type hypothesis using dE/dx information. It allows to determine the type of the low-momentum particles which do not reach PID systems of the detector (ARICH and TOP). To use ARICH and TOP subdetectors hits for particle identification, trajectories of the tracks are extrapolated in their volumes and matching hits are associated with the tracks. The particle type hypothesis is defined with likelihood functions, which give the probability that the track was created by a particle of the given type.

Reconstruction of the ECL cluster is done via a chain of modules, that perform clustering of the activated crystals, determine the shape and parameters of the showers, correct measured energy using calibration data, match clusters to reconstructed tracks (in case it is feasible), and perform $e^{\pm}$ identification. Reconstruction and selection of the clusters is configured by various criteria, such as total energy of the cluster, highest energy of the individual cell in the cluster, timing information etc.

Reconstructed events are stored in the ROOT files in mDST format for further skimming and physics analyses. All irrelevant information, such as hits or intermediate data structures, is omitted in the storage process.

3.3.1. Geometry

Almost every module in the reconstruction chain needs geometrical parameters of the Belle II detector to perform a correct reconstruction of events. This means that all technical details of the subdetectors as well as its placement should be stored in the same database, and easily accessible by reconstruction or simulation algorithms. Simulation depends on the geometry description as it should reproduce reliable results, identical to the signal from the detector. During the reconstruction process, the positions of the each part of the detector should be precisely known. This is a critical point especially for the tracking algorithms, since they rely on geometrical positions of the hits. To fulfill these requirements, the position information of the subdetectors is updated with the time to take into account deformations of the detector. Large changes can be registered by measuring the relative position of the detector components, but relatively small variations can only be detected by the alignment software.

Alignment is a crucial part of the tracking software. Its task is to detect inconsistencies between the "real" detector geometry and the stored description, especially displacement of the VXD sensors. Alignment for the Belle II detector is based on the Millepede II package, which performs linear least squares fit and minimizes the systematical deviations of hit positions against reconstructed track trajectories. As result of such minimization, geometrical correction factors are calculated and reconstruction can be performed with the updated detector geometry.

3.4. Simulation

All reconstruction modules are being tested using simulated events to test the performance and reliability of the algorithms. The main purpose of the simulation is to reproduce physics events and the detector response.It includes various tools:

- generators
- detector simulation package
- digitization tools

3.4.1. Generators

Generators are used for the reproduction of physical processes occurring in the e^+e^- collisions, such as decays of B mesons or beam background production. They generate lists of parameters of particles in the final state based on the current knowledge about physics processes.

EvtGen [28] is used for B-mesons decay simulation as it provides reliable results and has been used by the Belle experiment, and tested over the years by other collaborations. It provides the possibility to generate inclusive B meson decay modes as well as specific user-defined modes. To introduce radiative corrections to the decays, the PHOTOS [30] generator is used. Continuum processes are generated by Pythia8 [29] and EvtGen. The PHOKHARA [32] generator performs the simulation of electron-positron annihilation into hadrons with high order radiative corrections. In order to generate single particles in the event, a particle gun generator is implemented within BASF2. It allows to set the specific kinematic configuration of the generated particles to cover wide spectrum of the technical tasks.

3.4.2. Detector Simulation

The detector simulation within the BASF2 framework is done by the GEANT4 package. It uses the geometry database to simulate sensitive detector parts and uses generated particles information as input. GEANT4 simulates interaction of final state particles (primary particles) with the detector material, producing the expected detector response to those interactions. It results consist of simulated hits and secondary particles. To provide the correct detector response to the simulated hits, digitization modules are used.

Digitization process is different for each of the detector components due to the different hit and signal formation processes. Each subdetector has its own digitization module, which takes into account all detector-specific processes, e.g. collecting of ions in the CDC volume by sensible wires in presence of the

magnetic field (detailed description is given is Sec. 5.1). The digitization results in the simulated data, having the same format as a raw data, which can be used in the reconstruction chain.

4. Overview of Tracking Approaches and Algorithms

Together with the development of high energy physics experiments, pattern recognition techniques were evolved and improved. The tracking algorithms play a crucial role in studies at high energy physics experiment, as they are intended to reconstruct products of the reactions being studied at the experiment.

The general tasks of the tracking algorithms could be classified as:

- finding of patterns of hits, which are likely created by the same particle
- determination of the trajectories and parameters of the tracks
- providing of the information about event to other parts of the reconstruction chain

Tracking algorithms vary upon the tasks they are designed to resolve. For example, in modern online trigger systems which are strongly dependent on the execution time, a tracking part of the reconstruction intended to determine a number of track and roughly estimate their parameters, while offline tracking algorithms are designed for the accurate reconstruction of the hits pattern and precise determination of the tracks' kinematic parameters.

It's possible to split tracking tasks into two subsets: pattern recognition and fitting, each of them designed to solve a specific set of tasks. The goal of the pattern recognition is to reconstruct patterns of hits, track trajectories and roughly estimate track parameters. Then, based on results of the pattern recognition, filter-based fitting procedures determine track parameters with precision level, which is sufficient for physic analyses. Usually, a pattern recognition and a fitting are designed as independent algorithms, but in some tracking approaches (such as elastic arm approach [46]) they are combined and performed simultaneously.

In this chapter an overview of different pattern recognition methods will be given. Each approach has its own strengths, and can efficiently perform for a specific set of tracking tasks.

4.1. Pattern recognition approaches

The pattern recognition algorithms and approaches could be divided into two groups: local tracking approaches and global tracking approaches, and each of them has its own distinguishable features. While the main goal of all pattern reconstruction algorithms are mostly the same, the methods of the track detection are different.

The local tracking approach rely on short-range correlations between hits while performing the track reconstruction. These correlations in general imply mutual disposition of hits and their agreement with the local track model. The global tracking approach implies recognition of patterns of hits left by charged particles in the whole event, and rely on the long range correlations among hits and their agreement with the track model. All hits are simultaneously treated in the same way, independently on hits ordering and direction of the track. The local tracking approaches are able to take into account multiple scattering, but weaken in case of missing hits or high local hits density, while the global tracking approaches may operate with decreased hit efficiency, but weaken in case of tracks that deviate out of the track model.

4.1.1. Local Tracking Approaches

The local pattern recognition is often called track following [47], since most of the methods are based on the propagation of the trajectories through the detector volume and assignment of consistent hits. It is essential to define a track model that can be employed during extrapolation and for track parameter determination. In this case, initial track parameters should be defined and treated as seeds for the local track finding procedure to set the starting point of hit following.

Seed parameters are usually defined by combining subset of hits. There are various approaches how to perform seed determination, each of them has its own benefits. For example, in outward-inward tracking algorithms, neighboring hits from the last and the penultimate layers are combined into pairs (or triplets) to determine the direction of trajectory propagation. But with this approach parameters of the initial trajectory have a large uncertainty.

Naive Track Following

Different approaches of hit assignment during the track following can be applied. The basic one is the Naive Track Following, where track is extrapolated through the detector volume and hits along its expected trajectory are assigned. However this approach gives ambiguous results in case of high hits density and overlapping tracks. To solve the problem of uncertain hit assignment combina-

torial track following could be applied. It involve branching of the track evolution in cases of multiple choices of the track continuation.

The Hopfield Model and the Denby-Peterson Method

A neural network approach can be successfully used to solve the problems of the pattern recognition. In this approach, network is represented as net of neurons which interact with each other. In the Hopfield model [48] each neuron interacts asymmetrically with others, setting its state ("active" or "inactive") according to the state of the other neurons. The system can be characterized by the energy function [48]

$$E = -\frac{1}{2}\left(\sum_{ij} w_{ij} S_i S_j - 2\sum_{i} s_i S_i\right) \tag{4.1}$$

with the neuron state function

$$S_i = \Theta\left(\sum_{j} \left(w_{ij} S_j - s_i\right)\right) \tag{4.2}$$

where s_i are the threshold values, w_{ij} are the weights, which determine the strength of each interaction, i and j are the indexes of the neurons.

The Hopfield model has been adopted to the track finding needs by Denby and Peterson [49, 50]. In the method, each possible pair of hits is associated with the neuron, which then can be combined to build the track. Neuron can be activated only in case if both hits belong to the same track. The neurons can connect with each other and build a sequence only a case that they successively share hits, and follow connection rules. This means that connected neurons should be track-like, i.e represented by a smooth curve.

The dominant limitation of the method is that it is not suitable for the 3-D track finding. In principle, the problem could be solved by forming space point out of the hits. The method, referred as **Cellular Automaton** [51], used space points combination and the hits following as the track reconstruction method.

Cellular Automaton

Cellular automata are dynamical system, which evolve in discrete space, consisting of cells [52, 53]. The evolution of the system is determined with the set of rules, in which the new state of each cell is calculated based on the state of its neighbors. The changes of the state are performed simultaneously and in parallel.

In general case, a cellular automaton constructed using the following definitions [52]: define a cell and its possible states, define neighbors, define rules of the evolution, define time evolution.

For the tracking purposes, the tasks of cellular automaton are reduced to the solution of the longest path problem, which is stated in terms of graph theory [54]. The cellular automaton could be applied to construct segments using triplets of hits as well as combine segments to build the tracks. The cellular automaton, developed for the Belle II tracking uses novel weighted implementation of the algorithm, in which each cell has its own weight.

4.1.2. Global Tracking Approaches

Global tracking usually allows to perform efficient track finding, giving trajectories of possible tracks and their forming hits, but the reliability of the approach decreases if the particle experiences scattering and produces kinks in the trajectory, or strongly affected by energy losses in the material of the detector. In this section global tracking approaches and their application will be discussed [47].

Template Matching Technique

Template matching technique is a method, which searches for matches of hit patterns to predefined masks, which describe possible good tracks in the detector. This method has been applied in the ARGUS trigger system [55]. Predefined masks are compared with the hit pattern from the detector. In case of a match, patterns on the matched hits are defined as the track. For speedup purposes it's possible to disable all masks, which contain wires without hits from the detector.

The benefit of this method is the simplicity of the implementation and of the mathematical model. On the other hand, it's not well scalable, as it strongly depends on the number of possible combinations of the detector's sensible elements.

Radon Transform

Radon tracking technique is based on restoring track properties based on the representation of hits in the track parameter space. It is possible to represent distribution of the track parameters as a function $D(p)$, where p are parameters of the track. Density of the hits $\rho(x)$ in the event can be described with the relation [47]:

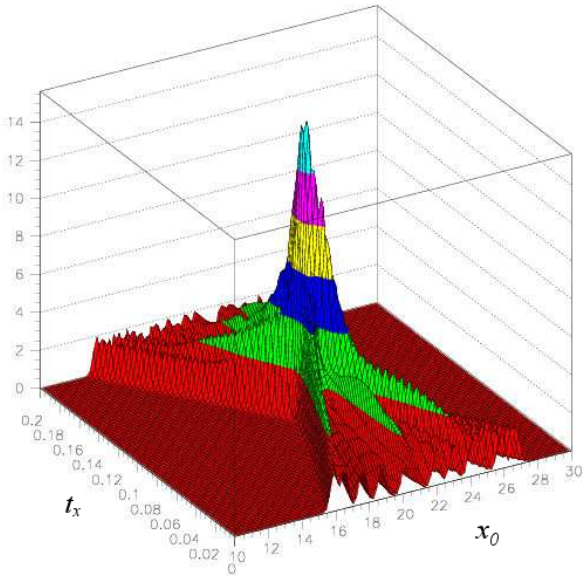

Figure 4.1.: An example of the Radon transformation for the event with a single track [47]

$$\rho(x) = \int_P \rho_p(x) D(p) dp, \tag{4.3}$$

where $\rho_p(x)$ is a response function in the parameter space, x is a set of general descriptions of the hit quantities, which can be interpreted as points on the track trajectory. By inverting equation (4.3) and constructing response function which takes into account detector resolution, it's possible to restore initial track parameters:

$$\widetilde{D}(p) = \int_X \rho(x) \rho_p(x) dx, \tag{4.4}$$

An example of the Radon transformation for the track in the tracking system without magnetic field is shown in Fig. 4.1. The track represented in parameter space of the track's slope t_x and impact parameter x_0. Each track hit contributes to the bins of total histogram with varied weights, which are mainly derived from the detector resolution. In case of discrete parameter space the Radon transformation transforms into the Hough transformation.

Hough Tracking

The Hough transformation [56] is widely used in track finding algorithms as well as in digital picture analyses to solve the problem of automated figure detection, such as lines, circles or more sophisticated shapes. The method was originally developed for detecting lines or arcs of hits in the pictures of bubble chambers, with the following reconstruction of particle trajectory. The general idea of the method lies in detection of parameters of the given figure if it presented in the picture. On the picture each point, which is of interest, gives vote for possible parameters of the figure, and votes from each point are grouped around most probable parameters of the figure.

The simplest case is the line detection. The Hough transformation uses the normal form of line on the plane:

$$\rho = x \cos\theta + y \sin\theta, \tag{4.5}$$

where ρ is the distance from the origin to the line, θ is the angle between x-axis and normal to the line, x and y are points, belonging to the line. Parameters of the possible line can be obtained by applying transformation 4.5 to the points of interest (in case of tracking - hits) and accumulating resulting set of parameters ρ and θ as votes. The most probable value will be represented as a cluster in (ρ, θ) parameter space (see Fig. 4.2). In case of presence of the homogeneous transverse magnetic field, it's possible to patterns of hits of charged particles have a circular trajectory. By applying the transformation

$$\begin{aligned} u &= \frac{2x}{x^2 + y^2}; \\ v &= \frac{2y}{x^2 + y^2}. \end{aligned} \tag{4.6}$$

circular patterns of hits are mapped into straight lines (detailed description of the conformal mapping is given in Sec. 6.1), allowing to use Hough tracking as efficient global tracking technique.

Legendre Tracking

The CDC of the Belle II detector can provide wire coordinates and drift time of the hits, which can be used for the accurate trajectory reconstruction. Whereas the Hough tracking is efficient for finding tracks which are coming from the interaction point (IP), it should be provided with the proper 2-dimensional position of the hits. The Hough transformation can not take into account the drift time of hits, so accuracy of the method drops. To solve this problem, tracking which is based on the Legendre transform can be applied.

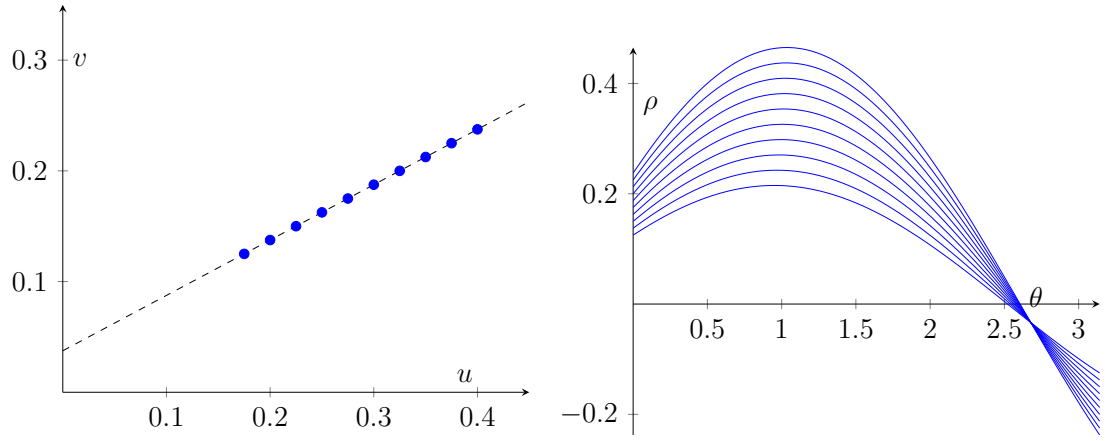

(a) Straight pattern of hits (b) Hits after the hough transform

Figure 4.2.: An example of the Hough transformation for the straight pattern of measurements

The idea of the Legendre-based tracking lies in the transformation of the drift circles using Legendre transform and mapping of hits onto Legendre plane [1]. This transform represents equation of all possible tangents to the given drift circle. Drift circles can be represented as concave and convex parts (Fig. 4.3a) with the next equation:

$$f(x) = \begin{cases} f_1(x) = y_0 + \sqrt{R^2 - (x - x_0)^2} & \text{for concave part} \\ f_1(x) = y_0 - \sqrt{R^2 - (x - x_0)^2} & \text{for convex part} \end{cases} \tag{4.7}$$

where (x_0, y_0) is the center of the circle, R is the radius of the circle.

With the normal line representation 4.5, Legendre transform becomes

$$f(x) \overset{\mathcal{L}}{\longleftrightarrow} = \begin{cases} \rho = x_0 \cos\theta + y_0 \sin\theta + R & \text{for concave part} \\ \rho = x_0 \cos\theta + y_0 \sin\theta - R & \text{for convex part} \end{cases} \tag{4.8}$$

and represents two equations of tangents to the drift circle in real space (fig 4.3b), or two sinograms, in the Legendre space (Fig. 4.3c), for each circle [1]. The sinogram in the Legendre space contains all possible combination of tangent parameters (ρ, θ) to the given drift circle (Fig. 4.4). In case of few drift circles, which sharing the common tangent, **the intersection of sinograms** in Legendre space corresponds to the parameters of **the common tangent** (Fig. 4.5). With the limit $R \to 0$, the drift circle reduces to the point, and the Legendre transform reduces to the Hough transform of the point (x_0, y_0), providing a single sinogram in the Legendre space instead of two.

As in the Hough tracking, the Legendre tracking implies detecting regions with high sinogram density in Legendre space. This can be done by filling 2-

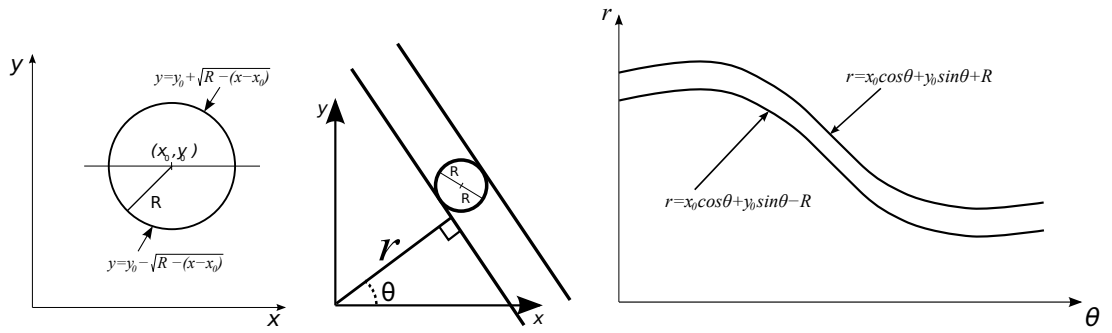

(a) A drift circle

(b) Possible tangents to a concave and a convex parts of a circle

(c) Legendre transformation of a drift circle

Figure 4.3.: An example of the Legendre transformation of a single drift circle

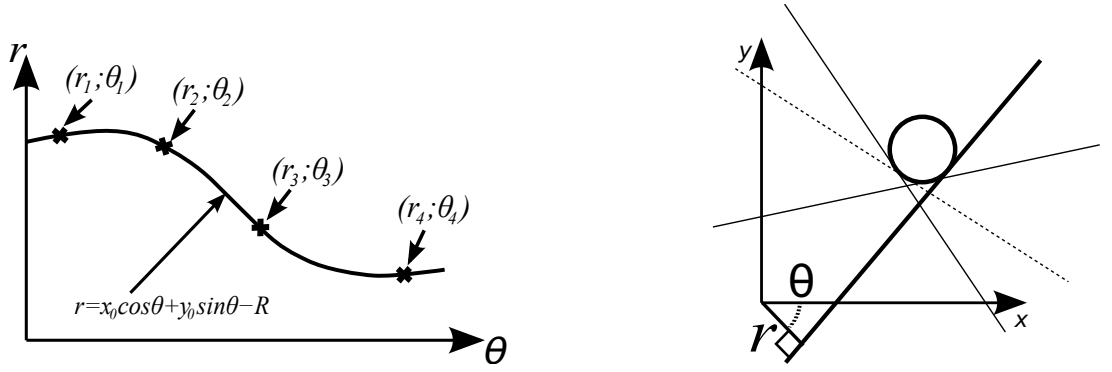

(a) Legendre transformation of a concave part of a drift circle with possible tangents

(b) Example of possible tangents to a concave part of a drift circle

Figure 4.4.: Relations of the Legendre transformation to tangents to a drift circle

dimensional (ρ, θ) histogram or concurrent 2-dimensional binary search alike to Fast Hough algorithm [57].

Main issue of the Hough and Legendre tracking is particles with hard energy losses and particles produced not in IP region (so-called non-prompt tracks). Both effects lead to a bending-like distortion of the hit patterns in the conformal space. Thus, depending on the strength of the distortion and granularity of the look-up histogram, efficiency of the method decreases.

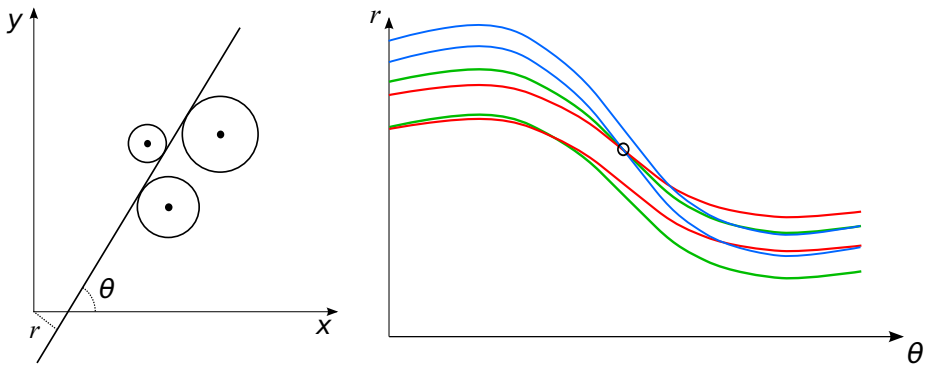

(a) Drift circles, sharing a common tangent

(b) Representation of a common tangent in the Legendre space

Figure 4.5.: Representation of a common tangent to drift circles

4.2. Fitting Algorithms

Fitting plays important role in pattern recognition algorithms for successful determination of trajectories of the track candidates as well as for analysis purposes. It is important part of the track finding process, in which parameters of the track are determined precisely. Fitting procedures could be classified into two subgroups:

- fast fitters, which are performing parameter determination of a given hit pattern according to a simplified track model
- filters, which are based on a complex track model and can perform along with a parameter determination

4.2.1. Fast Circular Fitters

In case of presence of the magnetic field in the tracking parts of the detector, projection of the particle's hit pattern forms circular trajectories. Fast circular fitters in general are based on least-squares regression methods, with determination of the parameters of the circle which interpolate the given pattern of hits. The task of the fitting could be reduced to χ^2 minimization problem:

$$\chi^2 = \sum_i d_i^2 w_i, \tag{4.9}$$

where d_i is the measurement displacement relative to the trajectory, and w_i is the weight of the measurement.

Kärimaki Fitter

Kärimaki circular fitter is a fast non-iterative fitting method, with Gaussian distributed fitting parameters [58]. The method provides an explicit solution instead of iterative solution for the non-linear least squares problem. The function (4.9) is minimized with parametrization of residual d_i

$$d_i = \pm \left[\sqrt{(x_i - a)^2 + (y_i - b)^2} - R \right], \tag{4.10}$$

where x_i, y_i are measurements, a, b are the coordinates of the center of the circle, R is the radius of the circle. To eliminate non-linearity coming from eq. (4.10), with the condition $|d_i| \ll R$ residuals could be represented with the approximation

$$d_i \approx \pm \frac{1}{2} R^{-1} \left[(x_i - a)^2 + (y_i - b)^2 - R^2 \right]. \tag{4.11}$$

The parametrization chosen for the trajectory includes the curvature $\rho = \pm 1/R$, the distance of closest approach d, direction of the propagation ϕ at the position of the closest approach. The parameters ρ, ϕ and d are Gaussian and don't produce truncation problems for high p_t tracks.

Riemann Fitter

Fitting of Riemann sphere [59] based on mapping of two-dimensional measurements onto the Riemann sphere. Circles and lines on the plane are uniquely mapped onto circles on the Riemann sphere. Thus circular pattern of hits mapped onto Riemann sphere will define a unique plane in the space. The method does not require iterations or initial seeds for the trajectory parameters to solve the problem.

4.2.2. Filters

Comparing to fast circular fitters, filters are able to analyze or predict behavior of the track. The track in space is considered as dynamical system in the filter analysis [60]. The state of the system can be described by the state vector of 5 parameters, which correspond to the parameters of the track, and can be written as a function of a suitable coordinate [60]:

$$\mathbf{x} = \mathbf{x}(z) \tag{4.12}$$

Evolution of the state vector $\mathbf{x}$ can be described by a system equation, which takes into account states $\mathbf{x}_k$ in the interaction points z_k only:

$$\mathbf{x}(z_k) = \mathbf{x}_k = f_{k-1}(\mathbf{x}_{k-1}) + \mathbf{w}_{k-1} \tag{4.13}$$

Kalman Filter

Kalman filter is an efficient recursive filter, which estimates evolution of the state vector of the system. The evolution of the system may evolve in space or in time. In case of the track fitting procedure, hits are treated as consecutive measurements of the state vector. To estimate the current state of the system, the previous measurement and the noise are taken into account.

Kalman filter is the optimal filter to predict the state of the system, basing on previous measurements, to smooth the state of the system, and to filter the current measurement. The filter can take into account multiple scattering of the particle. It proceeds in two steps, processing measurements in forward and backward directions.

Deterministic Annealing Filter

Another fitting technique is based on the Deterministic Annealing Filter (DAF). It is an extension to the Kalman filter, introducing reweighting of observations. After the smoothing procedure, the track position can be predicted at each point. Basing on this prediction, weight of each measurement can be estimated and taken into account in the next iterations. If the weight of the hit reaches the lowest threshold, the hit is not taken into account in the next iteration.

5. Tracking in Central Drift Chamber

The CDC pattern recognition contributes greatly to the whole tracking chain. Precise and pure track trajectories are of interest for event reconstruction and analysis algorithms. Pattern recognition should satisfy the next requirements:

- correct **assignment of hits** left by the charged particle to the same pattern
- efficient **separation of the tracks**, so hits originating from different particles don't mix up
- low **ghost rate** and **wrong hits assignment rate**

Also, tracking should fulfill the next technical demands:

- operate with **low execution time** while preserving reasonable tracking performance
- store tracking output, compatible with other reconstruction algorithms

The tracking chain in the CDC uses all benefits of the detector, such as the cellular detector structure (see 5.1), relatively low energy losses and long hit patterns of the particles (number of hits depends on the kinematic parameters of the particle). The design of the CDC allows for the efficient use of global and local tracking approaches even for the events with high track multiplicity and with moderate background levels.

5.1. CDC Design and Characteristics

The CDC of the Belle II detector has a cellular structure, where cells are represented by the combination of field and sense wires. Each sense wire is surrounded with 8 field wires, forming a square-like shape. Neighboring cell share field wires (see Fig. 5.2) and are grouped into layers, formed by cell which are the equidistant to the z axis. The number of the cells in each layer is chosen to meet readout electronics and trigger requirements and has to be multiple to 32 [3]. Thus, number of cell varies from 160 (for innermost layers) to 384 (for outermost layers). Axial and stereo layers are grouped by 6 into superlayers. Furthermore, the innermost superlayer has 2 additional layers and consists of smaller cells with a cell's radial size 10 mm while cells from other superlayers have a radial size of 18.2 mm on average.

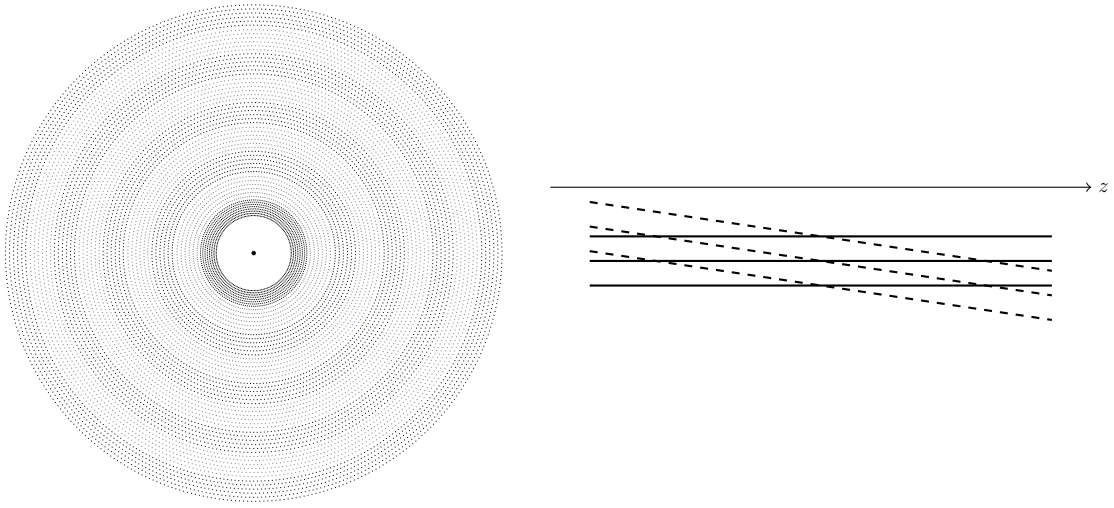

(a) Cross section of CDC in the $\rho - \phi$ projection at $z = 0$. Each marker corresponds to a sense wire, field wires are hidden; bold markers represent axial wires, mild markers represent stereo sense wires. The innermost superlayer corresponds to the small cell chamber.

(b) Schematic $\phi - z$ comparison of one axial and one stereo layers. Sense wires of the axial layer are parallel to the z axis, while stereo layers are tilted relatively to z axis. The stereoangle of stereowires introduces ambiguity of $\rho - \phi$ projection of stereohits in case of unknown z position of the hit.

Figure 5.1.: Schematic view of CDC

To provide stereo information about the track trajectory. there are two types of superlayers implemented:

- **axial** superlayers ("A"), in which sense wires are parallel to the z axis
- **stereo** superlayers ("U", "V"), which form a stereoangle with the z axis

The combination of axial and stereo hits, belonging to the same trajectory, can provide a complete 3-D trajectory of the charged particle in the CDC volume. To avoid biases in the polar angle measurement, stereo superlayers have two different orientations, "U" and "V", which differ by the sign of the stereoangle. Axial and stereo superlayers are alternating (AUAVAUAVA) between innermost and outermost parts of the CDC (see Fig. 5.1).

5.1.1. Drift Cells Structure and the Signal Registration

Electrons from the ionization process drift in the electric field. As they approach the sense wire, they produce a cascade and generate a signal on the sense wire. The behavior of the drift of the electrons and ions are different, and the main difference is that the drift time for electrons by orders of magnitude smaller than for ions. Thus, high positive potential is applied to sense wires and field wires are grounded. With this setup, electrons are collected within few hundred nanoseconds by the sense wire of the cell, while it takes up to microseconds for

Superlayer	Number of layers	Number of cells per layer	Radius, mm	Stereoangle, mdar
Axial 1	8	160	168.0 – 238.0	0.0
Stereo U 2	6	160	257.0 – 348.0	45.4 – 45.8
Axial 3	6	192	365.2 – 455.7	0.0
Stereo V 4	6	224	476.9 – 566.9	-55.3 – -64.3
Axial 5	6	256	584.1 – 674.1	0.0
Stereo U 6	6	288	695.3 – 785.3	63.1 – 70.0
Axial 7	6	320	802.5 – 892.5	0.0
Stereo V 8	6	352	913.7 – 1003.7	-68.5 – -74.0
Axial 9	6	384	1020.9 – 1111.4	0.0

Table 5.1.: Configuration of the CDC sense wires [3].

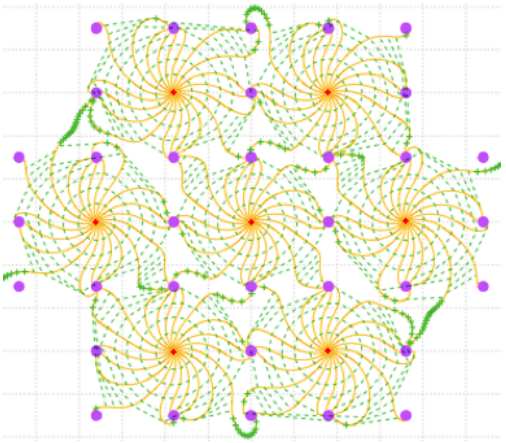

(a) Equipotential lines of the electric field (green dashed lines) and drift paths of electrons (yellow lines) in the CDC cells [61]

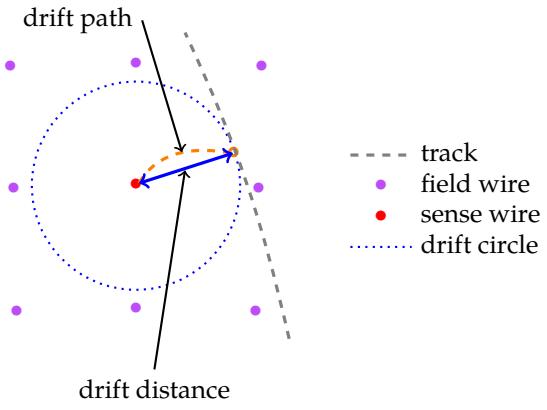

(b) a schematic structure of a single CDC cell with a hit

Figure 5.2.: Drift cells structure. [47]

ions to recombine on the field wires. The strength of the electric field E in the cell decreases with the distance to the sense wire as

$$E \approx \frac{U}{r} \tag{5.1}$$

where U is the voltage on the sense wire, r is the distance to the wire. Fig. 5.2a shows an example of electric field lines in the CDC cells.

It is possible to estimate the distance from the track's trajectory to the sense wire by measuring the drift time

$$t_{TDC} = t_{drift} + t_0 + t_{tof} \tag{5.2}$$

where t_{TDC} is the time measurement by the TDC device, t_{drift} is the drift time, t_0 is the event time, t_{tof} is the time of flight of the particle from its production vertex to the given CDC cell. The distance of the closest approach of the track to the sense wire can be estimated using the space-time relation (x-t relation), in which x represents a distance of the track closest approach to the sense wire. In the simple case, the linear x-t relation can be presented as

$$r = t_{drift}\, v_{drift} \tag{5.3}$$

where r is the drift distance, v_{drift} is the drift velocity (for CDC of the Belle II detector $v_{drift} \approx 4$ cm/µs [62])

More precise space-time calibration needs a more complex x-t relation. The simulated x-t relation is affected by the ion statistics, gas composition and the field inhomogeneity. It is intended to approximate the real detector response and is parametrized with a fifth-order polynomial (for the inner part of the cell) and a linear function (for the boundary regions), and named realistic x-t relation. It also takes into account the influence of the magnetic field on the electron drift trajectories and effects of the field inhomogeneities at the cell boundaries. Also, due to the presence of the magnetic field, electrons experience the Lorenz force and as result drift trajectories are bent 5.2a.

An example of the simulated realistic x-t relation is shown in Fig. 5.3. The deviation of the realistic x-t relation from a linear x-t relation becomes more observable for the outer parts of the CDC cell (higher drift length). Also, for the different track's incident angle x-t relation differs.

5.2. Tracking Flow

With the current setup, development of the CDC tracking is performed using the detector simulation. All components of the simulation chain, described in Sec. 3.4 (generators, detector simulation, digitization), are used to replicate the

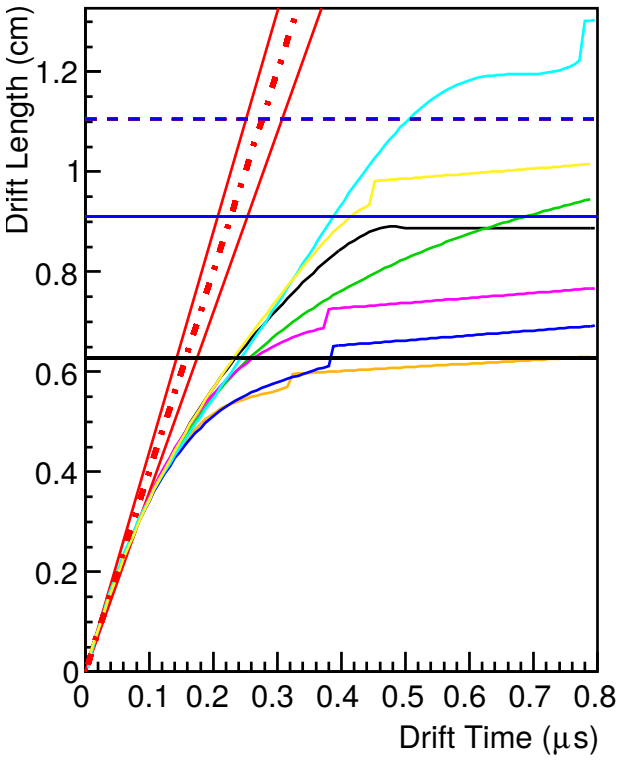

Figure 5.3.: An example of the simulated x-t relation. Colored curves correspond to the simulated x-t relation with the different incident angle, red dot-dashed curve represents default linear x-t relation. Black solid line corresponds to the cell width in ϕ direction, blue solid line corresponds to the distance between the sense wire and the inner (outer) field wire, blue dashed line corresponds to the distance from the sense wire to the corner inner (outer) field wire. (taken from [62])

expected detector response to the e^+e^- collisions. The simulated hits in the CDC are used as input for the CDC tracking chain, which combines them into track-like patterns. The pattern recognition in CDC is designed in the way to reconstruct tracks efficiently and provide tracking information to other subsystems of the detector or for further physical analyses.

The general architecture of the CDC tracking chain is shown in Fig. 5.4:

- **WireHitTopologyPreparer** - prepares the digitized CDC hits for further usage in the pattern recognition algorithms
- **SegmentFinderCDCFacetAutomaton** - based on the Cellular Automaton tracking approach, reconstructs track segments within single superlayer (both axial and stereo superlayers)
- **TrackFinderCDCLegendreTracking** - pattern recognition, based on the Legendre transformation, reconstructs global track trajectories using axial hits only
- **StereoHitFinderCDCLegendreHistogramming** - module, which assigns stereohits to the axial-only tracks
- **SegmentTrackCombiner** - combines reconstructed segments and tracks to restore complete track trajectories
- **TrackQualityAsserterCDC** - a module which assures the quality of the reconstructed tracks, performs correction of the trajectories and normalizes them

As one can see, the CDC tracking is a mixture of global and local approaches. It employs Cellular Automaton based local tracking to reconstruct segments of tracks within one superlayer, while Legendre based global tracking approach is intended to find complete track patterns using hit information from all axial superlayers. It worth to mention that stereo superlayers are not considered in the Legendre tracking since stereohits have a large $\rho - \phi$ projection ambiguity in case of unknown z position of hit. Assignment of stereohits is performed afterwards, when $\rho - \phi$ trajectories are defined.

All tracking modules are using the same hit objects, created by WireHitTopologyPreparer module and exchanged via DataStore interface. It brings a possibility to mask already used or bad hits, and to forbid to use them. TrackFinderCDCLegendreTracking module combine hits into tracks independently of SegmentFinderCDCFacetAutomaton, and do not take into account the information about the available segments. The combination of the global and local approaches take place on the later stage, when SegmentTrackCombiner module appends segments with unused hits to the suitable global tracks.

Details about application of the tracking methods are given in the following sections.

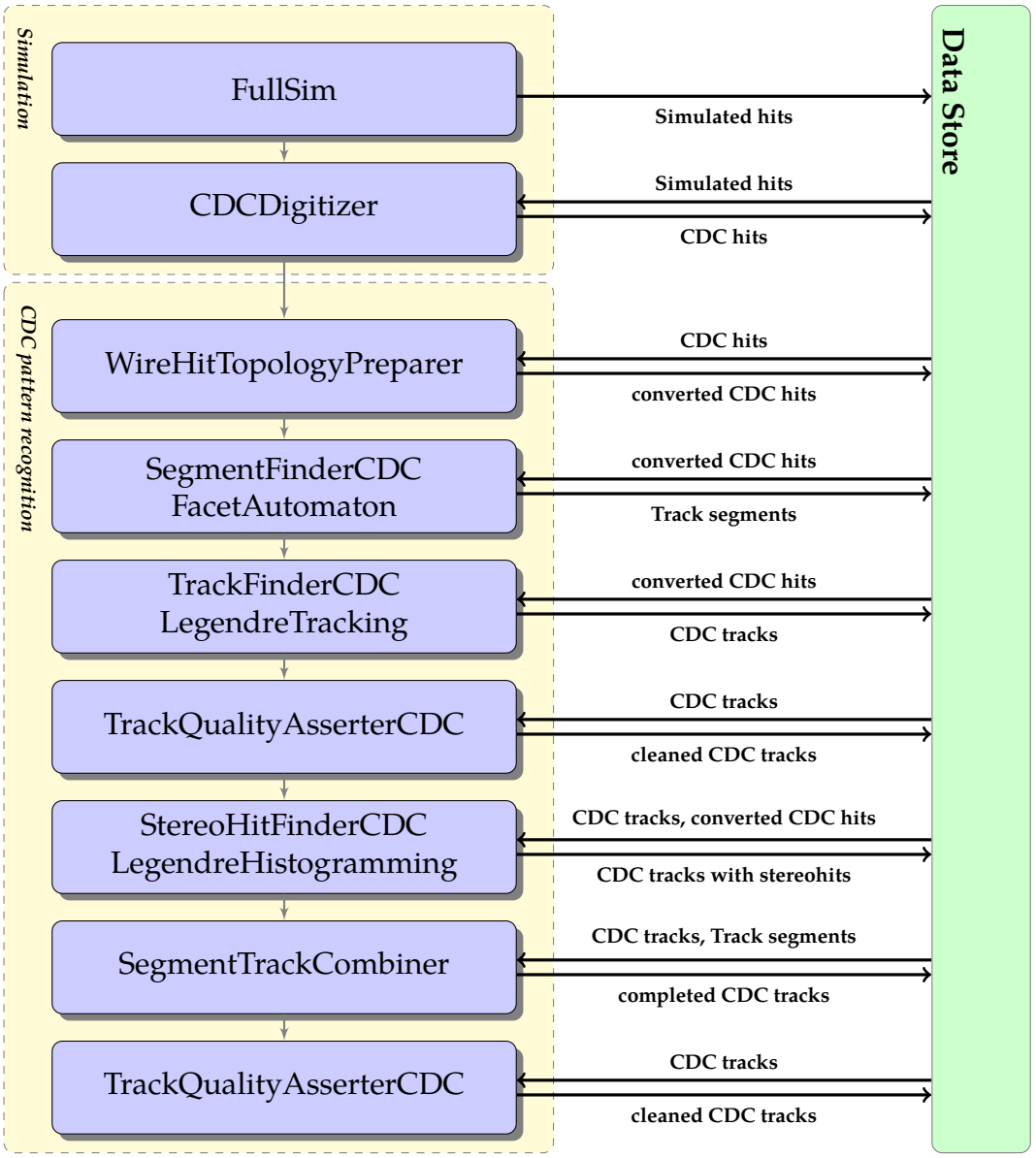

Figure 5.4.: Schematic view of the CDC pattern recognition flow, ordering of the modules and data exchange are shown. The common data objects (hits, segments, tracks) are stored in DataStore and delivered to each module on demand.

5.2.1. Cellular Automaton

Since CDC has a cellular structure, in which cells are combined into layers, it is reasonable to involve Cellular Automaton tracking technique as a local tracking algorithm [54]. The neighboring hits within one superlayer combined into hit triplets, which are feed to the weighted Cellular Automaton and combined into the segments. This approach allows to create complete hits segments within one superlayer and to avoid track losses due to imperfect trajectories. The main difficulties appear on the segment combination stage, where segments are combined into tracks based on their kinematics. Since segments consist of relatively low number of hits to determine trajectory parameters precisely, combination ambiguities can appear.

The results of the Cellular Automaton can be efficiently used for beam-background suppression purposes. Beam background in the CDC usually is represented by single hits, clusters of hits and low-momentum track-like trajectories. Background suppression is based on a trained boosted decision tree (BDT) which identifies single hits, clusters, or segments as a background [63]. The BDT is trained using the TMVA toolkit, and takes cluster and segment parameters as input for the training. By cutting on the BDT output it is possible to reject up to 95% of the background hits. The main advantage of using a BDT is that track-like patterns and background-like patterns are effectively distinguished, leading to least losses in the track reconstruction efficiency.

5.2.2. Legendre Finder

Legendre pattern recognition has been chosen as the global pattern recognition algorithm. As it was shown in Chapter 4, it strongly depends on the precision of the hit's drift length information, as well as on the beam-background level. As the method involves a conformal transformation as intermediate step of the pattern recognition, it leads to efficient reconstruction of the tracks coming from the IP. However, the method's efficiency drops in case of tracks with the high energy losses.

The method is suitable for the reconstruction of 2-D trajectories, and it uses hit's $\rho - \phi$ projection for the pattern recognition. Due to this fact, the method only can work with the axial hits, since the $\rho - \phi$ projection of the stereohits are correlated with the chosen z reference coordinate and the hit's z position.

More detailed description of the method will be given in Chapter 6.

5.2.3. Stereohits assignment

To complete trajectories with the z stereo information, a stereohit assignment module is put in the pattern recognition chain. Its main purpose is to assign

correct stereohits to the axial trajectories, so a complete 3-D trajectory can be restored. The method is based on the Hough-like transformation with the voting for the most probable λ and z_0 parameters of the trajectory. Hits, which comply determined λ and z_0 requirements are assigned to the track.

5.2.4. Tracks' Combination and Quality Estimations

In order to provide the complete trajectories, the complementary reconstructed tracks from the global finder and segments from the local finder are combined into the same pattern [63]. Thus, longer track trajectories can be restored, leading to more efficient determination of the track's kinematic parameters as well as particle type hypothesis.

On the other hand, imperfect trajectories with holes, wrong hits or kinks and wrong starting kinematic parameters cause faults during the fitting procedure. Thus, the utilities to check the track quality are involved into the CDC pattern recognition chain [63].

6. Legendre-Based Pattern Recognition

In this chapter discussion on the Legendre-based pattern recognition is given. The method focuses on the determination of the circular patterns of hits with the further estimation of the trajectory parameters. This global pattern recognition technique considers axial CDC hits and builds tracks, which are coming from the IP (so-called **prompt tracks**). It will be shown that the method with its features is able to reconstruct **non-prompt tracks** (tracks which can't be extrapolated to the IP) with high efficiency.

6.1. Main Idea of the Legendre-Based Method

Hits in CDC can be geometrically represented as circles with the center at the fired sense wire and radius which is equal to the hit drift length (see Fig. 5.2b). It is not possible to reconstruct exact hit position before the pattern recognition procedure, since the incident angle of the particle to the CDC cell is unknown. Moreover, z-component of CDC hits is also couldn't be measured before the combination of axial and stereo hits. While axial wires are parallel to the z axis and the projection of an axial hit onto xy plane does not depend on its z production position, stereo hits need the information about z production position to properly extract xy information. Due to this fact, only axial hits are taken into account in the method, as stereo hits can not provide a suitable information. Thus, only the xy projection of CDC hits is considered, and as result particle trajectories are reconstructed as 2-D circles (more details on the trajectory parametrization are in section 6.1.3).

In case of the Belle II detector, charged particles in presence of the magnetic field leave circular patterns of hits in CDC. Most of the charged particles come from the interaction point, meaning that all tracks are sharing the same production point (in some approximation). These facts allow to apply the conformal mapping, which transform all circles sharing the same point (namely origin) into straight lines. In this case the problem of pattern recognition reduces to the problem of straight lines detection. Furthermore, a particle trajectory is always tangential to the drift circles it induced, and this rule is true as well in a conformal mapped space, where trajectory is represented as a straight line. As

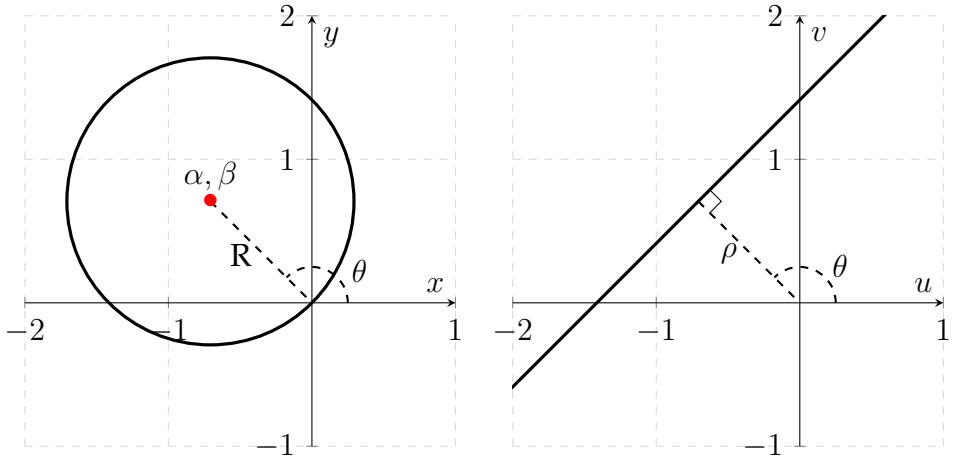

(a) Circle in real space

(b) Transformed circle in the conformal space

Figure 6.1.: An example of the conformal mapping of the circle, which passes through the origin, by the transformation $w = 1/\overline{z}$

it was described in the section 4.1.2, Legendre-based track finding is aimed to find **common tangents** to the set of drift circles. With this method it is possible to detect trajectories in the conformal space and distinguish patterns of hits, created by the same particle.

6.1.1. Conformal Mapping

The conformal mapping [64] is widely used in pattern recognition approaches in case of barrel tracking detectors placed in a longitudinal magnetic field. It is used to reduce the problem of circular trajectories detection to the problem of linear trajectories detection. The method considers domain plane as a complex plane.

A circle can be represented with the next equation:

$$(x - x_0)^2 + (y - y_0)^2 = R^2 \tag{6.1}$$

In the complex plane it's possible to represent a circle equation in the next form [65]:

$$|z - \gamma|^2 = R^2 \tag{6.2}$$

where $z = x + iy$ is points on a complex plane which form the circumference of the circle of radius R around the center $\gamma = \alpha + i\beta$. The equation 6.2 can be written in the next form

$$z\overline{z} - \gamma\overline{z} - \overline{\gamma}z + \gamma\overline{\gamma} - \rho^2 = 0. \tag{6.3}$$

By multiplication of 6.3 by a real constant A, one can get an equation for a generalized line:

$$Az\overline{z} + Bz + C\overline{z} + D = 0. \tag{6.4}$$

where A and D are real numbers, B and C are conjugate complex numbers. Equation 6.1 represents a circle in a case $A \neq 0$, and $B = -A\overline{\gamma}$, $C = -A\gamma$, $D = A(\gamma\overline{\gamma} - R^2)$.

Trigonometrical Representation of a Line

The point belonging to the complex plane could be represented in the trigonometrical form with polar coordinates (r, ϕ):

$$z = r\left(\cos\phi + i\sin\phi\right) \tag{6.5}$$

Therefore, center of the circle, γ, could be represented as

$$\gamma = R\cos\theta + iR\sin\theta \tag{6.6}$$

where θ is a polar angle of γ. By expressing equation 6.13 in terms of the trigonometric parameters of the center of the circle, one can get a trigonometric equation of a circle, mapped in the inverse conformal space:

$$\frac{\rho}{2} = u\cos\theta + v\sin\theta \tag{6.7}$$

where $\rho = 1/R$ is a curvature of the circle.

Conformal Mapping

A complex analytic function

$$w = g(z) \tag{6.8}$$

which transforms a point $z = x + iy$ belonging to the domain $\Omega \subset \mathbb{C}$ to a point $w = u + iv$ belonging to the domain $D = g(\Omega) \subset \mathbb{C}$. The mapping 6.8 required to be one-to-one, so each point $w \in D$ has unique corresponding point $z \in \Omega$. As result an analytic function $z = g^{-1}(w)$ is a map from D to Ω, and analytic on all of D. The derivative of the inverse function has form

$$\frac{d}{dw}g^{-1}(w) = \frac{1}{g'(z)} \tag{6.9}$$

thus the derivative of $g(z)$ must be nonzero in order to keep $g^{-1}(w)$ differentiable:

$$g'(z) \neq 0,\ z \in \Omega \tag{6.10}$$

The inversion of the complex plane could be defined as

$$w = \frac{1}{\overline{z}}; \quad \text{or} \quad u = \frac{x}{x^2 + y^2},\ v = \frac{y}{x^2 + y^2} \tag{6.11}$$

(add expressions in u,v coordinates) Applying this mapping to transform a generalized circle (6.4) one will get the next equation for the generalized circle in the conformal mapped space:

$$Dw\overline{w} + C\overline{w} + Bw + A = 0 \tag{6.12}$$

In the special case, when the circle passes through the origin (see Fig. 6.1a) by satisfying the exact equality $\gamma\overline{\gamma} = R^2$ (the coefficient $D = 0$), so (6.12) reduces to the equation of a line

$$C\overline{w} + Bw + A = 0 \tag{6.13}$$

or in the representation of (u, v) coordinates

$$2\alpha u + 2\beta v = 1. \tag{6.14}$$

6.1.2. Parametrization of the Legendre Space

According to the equations 4.8, the equation of a tangent to a drift circle has a form of

$$r = x_0 \cos\theta + y_0 \sin\theta \pm R_{dr}. \tag{6.15}$$

Each possible tangent to the mapped drift circle $(x_0, y_0; R_{dr})$ with the parameters (r, θ) represents a possible circular track's trajectory with the radius R and the center of (α, β). The parameters of the circular trajectory are related to parameters of the tangent as following:

$$\begin{aligned} R &= 1/\rho \\ \alpha &= R\cos\theta \\ \beta &= R\sin\theta \end{aligned} \tag{6.16}$$

As it has been shown, the conformal mapping 6.11 transforms the circle 6.1 into a line 6.7. In case of the Legendre tracking, the main goal is to find an equation of the common tangent to the pattern of drift circles in the conformal mapped space, with the following restoration of the corresponding circular trajectory. To make a conformal mapping compatible with the Legendre tracking method, the transformation 6.11 should have the next form:

$$w = \frac{2}{\overline{z}}; \quad \text{or} \quad u = \frac{2x}{x^2 + y^2},\ v = \frac{2y}{x^2 + y^2} \tag{6.17}$$

so the equation of the mapped circle 6.7 will be

$$\rho = u\cos\theta + v\sin\theta \tag{6.18}$$

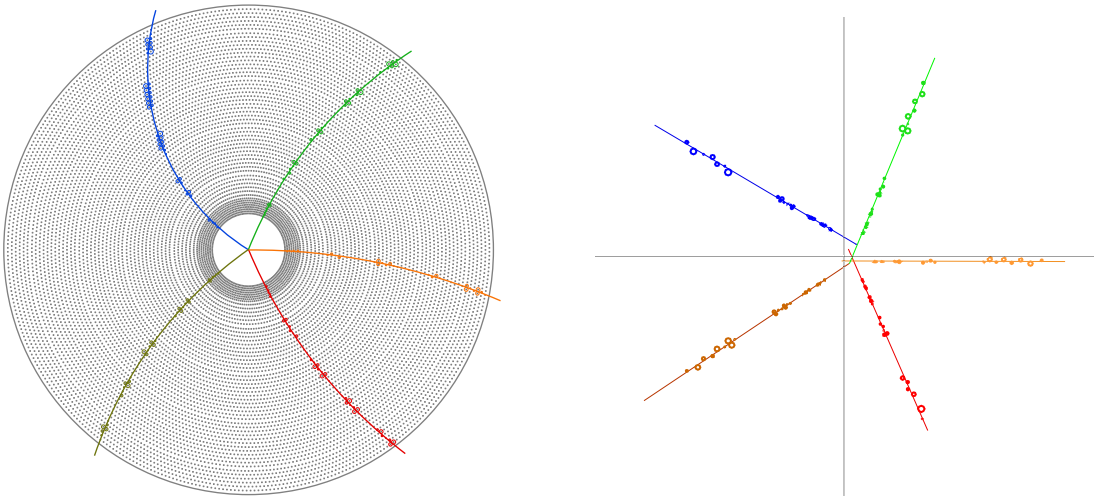

(a) $x-y$ projection of the CDC with 5 simulated tracks

(b) Simulated tracks after the conformal mapping

Figure 6.2.: An example of the conformal mapping of simulated event

which is consistent with the equation of tangent 6.15.

Since the Legendre transformation is based on finding of the common tangent to drift circles, the conformal mapping rules for the hits should be introduced. A drift circle could be parametrized with a standard circle equation

$$(x - x_0)^2 + (y - y_0)^2 = R_{dr}^2 \tag{6.19}$$

where (x_0, y_0) is the $x - y$ projection of the wire, and R_{dr} is the drift length. By applying conformal mapping 6.17, the conformal mapping rule for the drift circle can be obtained:

$$\begin{aligned} u_0 &= \frac{2x_0}{x_0^2 + y_0^2 - R_{dr}^2} \\ v_0 &= \frac{2y_0}{x_0^2 + y_0^2 - R_{dr}^2} \\ \tilde{R}_{dr} &= \frac{2R_{dr}}{x_0^2 + y_0^2 - R_{dr}^2} \end{aligned} \tag{6.20}$$

where (u_0, v_0) is the center of the mapped drift circle, $\tilde{R}_{dr}$ is the radius of the mapped drift circle. An example of the conformal mapping of the simulated event with 5 $\mu^{\pm}$ is shown in Fig. 6.2. Each pattern of hits in conformal space shares a common tangent to mapped drift circles.

6.1.3. Geometrical Representation of Tracks

The method uses 2-D representation of the track trajectories. Definition of the parameters are shown in Fig. 6.3. The interaction point is located at $(0; 0)$, while

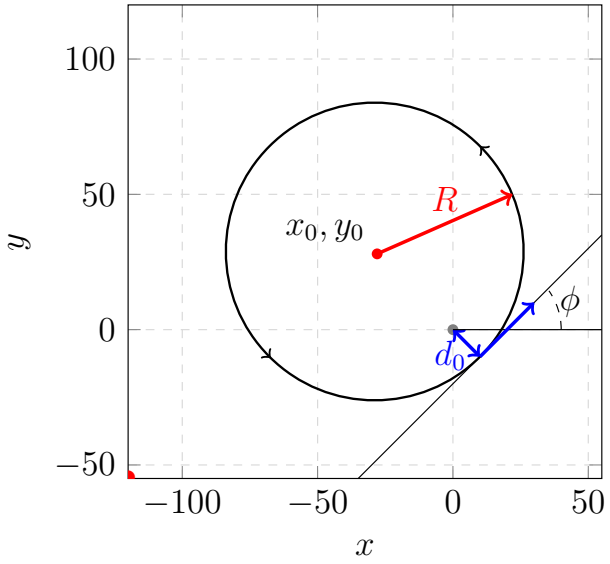

Figure 6.3.: A schematic representation of the track's trajectory

the center of the circle at $(x_0; y_0)$. The circle could be parametrized with using the following parameters [66]:

- R - is the radius of the track. It is connected to the curvature of the circle as $\rho = 1/R$.
- d_0 - distance of the closest approach of the circle to IP (distance to the perigee).
- ϕ - direction of the circle propagation at the perigee

Using this representation other parameters of the circle could be obtained. For example, the perigee position can be calculated as

$$\begin{aligned} x_{d_0} &= d_0 \sin\phi \\ y_{d_0} &= -d_0 \cos\phi \end{aligned} \tag{6.21}$$

The method has two kinds of trajectory determination: in comformal mapped space and in real space. In case of conformal mapped space all trajectories have $d_0 = 0$, since the conformal mapping assumes that trajectory passes through the origin, and as result only R and ϕ parameters are estimated. On the other hand, in real space trajectories are fitted using all available hits information with freed d_0 parameter, so at this point tracks could be separated to **prompt** and **non-prompt** tracks, based on the d_0.

6.2. Track Detection

It is possible to reduce the problem of the Legendre-based global pattern recognition to the problem of the identification of the most populated regions in the Legendre space. This task can not be solved analytically within the reasonable amount of time, dedicated to the event processing. Another option is to build discrete 2-D grid in the Legendre space and estimate density of hits in each cell. This leads to the histogramming method, which consists in filling of the 2-D histogram in the Legendre space with the transformed hits. In other words, each hit effectively contributes to the histogram by incrementing content of the bins to which it belongs.

There are few approaches of lookup of dense regions in 2-D space by filling histograms. The most conventional approach consists in splitting of the plane into $m \times k$ bins and filling each bin individually with appropriate entries. Tthis approach requires of check of all hits in the event for the consistency with all bin in histogram. Lets assume n hits in the event, and square matrix of size $m \times m$. Then, the time complexity will be $\mathcal{O}(n * m^2)$.

Another option is to use fast 2-D binary search, which consists in consecutive splitting of the plane into 4 bins. This approach is used in Fast Hough algorithm [57], and it takes into account regions on the plane, which are most likely contain the searched point. On the each iteration the most populated bin is selected and the next splitting applied to it. Assuming that there are l consequetive operations of splitting, the time complexity will be $\mathcal{O}(n * l * log(l^2))$. Thus, the most efficient way to determine most dense regions in the Legendre space is to use 2-D binary search.

6.2.1. 2-Dimensional Binary Search

Considering the problem of dense regions lookup, a 2-dimensional binary search can be effectively used as a tool to find the sinograms intersections. The 2-dimensional binary search can answer the question, how many of the Legendre transformed hits are in the given region, by splitting the selected region into 4 bins and checking how many hits crosses the bins boundaries. As it was mentioned, it is an iterative procedure, meaning that at each iteration the size of the examined plane reduces by a factor 4. At each iteration of the search, numbers of hits which belong to each of 4 bins are collected, and the most populated bin is considered for the next iteration. However, if the search do not succeed with the selected bin, the next most populated bin is considered. It means, that search do not start over again in case of the rejection of some of the bins, but proceed by considering other regions of the Legendre plane.

An example of 2-D binary search in Legendre plane is shown in Fig. 6.4. The whole Legendre space is divided into 4 bins, and number of hits which belong

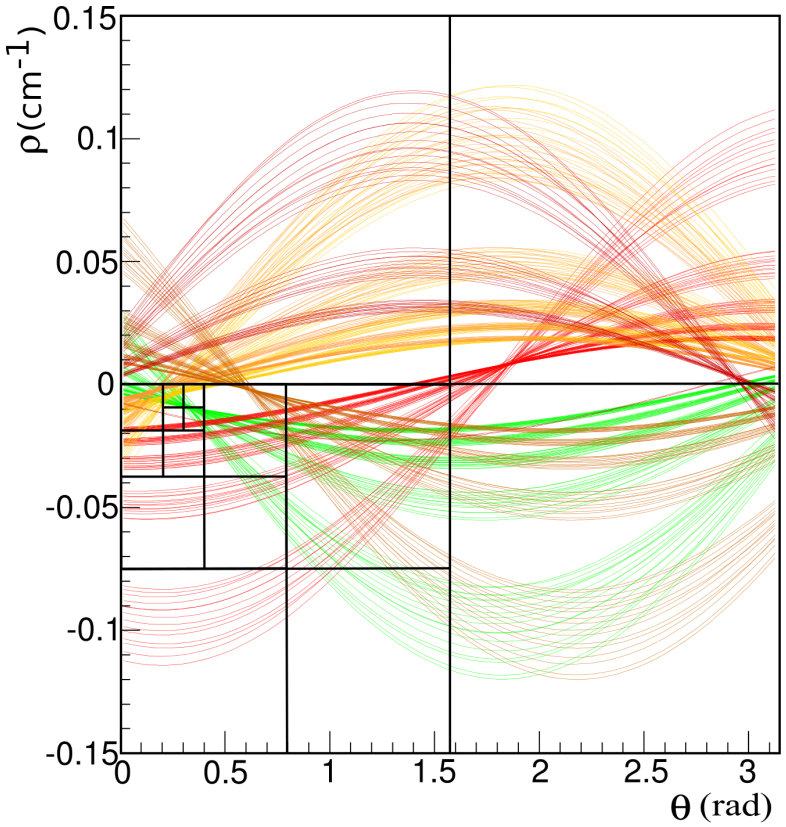

Figure 6.4.: An example of the simulated $B\bar{B}$ event with 6 tracks in the Legendre plane. 2-dimensional binary search is performed toward the possible track candidate

to each of the bin is accumulated. Then, the most populated bin is assumed to contain a track candidate and checked to satisfy the search criteria. In case it passes all conditions, it is splitted into 4 bin further. This search is performed until the lowermost level is reached or selected bin is rejected. In case of rejection, other bins at upper level are considered in the search. Such algorithm allows to cover the whole phase space, but takes into account only regions which are interested from point of view of the Legendre algorithm (i.e. regions with a high hits density).

6.2.2. QuadTree Data Structure

A QuadTree is a hierarchical data structure, in which each node has four children linked to it. It can be used to perform and to store results of the 2-D binary search, and to reuse them. The scheme of the tree is shown in Fig. 6.5. In general, in case all branches are decompounded down to the level lvl, the total number

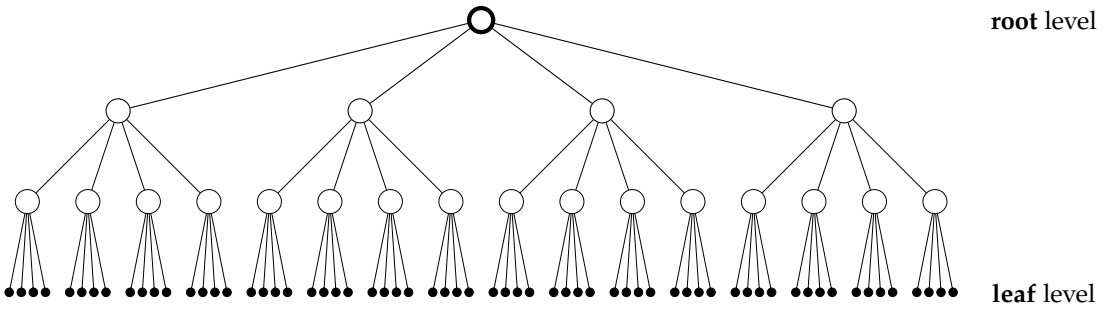

Figure 6.5.: QuadTree scheme

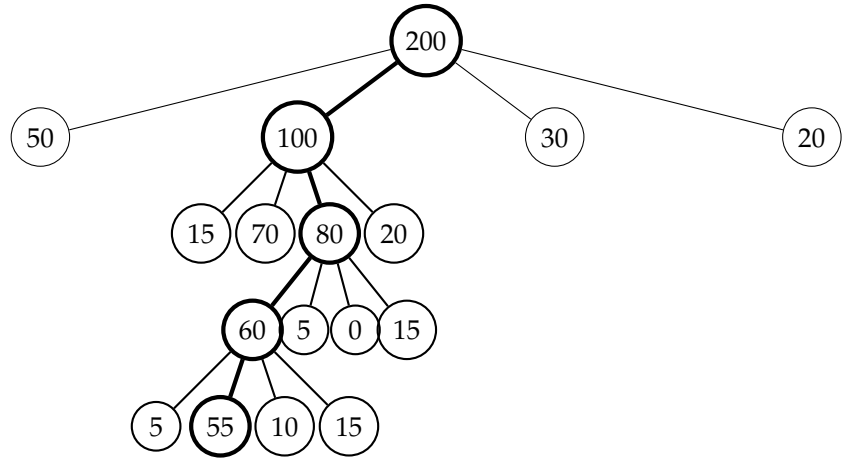

Figure 6.6.: QuadTree lookup scheme. Each circle represent a QuadTree node, with the number of entries in it. Subdivision of the nodes are preformed for the most populated node.

of the nodes in the QuadTree can be calculated as

$$n = \frac{1 - r^{lvl}}{1 - r}, \tag{6.22}$$

which is the sum of the geometric series, with common ratio r (for QuadTree $r = 4$ and is exactly the number of the children of each node).

A QuadTree structure can be efficiently applied for the fast lookup in the 2-dimensional space by following some given selection rules. An example of the QuadTree lookup is shown in Fig. 6.6. At each level bin with the most contribution (containing most of hits at the level) is investigated and in case it meet requirements of the search, the tree examination proceeds to its children until the lowermost level is reached. This algorithm do not require to fill the whole tree, bit it considers only the nodes which are of interest for the track finding. In best case, when none of the bins are discarded, the number of created QuadTree nodes will be

$$n = 4 \cdot lvl \cdot N_{trk}, \tag{6.23}$$

where N_{trk} is a number of found track candidates. In this case, each branch of the QuadTree will reach the lowermost leaf level, and result in a track candidate.

The QuadTree allows to incorporate search criteria, which will allow to accept or reject nodes during the binary search. The partly filled QuadTree can be reused among separate iterations of the tracks search with different search criteria, leading to introduction of the track search passes, which will be defined later in Sec. 6.4.3.

6.3. Features of the QuadTree

The QuadTree mainly plays a role of the object which handles information about the hits, but it also incorporate algorithm which performs 2-D binary search. The rules and conditions of the binary search can be configured by introducing various features into QuadTree implementation. There are two main way to configure the QuadTree: to define the bin splitting rule and to define the QuadTree deepness.

The standard way to split the plane during the binary search is to create 4 equal bins (see Fig. 6.4). But for the lower levels of the search, when distortion of the impact region is comparable with the size of the node, the splitting should be changed to take into account imperfections of the trajectories. Another way to take into account trajectories distortions and smearing of the sinograms intersections is to introduce criteria on the deepness of the binary search.

In this section discussion on the implemented features of the QuadTree is given.

6.3.1. Imperfect Tracks Detection

As it has been defined in Sec. 6.1.3, tracks in the CDC can be divided into two groups based on the impact parameter of the track. The distance of the closest approach, d_0, has a valuable influence on the representation of the track in the Legendre space. In case of $d_0 \to 0$, the sinograms intersections would be more localized compared to the tracks with a high d_0 (non-prompt tracks). Thus, in order to achieve efficient track finding, effect of the intersections smearing should be taken into account.

Non-prompt tracks can be reconstructed using a segment of the track. A trajectory of the non-prompt track could be partly approximated by the prompt circle (see Fig. 6.7) with some precision level. Thus, by setting the acceptable uncertainty of the approximation, it is possible to detect a segment of the non-prompt track. The detected segment can be restored to the whole track by extrapolation of the trajectory and assigning missing hits.

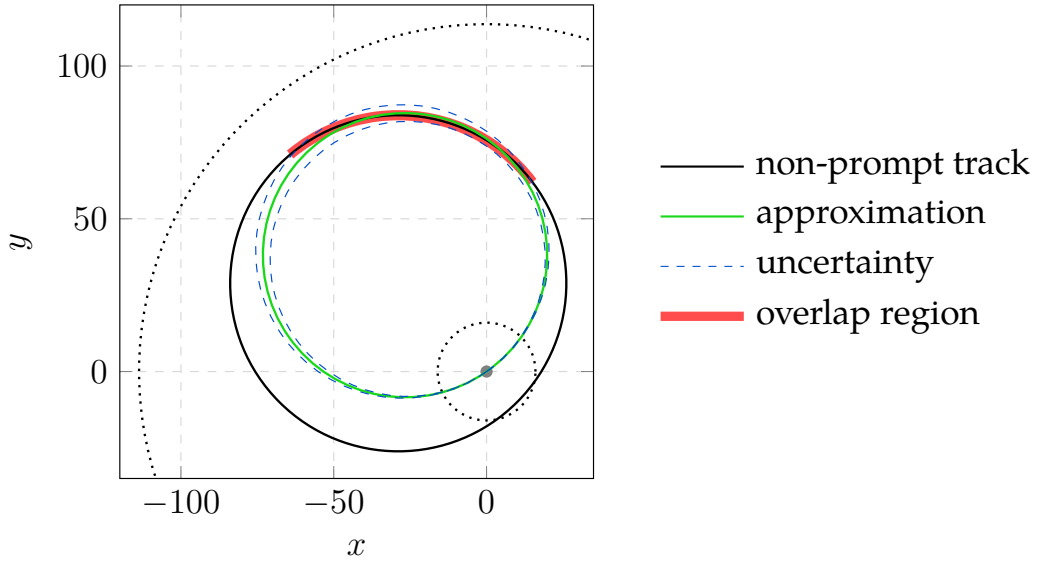

Figure 6.7.: An example of the non-prompt trajectory partial approximation with the prompt circle. The parameters of the approximation circle depend on the overlap region of the non-prompt trajectory

The tracks with a high energy losses also appears to be smeared in the Legendre space. This effect can be taken into account by setting the desired resolution on the leaf QuadTree nodes. Also, heavily smeared tracks in Legendre space can be splitted by the bin boundaries during binary search. To avoid this effect, the custom bin splitting procedure is implemented.

6.3.2. Resolution of QuadTree

As it was discussed, the QuadTree track finding is performed until it reaches the leaf level (the lowermost level of the QuadTree). There are two approaches of the leaf level definition - by defining the fixed deepness of the tree and by defining the desired resolution of the leafs. The fixed deepness of the tree implies filling the QuadTree down to the some predefined level, which is the same for the whole phase space, whereas resolution could be defined as a sophisticated function. Both approaches in some sense are equal, since the resolution of the node is the inverse to the level of the node in case of the standard (equal) splitting of the bins. A fixed deepness of the tree sets limitations on the nodes splitting strategy and is suitable for the simplified track finding. In case of non-standard bin splitting (e.g., total area of children nodes is not equal to area of the parent node) the area, which the each leaf node covers, is different for the same QuadTree depth and depends on the bin splitting definition.

The most natural way to define a resolution function is to make it dependent on the curvature ρ of the track candidate. The , whereas curvature ρ is a param-

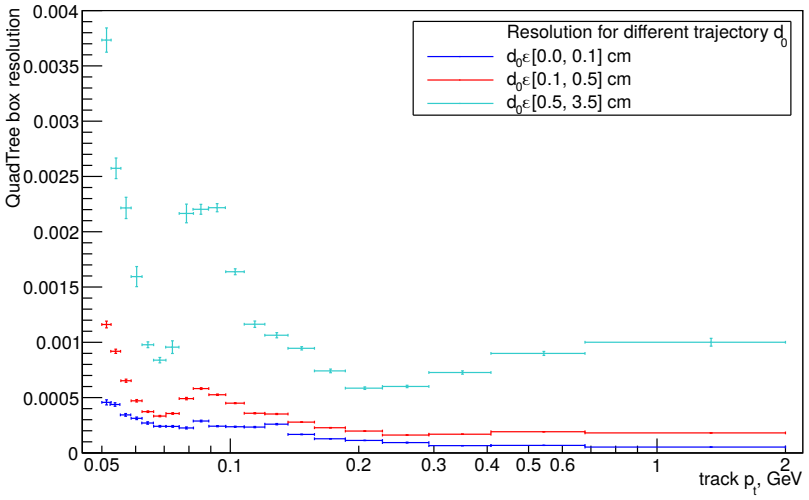

Figure 6.8.: Resolution curve

eter of the QuadTree and uncertainty of the trajectory curvature is inversed.

$$\rho = \frac{1}{R} \tag{6.24}$$

This allows to take into account smearing of the track in the Legendre space due to the energy losses of the charged particle. The smearing of the non-prompt tracks also could be taken into account by a resolution function, but this effect is more significant compared to the energy losses. Since the Legendre space is dependent on the ρ and θ of the track, and d_0 variable is not accessible within QuadTree search, it's reasonable to introduce different ρ-dependent resolution functions for the different d_0 factors.

The resolution curves are estimated using Monte Carlo simulations with a Particle Gun generator, which allows to tune the parameters of the generated track, such as p_t and d_0 which are in interest of the resolution studies. The resolution is estimated in Legendre space by adjusting the boundaries of a single QuadTree node, with which 80% of hits belong to the single node. Fig. 6.8 shows the resolution estimation for tracks with different distance of the closest approach.

6.3.3. Bins Splitting

An introduction of the resolution functions brings a possibility to apply non-standard splitting of bins. Since the most of tracks in the Legendre space are affected by a smearing around the true parameters spot of the track, a possibility

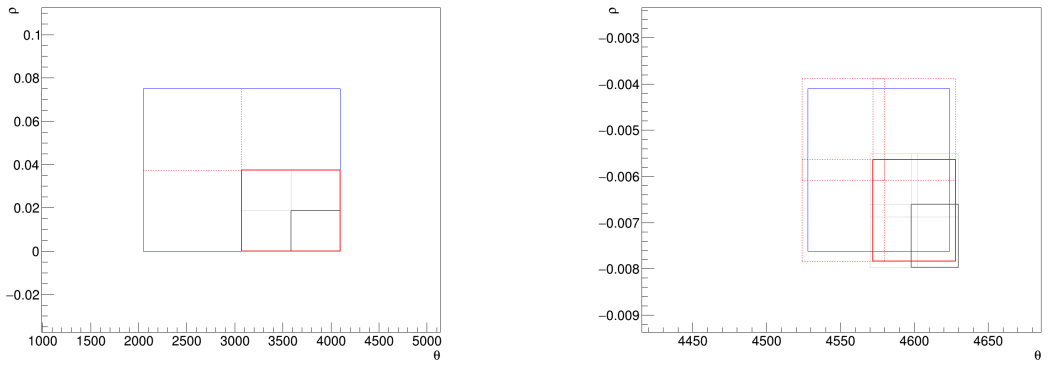

(a) Normal binning (lvl=2)

(b) Bins overlapping (lvl=12)

Figure 6.9.: An example of the bins overlapping

of track splitting among two neighboring nodes exists. The significance of this effect could be reduced by allowing the neighboring bins to overlap.

Overlapping of bins are defined as following: the boundaries of the each child node are extended by 25%, and the new extended boundaries are used the check of impact of hits with the child node. This allows to suppress losses of hits due to smearing of the intersection region.

Another improvement comes in case of wrong selection of the QuadTree evolution path: at the uppermost level track candidates with the near parameters can effectively contribute to the neighboring node by increasing number of hits in it. In case of the further evolution of the QuadTree to the lowermost levels, the spread of sinograms in Legendre space would lead to reconstruction of the segment of the track candidate and losing other hits. By applying overlapping of bins, all hits which can effectively contribute to the track candidate would be collected by the investigated node.

Sliding Bins

Overlapping of bins introduces an another effect to the evolution of the QuadTree structure. The new node boundaries are used for the subsequent children creation, which means that position of the children nodes will be shifted compared to the standard binning without extending the boundaries. An example of this effect is shown in Fig. 6.10. The children nodes (red boxes) are displaced compared to the standard QuadTree grid and tend to follow to the most dense region in the Legendre space.

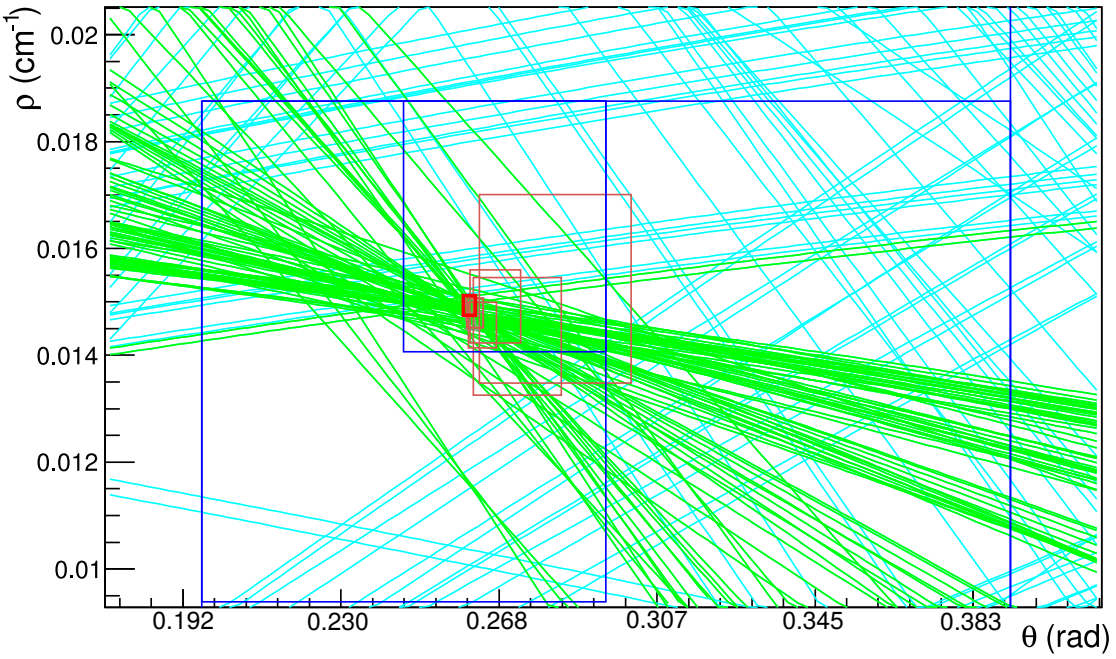

Figure 6.10.: "Sliding bins" example

6.4. Event Processing

The QuadTree is used as a core tool to find track candidates. The binary search, which QuadTree performs, is configured with various criteria. During the search, curvature of the trajectory, number of hits in the possible candidate and resolution of the nodes are checked. If the search reaches the desired resolution and satisfy all trajectory criteria, a **track candidate** is created.

Each new track candidate is fitted with a fast circular fit, and extended with new hits, which are consistent with its trajectory. There are two kinds of hits assignment: based on the distance from the hit to the trajectory, and based on the custom conformal transformation.

Specifics of the track detection and event processing are given in the following subsections.

6.4.1. Track-by-Track Finding

In the method, the track-by-track finding approach is used. It implies reconstruction of the track candidates which takes as much correct hits as possible. This can be done by processing of each event multiple times with different search criteria and excluding used hits after each iteration of the search. The search is performed with different conditions for the possible track candidates, so each iteration is focused on the specific kind of tracks.

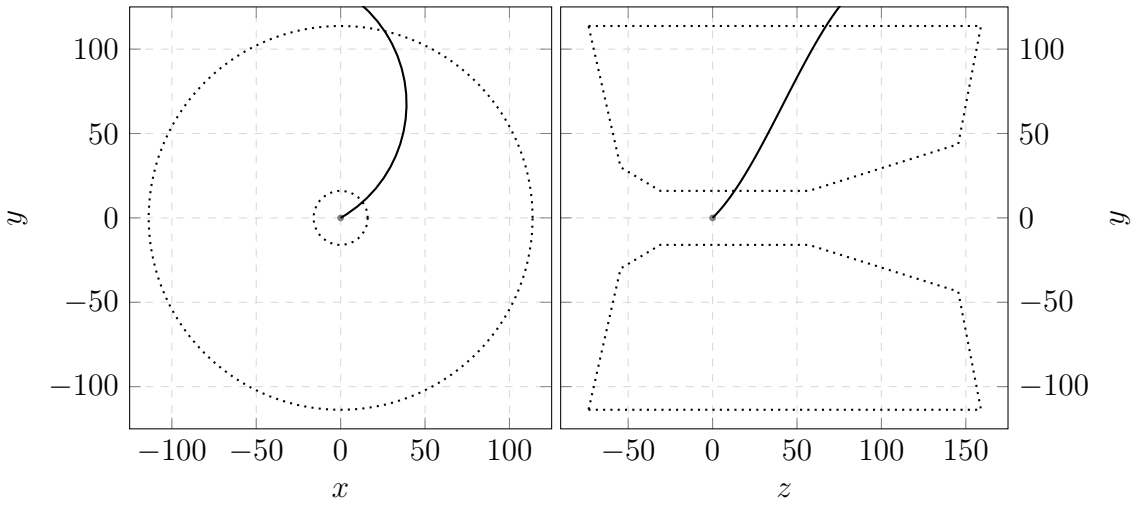

(a) High-p_t track

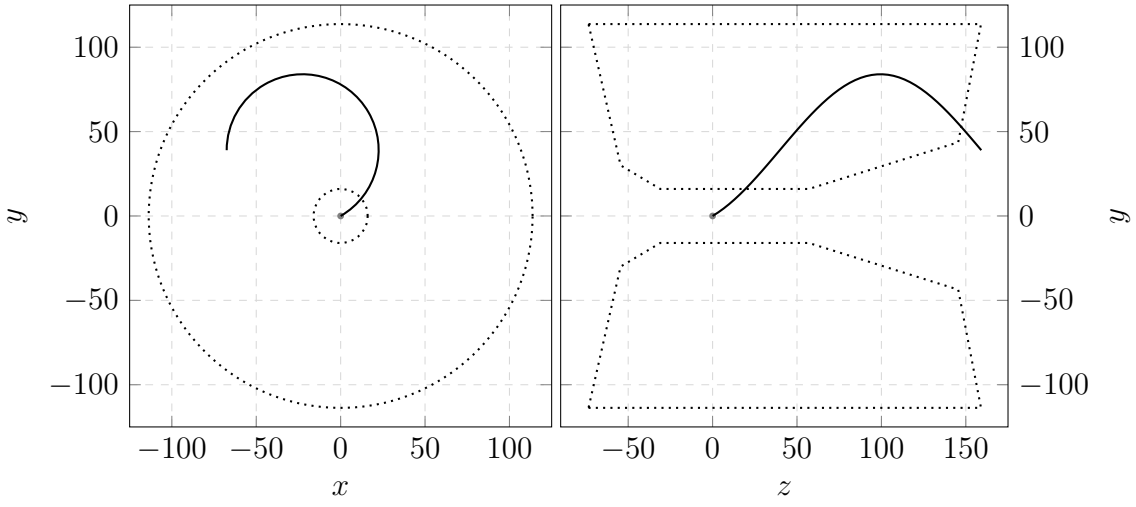

(b) Curling track

Figure 6.11.: An example of tracks in CDC.

Curvature Threshold

Two regions of the trajectory curvatures are defined: curling tracks and non-curling tracks. As it shown in Fig. 6.11, the tracks which do not reach the outer wall of CDC could pass through the CDC volume and try to reach the interaction region. Moreover, curling tracks are more affected by energy losses in the detector volume. Thus, the number of hits and distortion of the trajectory are different for curling and non-curling tracks.

In order to increase the performance of the track finder, the search procedure is divided into two steps: lookup of high-p_t tracks, which are assumed to be in better agreement with the defined track model and as result are "perfect" from point of view of the pattern recognition, and lookup of curling tracks, which are more affected by different kind of the trajectory distortion. Thus, by storing the ideal tracks at the first steps of track finding, the probability of misreconstruction is decreased.

Number of Hits Threshold

Number of hits in the hits pattern is proportional to the length of the particle's path in the detector volume. The path's length also depends on the kinematic parameters of the particle, as it shown in Fig. 6.11. The high-pt tracks with $\theta \in (\approx 30^o; \approx 130^o)$ will traverse through the whole CDC volume and will leave at least one hit in each CDC layer and two hits in most cases. Thus, for high-pt tracks tight cut on the number of hits could be chosen as ≈ 50 and loosen to ≈ 30. For the curling tracks tight cut must be increased to take into account hits in the outgoing arm of the trajectory and has been chosen as ≈ 70 hits.

6.4.2. Legendre Space Definition

CDC hits in the Legendre space have form of a sinusoid curve (see eq. 6.25), and are being limited in the ρ direction by the amplitude of the sine wave (which is determined by the conformal coordinates $(x'; y')$ of the hit). The period of the sine wave is the same for all hits and is exactly 2π. Taking into account these properties, it is possible to set the boundaries for the Legendre space.

The equation (4.8) could be represented in the next form:

$$\begin{cases} \rho = \sqrt{\tilde{x_0}^2 + \tilde{y_0}^2}\ \sin(\theta + \lambda) + R \\ \rho = \sqrt{\tilde{x_0}^2 + \tilde{y_0}2}\ \sin(\theta + \lambda) - R \end{cases} \tag{6.25}$$

where $tg\lambda = \frac{\tilde{x_0}}{\tilde{y_0}}$. The amplitude $\sqrt{\tilde{x_0}^2 + \tilde{y_0}^2}$ of the sine wave defines the boundaries of the ρ variable in the Legendre space. In the conformal space (after applying transformation (6.20)) CDC hits from outermost layers would be closer

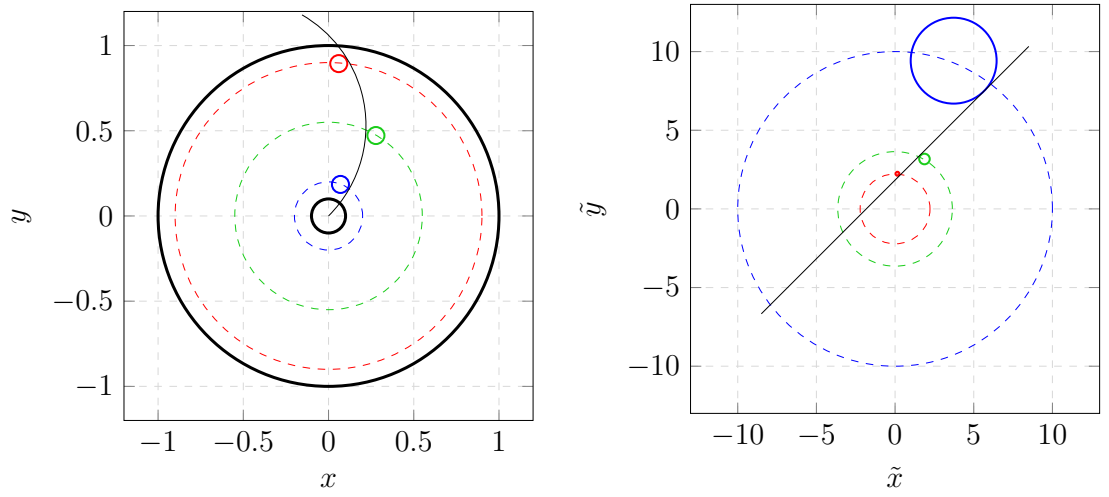

(a) Hits in real space

(b) Hits after the conformal transform

Figure 6.12.: An example the conformal transformation. Hits in real space and in the conformal space have the same color.

to the origin of the space than hits from the innermost CDC layer (Fig. 6.12). Thus, the distance to the innermost CDC hits defines the upper limit on the track's curvature ρ. Taking into account that inner radius of the CDC is 16 cm, we get

$$\rho_{max} = 0.125 \text{ cm}^{-1} \tag{6.26}$$

6.4.3. Passes Definition

In the Legendre space representation of the hits pattern of the same track vary depending on the parameters of the track. Number of hits belonging to the track candidate is strongly depends on the kinematic parameters of the track. For example, for track with low momentum and do not reaching the outer parts of the detector, the number of the produced hits is much higher than for the high-p_t tracks which are likely absorbed by the ECL or leaving the detecting parts of the detector (in case of μ). Another effect arise for non-ideal tracks (from point of view of the pattern recognition) and consists in delocalization of intersections of the sinograms of hits in the Legendre space.

The track finding procedure performed in three stages (so-called **passes**), each of them mainly focused on the specific kinds of track candidates. Together with track-by-track tracking approach the method produces tracks with high hit assignment efficiency (most of the hits produced by the same particle reconstructed within the same pattern) and relatively low fake rate. The weak point of the method is tracks with kinks and long tracks, resulting in increased clone

	curvature threshold		hits threshold		resolution function
	start	stop	tight	loose	
Non-curlers		0.005	50	25	fine
Curlers	0.007	0.15	70	30	rough
Full range		0.15	30	10	rough
Ideal high-pt tracks		0.005		50	fine
Ideal curling tracks		0.07		50	fine

Table 6.1.: Definition of the track finding passes.

rate.

The general definition of the passes is shown in Table. 6.1. Each pass has its own tight and loose cut on the number of hits in the pattern, start and stop value for the trajectory curvature and QuadTree resolution function. Within each pass, track finding is performed with the given cut on the number of hits within defined curvature region, and all possible candidates stored. For the next iteration of the track finding within the pass, the hits threshold is lowered by a factor 0.75, until it reaches the loose cut on the number of hits. Then, the curvature boundaries are extended (by a factor 2) in case such possibility is defined.

Non-curlers pass has cuts, which are optimized for the high-p_t tracks finding. **Curlers** pass covers the whole p_t (curvature) ranges and has tight initial cut on the number of hits, leading to efficient determination of the long tracks. **Full range** pass is used to collect the remnants, short tracks and/or tracks segments. Also, there are two special track finding steps, performing **Ideal high-p_t tracks** and **Ideal curling tracks** finding, both of them runs before the each pass. Ideal high-p_t tracks finding has the cut on the number of hits, which corresponds to the ideal case of the non-curling track, when it traverse the whole CDC, and has curvature $\rho > 2/r_{CDC}$. Ideal curling tracks finding has the cut on the curvature $\rho < 4/r_{CDC}$, corresponding to the tracks which reach fifth CDC superlayer and curling back in the direction of origin, leaving a full circular patter of hits in the CDC.

6.4.4. Fast Track Fitting

The found track candidates are fitted using Kärimaki fitter [58]. The fitter is able to restore trajectory of the prompt and non-prompt track candidates by calculation the parameters of the circle. The fitter couldn't take into account multiple scatterings and energy losses of the charged particle but performs fast non-iterative fitting. The advantage of using fast circular fitter in comparison

to the output of the QuadTree search (which is also providing parameters of the track candidate) is that it is able to restore trajectories of the non-prompt tracks.

In case of the non-prompt track or false positive hits assignment, determination of the d_0 is important on a par with the ρ and θ. Then, new hits could be assigned to the extrapolated trajectory in conformal and real space.

6.4.5. Conformal-Based Hits Assignment

The smearing of the tracks in the Legendre space (due to the energy losses, multiple scatterings and non-promptness of the track) leads to the lowered hit efficiency and splitting of the track into few segments. There are two approaches of the assignment of the missing hits implemented: assignment based on the distance of the hit to the trajectory in real space and assignment of the missing hits in Legendre space (so-called **conformal-based hits assignment**). Both methods rely on the correctness of the determined trajectory of the founded track candidate.

The conformal-based hits assignment is a method which consists in defining of the new reference point of the conformal transformation as a point belonging to the trajectory of the track with further Legendre transformation. Fit of the reconstructed segment provide a correct averaged parameters of the trajectory. Taking a point on the averaged trajectory as a reference point of the conformal transformation leads to a better agreement of the hits pattern in conformal space with a straight line. Legendre transformation of the corrected conformal hits pattern appears to be localized as promt-like track compared to the default reference point (origin).

6.4.6. One Hit - One Track Relation

As we reconstruct track candidate, all hits which are possibly belong to the track are marked as **used** and not taken into account in the next iterations of the track finding. Thus, a hit could be assigned to the one track only. In case of removing of hits out from the track candidate, the released hits are marked as unused and could be considered during the upcoming iterations of the pattern recognition.

6.5. Tracks Postpocessing

Tracks which are found during the step-by-step track finding procedure with the QuadTree, are stored and used in the further postprocessing stage. The main purpose of the postprocessing is to improve the quality of the reconstructed

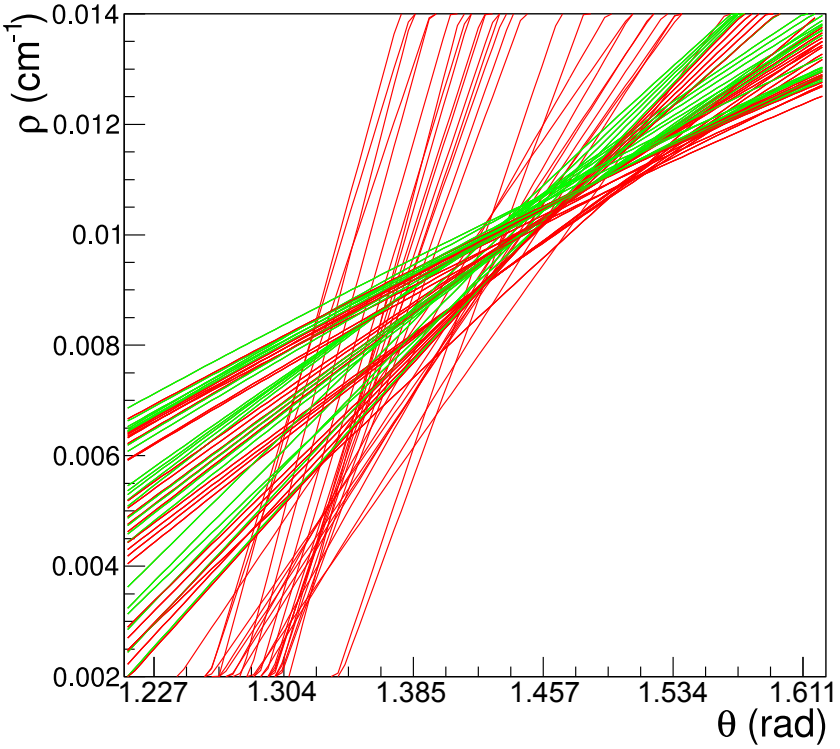

(a) Reference to (0; 0)

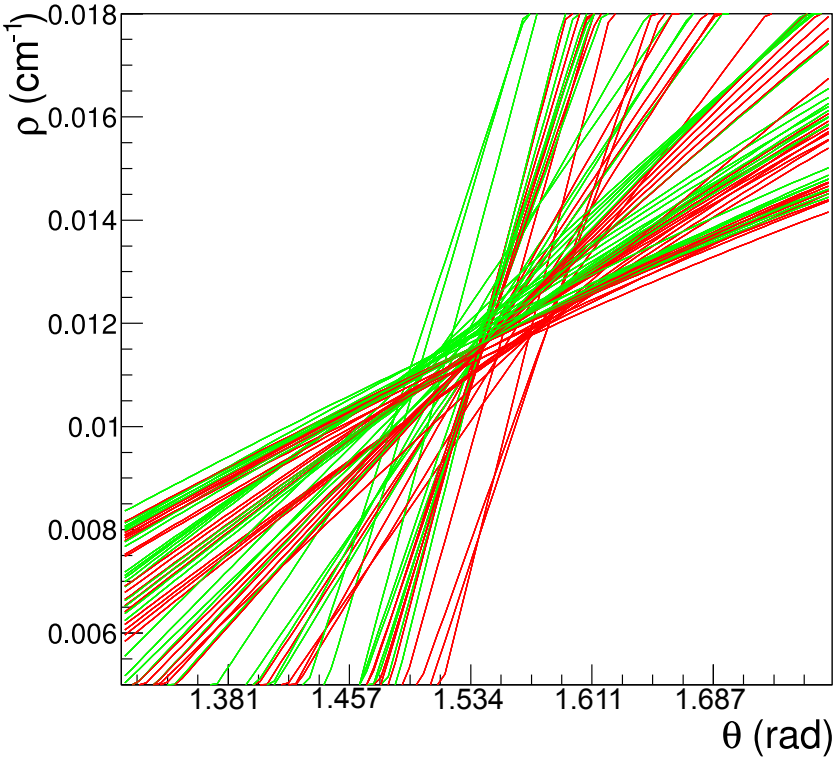

(b) Reference to POCA after the fitting

Figure 6.13.: CDC hits in the Legendre phase-space before (a) and after (b) conformal transformation with respect to a new reference point

event by checking the patterns of hits as well as the relations among tracks. The postpocessing could be grouped into three tasks: checks of the hits assignment to the trajectory, merging of the tracks, quality checks of the hits patterns.

6.5.1. Fitter-Based Merging

As it was mentioned, the global tracking approach may end up with the tracks splitted into segments. Beside to the restoration of the whole trajectory via its extrapolation and assignment of the matching hits, segment merging approach could be applied. In case of segments of track which couldn't be fitted properly and as result extrapolation gives wrong results, merging of the reconstructed segments provides reasonable reconstruction of the track and increase in the hits efficiency.

The general procedure is shown in Fig. 6.14. The list of tracks is sorted by the number of hits forming the track, so more complete tracks would be at the beginning of the list, and segments of tracks would be at the end. The track, which would be extended the merging ("merge into") is combined with the rest of the tracks in the list. The combination is performed in the following way:

- throw all hits of "merge into" and test tracks into the same pattern
- find the common circular track-like pattern of hits
  - fit the resulting pattern and get the common trajectory
  - remove hits which are not consistent with the trajectory (basing on the distance to the trajectory)
  - tighten the throw out criteria and repeat filtering out of hits
- if the final pattern of hits contains more hits than "merge into", tracks could be possibly merged
- the test track candidate marked as possible track to merge with, probability of merging is stored.

Probability of merging is estimated basing on the χ^2 criteria and is a quality criteria of the track, which will be discussed in Sec. 6.5.3. Using described procedure, the candidate to merge with the higher probability is marked as "the best candidate". "The best candidate" is tested for the compatibility with other tracks to assure that "the best candidate" has the only possibility to be merged in the "merge into". For this purpose "the best candidate" is attempted to merge with the other tracks resulting in "the best candidate for the best candidate". In case it is the same track as "merge into", it could be merged with "the best candidate", otherwise the procedure takes the next track to test merging possibilities.

Merging of tracks decreases the clone rate of tracks in the event as well as increases hit efficiency of tracks, providing more complete hits pattern.

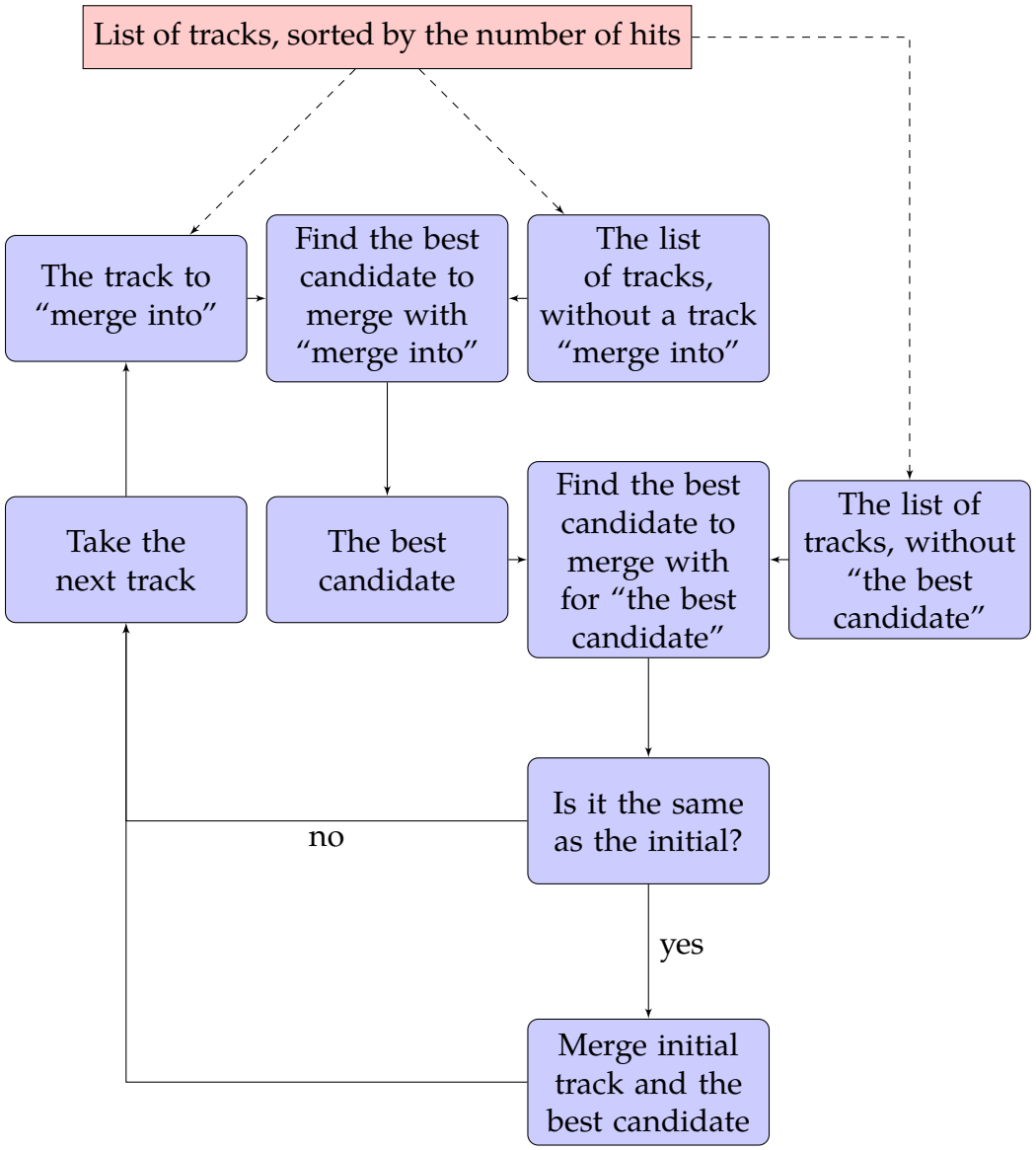

Figure 6.14.: The scheme of the tracks merging procedure.

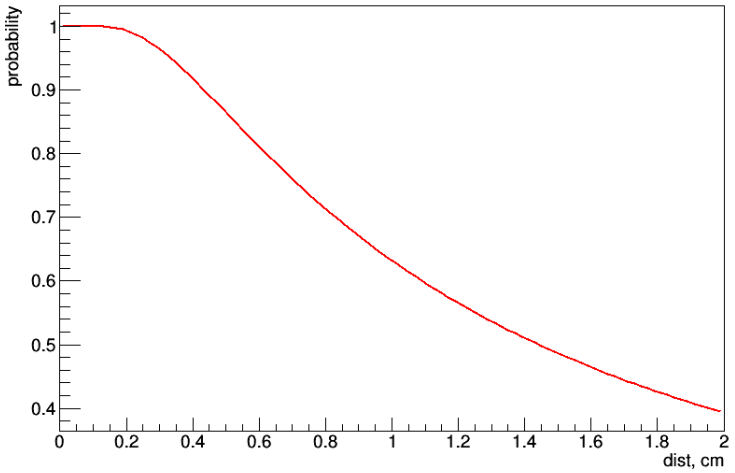

Figure 6.15.: The hits assignment probability

6.5.2. Hits Assignment Check

When tracks trajectories are defined, the procedure of hits reassignment is performed. It includes assignment of the new hits, removing of hits with do not satisfy assignment criteria, and reassignment of hits among the tracks in case the hit fits better to the pattern of another track. Each change of the pattern of hits accomplished by the update of the trajectory, so the next iteration is performed with the corrected track's parameters.

Hits Assignment The assignment of hits is based on the assignment probability. The assignment probability was estimated using the simulated events, and depends on the distance of the drift circle to the trajectory of the track (see Fig. 6.15). The hits with probability $> 80\%$ are assigned to the track candidate. Also, in case of the hits reassignment among concurring tracks, the hit is assigned to the track which has the higher probability.

Hits Removing The hits, which do not meet requirements on the minimal assignment probability are rejected form the track and marked as unused. This procedure is performed after each step of the trajectory update, so hits which are not in agreement with the trajectory would not take part in the following steps of the track evaluation.

6.5.3. Track Quality Check

The quality of the track is checked using global and local criteria. The global criteria implies check of the consistency of the hits pattern to the fitted trajectory, while the local criteria requires the continuity of the pattern of hits (without holes) along the whole trajectory. This basic checks are intended to prepare the track candidates for the next processing step, namely fitting with DAF and Kalman filter (see Sec. 4.2).

The global quality criteria is based on the check of p-value of the trajectory, which is obtained from the χ^2/ndf of the fit. Since the track's model in the method is simplified to the circle and does not take into account energy losses, the χ^2 value of the trajectory fit is biased to the higher values, and as result the p-value is also overestimated. Thus, the arbitrary cut for the p-value is used.

7. Performance of the CDC Track Finding

The performance of the CDC pattern recognition should be estimated from the point of view of the reconstruction of measurable tracks. By the measurable track meant a track of a charged particle in the acceptance region of CDC ($\theta \in (17°; 150°)$, $p_t \gtrsim 50$ MeV), and has left enough hits in the CDC volume. The testing of the tracking algorithms are based on the comparison of the reconstructed event to the Monte Carlo information. Monte Carlo simulated events in this study are generated using EvtGen physics generator and Geant4.

7.1. Definition of Reconstruction Efficiency and Purity

The estimation of a reconstruction performance of the the pattern recognition is based upon comparison of the output of two algorithms, which perform simultaneously: CDC pattern recognition and Monte Carlo tracking. The CDC pattern recognition is an algorithm being studied (Belle II CDC tracking), while the Monte Carlo tracking is an "ideal" pattern recognition algorithm. The "ideal" tracks will be called **MCTrack**, and reconstructed tracks are **PRTrack** (pattern recognition tracks).

Relations between simulation (MC particle and CDC hits) and reconstructed

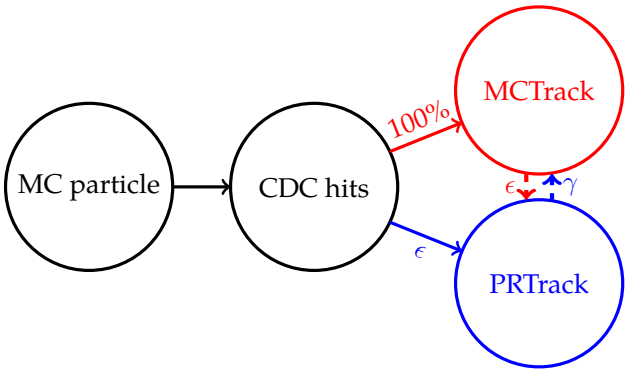

Figure 7.1.: Relations between MCTrack and PRTrack

MCTrack and PRTrack are shown in Fig. 7.1. The Monte Carlo tracking creates tracks based on the relations between CDC hits and generated particle. All hits left by the same particle will be assigned to the same track, meaning that all tracks in CDC will be found and reconstruction efficiency of the Monte Carlo tracking is 100%. On the other hand, pattern recognition assigns ϵ fraction of CDC hits (see Fig. 7.1), belonging to the same particle. Knowing which hits are owned by MCTrack and PRTrack, it is possible to match reconstructed tracks to "ideal" tracks and check a reliability of the pattern recognition. There are two kinds of relations between PRTrack and MCTrack: hit purity and hit efficiency relations. Hit efficiency ϵ indicates how many of MCTrack hits are contained in PRTrack, while hit purity γ shows which fraction of PRTrack hits is present in MCTrack. In other words, hit efficiency shows how well MCTrack is described by the given PRTrack, and hit purity reveals the quality of the PRTrack reconstruction. MCTrack is claimed to be **matched** to PRTrack when the highest purity MCTrack is the same as the highest efficiency MCTrack of this PRTrack. This means, that tracks are matched when most of MCTrack hits are in PRTrack and most of PRTrack hits are owned by the same MCTrack.

An efficiency of the pattern recognition is a measure which describes the fraction of MCTracks reconstructed by the pattern recognition (matched MCTracks). It can be written as

$$\varepsilon = \frac{n_{PR}}{N_{MC}} \tag{7.1}$$

where N_{MC} is a total number of MCTracks, n_{PR} is a number of matched reconstructed tracks (PRTracks).

A purity of a tracking sample is a fraction of matched (reconstructed) ideal tracks (MCTracks) in a track sample of a pattern recognition. In other words, it characterizes accuracy of the tracking algorithm and how many fake tracks it produces. The purity can be expressed as

$$p = \frac{n_{PR}}{N_{PR}} \tag{7.2}$$

where N_{PR} is a total number of PRTracks, n_{PR} is a number of the reconstructed tracks, that can be matched to the MCTracks.

7.2. Study of the Tracking Performance

To show performance of the Belle II CDC tracking chain, a comparison to the legacy track finder from the Belle experiment has been done. The legacy track finder (**Trasan**) has been adopted to the Belle II software framework to be used at the early stages of pattern recognition development as the reference. The CDC tracking chain used for the performance studies includes the following pattern recognition modules: WireHitTopologyPreparer, SegmentFinderCDCFac-

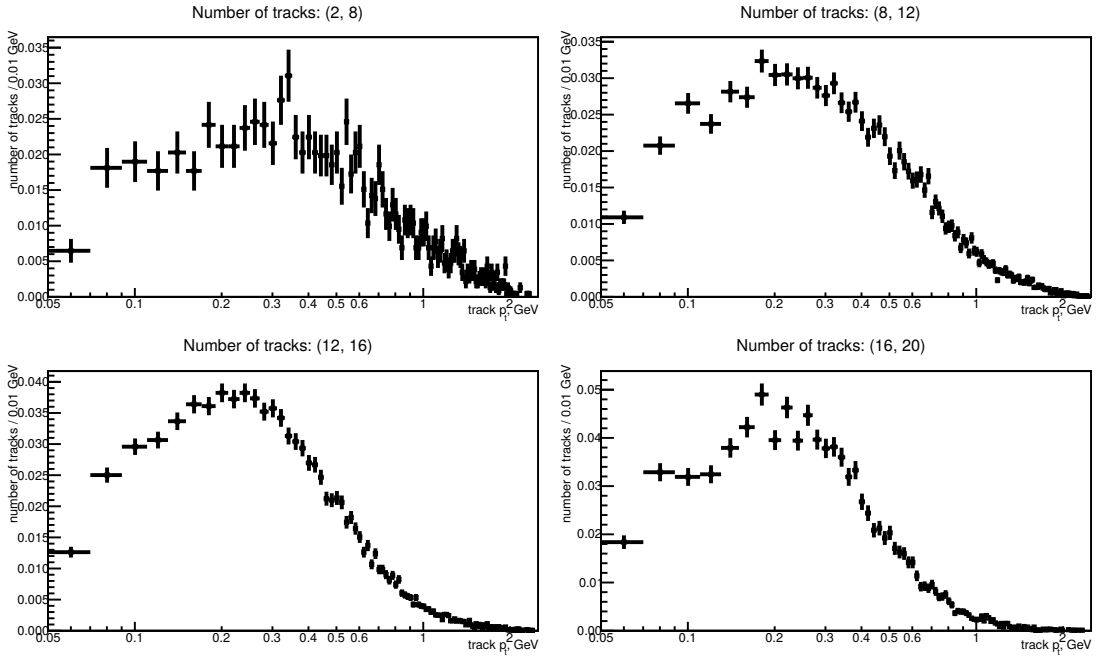

Figure 7.2.: Distribution of Monte Carlo generated tracks in bins of p_t

etAutomaton, TrackFinderCDCLegendreTracking, StereoHitFinderCDCLegendreHistogramming, SegmentTrackCombiner. TrackQualityAsserterCDC modules were excluded from the execution chain as the main purpose of them is to remove tracks which are unreasonable from point of view of the fitting algorithms, but acceptable from point of view of the pattern recognition.

The efficiency study were performed on the Monte Carlo generated sample of inclusive $B\bar{B}$ decays, created in $e^+e^- \rightarrow \Upsilon(4S) \rightarrow B\bar{B}$ decay chain. The efficiency and purity dependence on p_t, d_0, number of tracks in event and combination of these quantities has been estimated. The efficiency studies of the exclusive $B\bar{B}$ decays ($B \rightarrow \mu\nu$, $B \rightarrow D^0\pi$) can be found in Appendix A.

Plots of efficiency are studied in four event multiplicity (number of MCTracks in event) bins. The reason lies in the fact that reconstruction efficiency depends on the number of MCTracks in the event. The distribution of the Monte Carlo generated tracks in bins of event multiplicity is shown in Fig. 7.2. As one can see, the p_t distribution of tracks has the same shape, but maximum of it is shifted to the lower p_t values for high multiplicity events.

7.2.1. Dependence on p_t

The efficiency of the CDC pattern recognition compared to the legacy track finder is shown in Fig. 7.3. Prompt tracks only with $d_0 < 1$ cm are considered for the study. The CDC pattern recognition has much higher efficiency

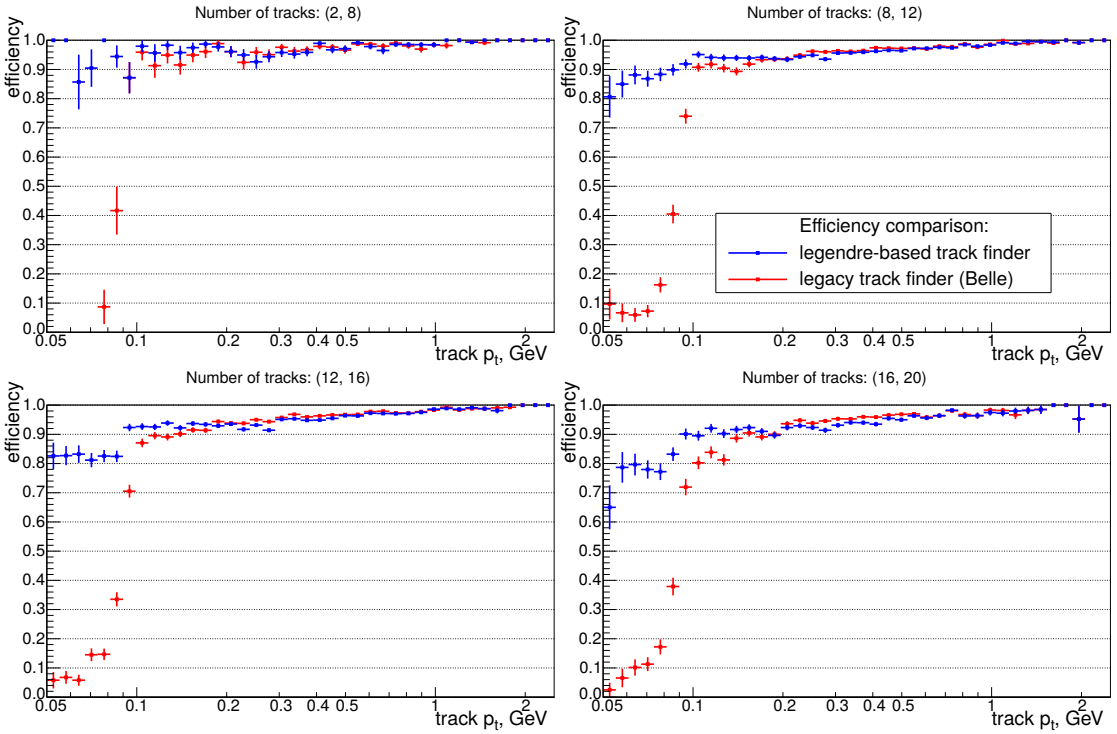

Figure 7.3.: Comparison of the efficiency of the Belle II track finding chain to the legacy track finder (the Belle experiment) based on the number of generated tracks in event (event multiplicity) in bins of track p_t

for the $p_t < 0.1$ GeV region compared to the efficiency of Trasan in the same region. Trasan finder requires stereo hits to create a track, so it results in the biased reconstruction efficiency for low-p_t tracks, which do not reach the first stereo superlayer. The CDC pattern recognition do not have such conditions, since tracks are build using axial hits, and stereo hits are assigned afterwards to existing tracks. It is a considerable improvements, since low-p_t region has a substantial amount of tracks (see Fig. 7.2). It can be seen than reconstruction efficiency rises with the p_t of the generated track as well as it drops with the event multiplicity. The interpretation of the efficiency behavior can be found in the track-track influence during the pattern recognition.

Dependence of the reconstruction efficiency on the event multiplicity tends to be lower by few percents for high multiplicity bin compared to low multiplicity efficiency. For example, in Fig. 7.2, efficiency distribution in fourth multiplicity bin ($16-20$ MCTracks) is decreased compared to the first multiplicity bun ($2-8$ MCTracks). The explanation of this effect can be found in the algorithm itself. The track search is based on the finding of the dense regions in the Legendre space, which is turned out to be more populated in case of high multiplicity events. The higher population of the Legendre space leads to the increased hit miss-assignment rate, which also includes merging segments originating from

different tracks into the same PRTrack. In such cases there are mo matching between MCTrack and merged PRTrack. But this effect is comparable with efficiency fluctuations along p_t.

Reconstruction efficiency dependence on track p_t is stronger than on the event multiplicity. This effect comes both from algorithm specifics as well as from detector features. The fact that the size of cells of the CDC is the same for all superlayers, leads to different separation of tracks in different p_t regions. Since the metrics in conformal mapped space is proportional to real space as $\sim 1/r$, the transformed cells from inner layers will be much larger than from outer layers. It results in different resolution and track separation for high- and low-p_t regions.

To summarize influence of both effects, one can compare pattern recognition efficiency of low multiplicity events (namely first bin in Fig. 7.2) to other bins. A pattern recognition in case of low multiplicity events implies a single track reconstruction in nearly absence of other tracks. This means that the each track can be considered as an independent one as long as its pattern do not intersects with other tracks, and both efficiency decreasing effects hardly affect the pattern recognition. In case of the increased multiplicity of the event, an influence of the track-track interaction strengthens, resulting in reconstruction efficiency shape which shown in Fig. 7.2 (2-4 multiplicity bins).

7.2.2. Dependence on the Particle Type

Particles of different type interact with the detector volume differently, resulting in different reconstruction efficiency. Fig. 7.4 shows p_t dependence of the reconstruction efficiency of the prompt particles of different type. As expected, a reconstruction efficiency of $K^{\pm}$ is lower than for $\pi^{\pm}$, as well as efficiency of leptons (e, μ) is higher. But, the overall behavior of the reconstruction efficiency follows the same rule – lower for the low-p_t region and tends to 100% efficiency. This efficiency behavior can be explained from point of view of material effects, which include energy losses dE/dx and multiple scatterings.

The dE/dx falls with increasing the energy of a particle until it reaches the minimum ionization, and then rises due to bremsstrahlung effect. The minimum ionization differs for each kind of the charged particles, and depends on the mass of a particle. For leptons (especially e) bremsstrahlung have more significant influence in high-p_t region than for hadrons, leading to efficiency drops. Hadrons have stronger energy losses due to the material effect in low-p_t region. Influence of this effect can be clearly seen in Fig. 7.4, where particles of different kind have different reconstruction efficiency.

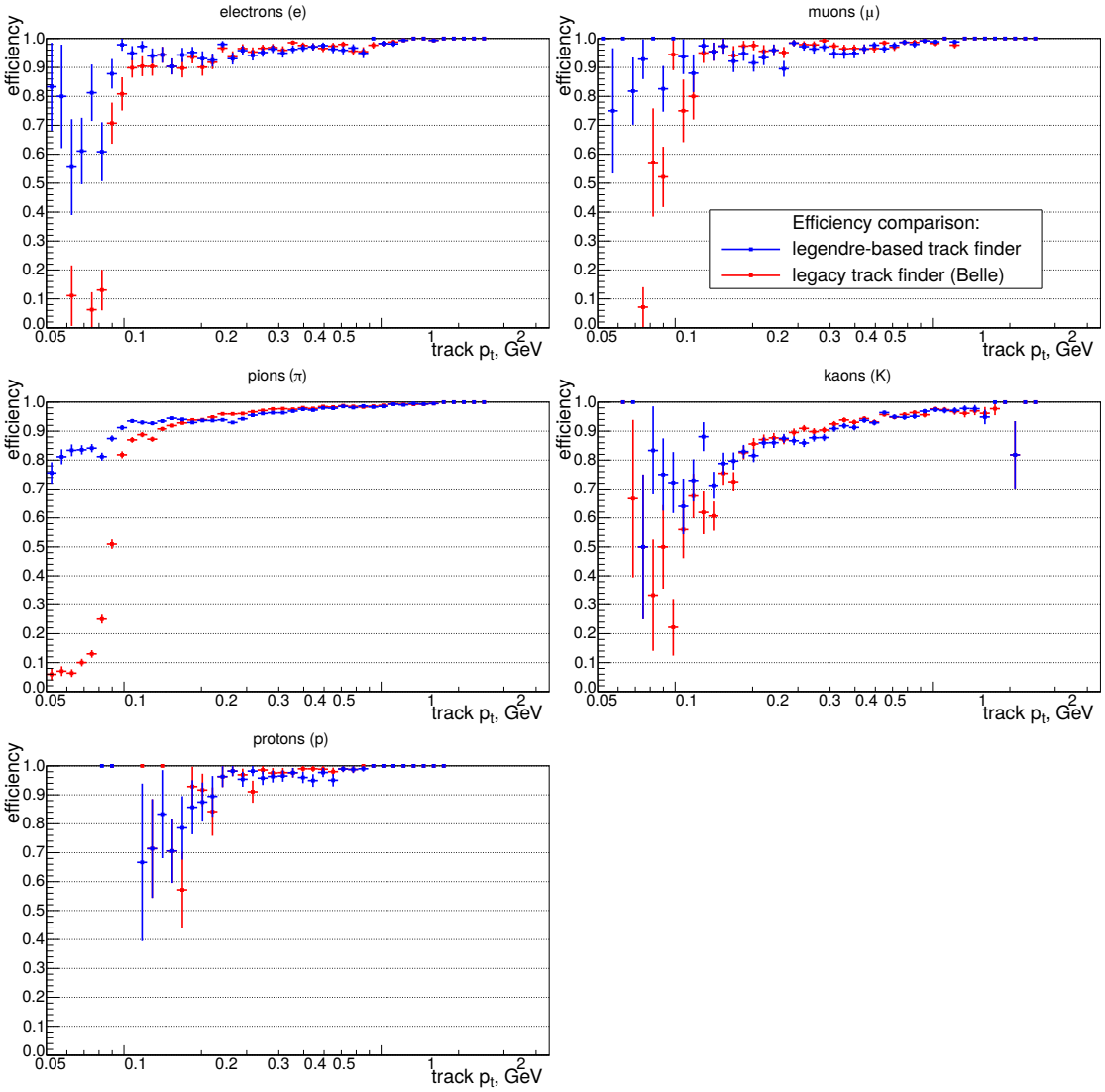

Figure 7.4.: Comparison of the efficiencies of Belle II track finding chain to legacy track finder (the Belle experiment) based on the particle type in bins of track p_t

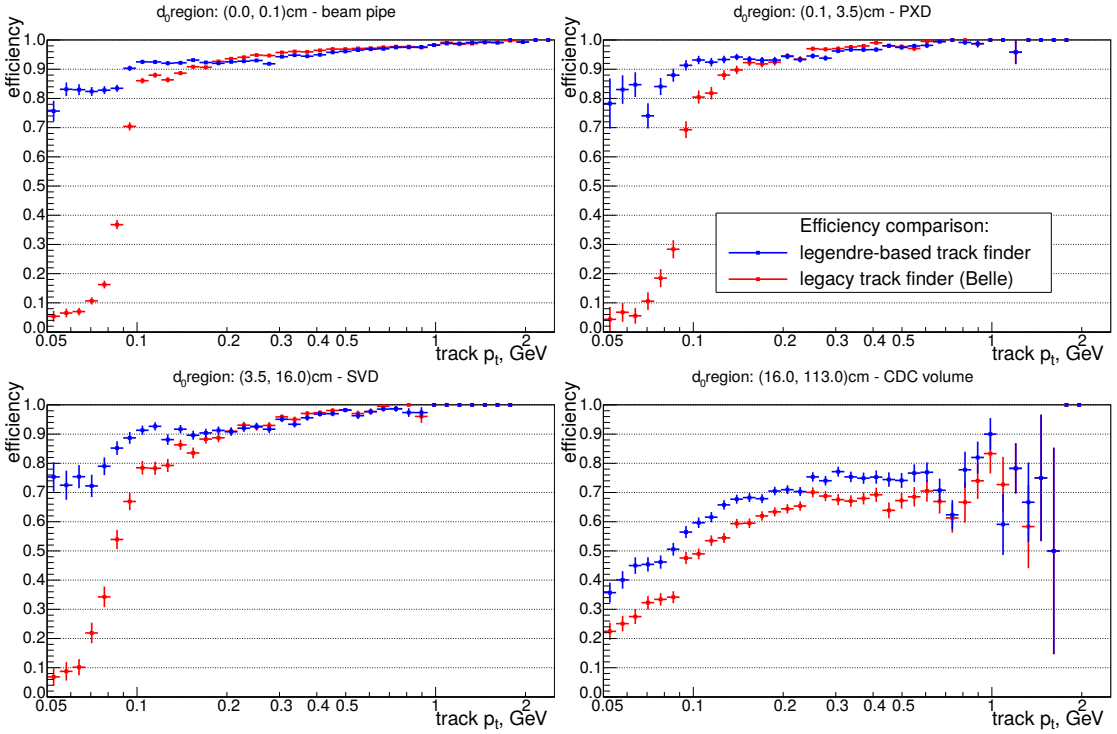

Figure 7.5.: Comparison of the efficiencies of Belle II track finding chain to legacy track finder (the Belle experiment) based on the production position of the track candidates in bins of track p_t

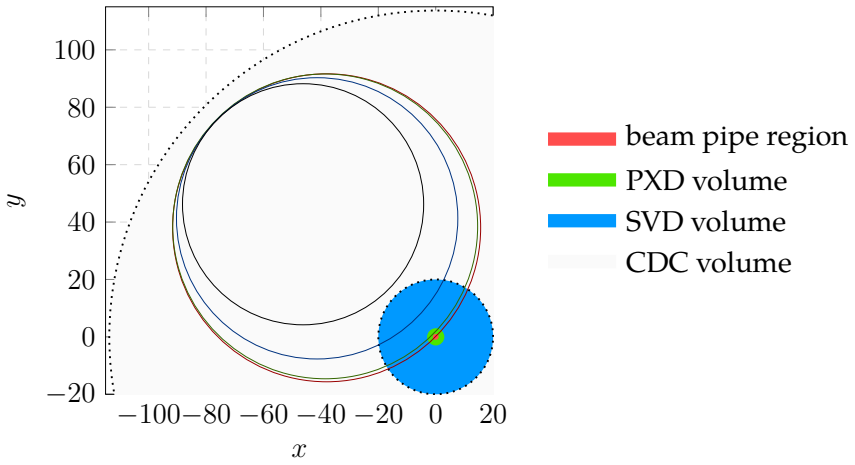

Figure 7.6.: An example of the non-prompt trajectories. Volumes of the different parts of the detector are highlighted with different color.

7.2.3. Dependence on d_0

As it was shown in Sec. 6, the Legendre based track finding was also developed to reconstruct non-prompt tracks. The information about particle production vertex can only be obtained at the Monte Carlo level, and is not of interest in pattern recognition analyze. The reason is that pattern recognition can not determine track production vertex and distance to it. Much important quantity is a distance of the closes approach of the track to the origin (d_0), which is the one of the 2-D trajectory parameters (see Sec. 6.1.3). From point of view of the pattern recognition, a track is classified as a non-prompt track as long as its d_0 parameter higher than a threshold (in the current work it is defined to be $d_{0_{max}}^{prompt} = 1$ cm) and vice versa.

Efficiency comparison of the Legendre based pattern recognition to Trasan is shown in Fig. 7.5. There are four d_0 regions selected for the study, depending on the detector geometry: track inside the beam pipe, inside the PXD volume, SVD volume and CDC volume. An example of trajectories passing through the different regions of the detector is shown in Fig. 7.6. Tracks, whose trajectories passes through the inner parts of the detector (this includes beam pipe, PXD and SVD volumes) have high reconstruction efficiency which stays on the nearly the same level (see Fig. 7.5, $1-3$ bins of d_0). In case of tracks which are contained in the CDC volume only, the reconstruction efficiency is on a relatively high level to perform a pattern recognition, although the algorithm is mainly focused on the prompt track reconstruction.

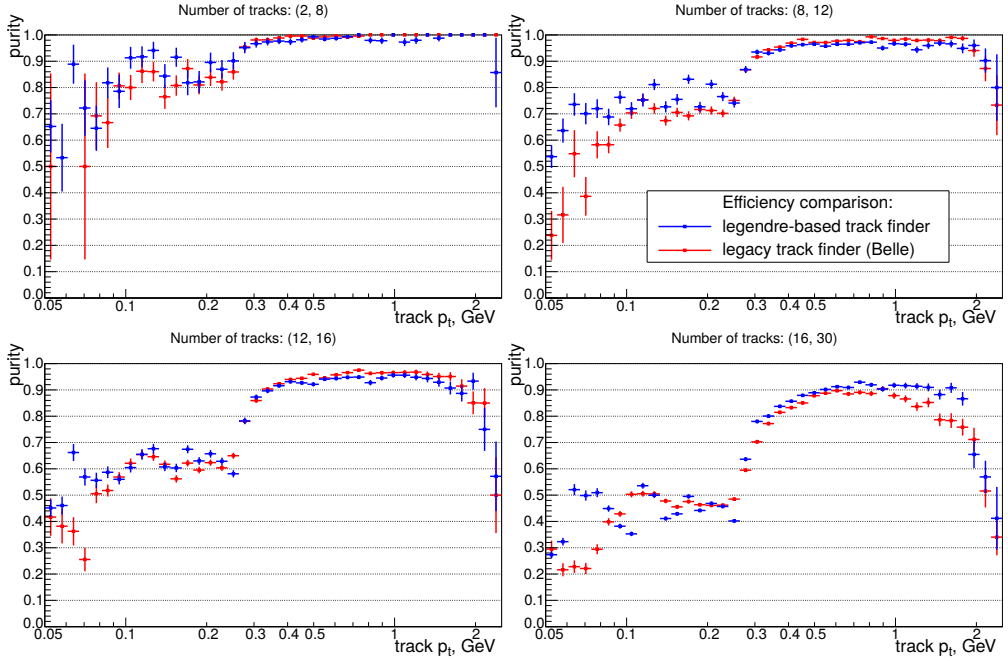

Figure 7.7.: Comparison of the purities of Belle II track finding chain to legacy track finder (the Belle experiment) based on the number of generated tracks in event (event multiplicity) in bins of track p_t

7.2.4. Purity

The purity of the tracking sample plays an important role for the event reconstruction (for example, Full Event Interpretation) and physics analyses. Reconstructed tracks can be classified into three classes: matched tracks, clones and fakes. Fake tracks are tracks which do not have any suitable Monte Carlo track to match, while clones have a matching Monte Carlo track, but this Monte Carlo track could be describes with other reconstructed track which contains most of the hits.

The purity of a pattern recognition is shown in Fig. 7.7. A lower purity can been observed in the low-p_t region, which corresponds to the curling tracks. In this region, the fraction of clone and fake tracks is relatively high (see Appendix A). Curling tracks usually have a long trajectory in the CDC volume and a large amount of hits. This results in different curvatures at the beginning and ending of the trajectory, and splitting of the track into two tracklets. The track merging procedure decreases the amount of clones, but could not take into account multiple scattering effect and high energy losses of tracks.

7.2.5. Examples of Missed Tracks

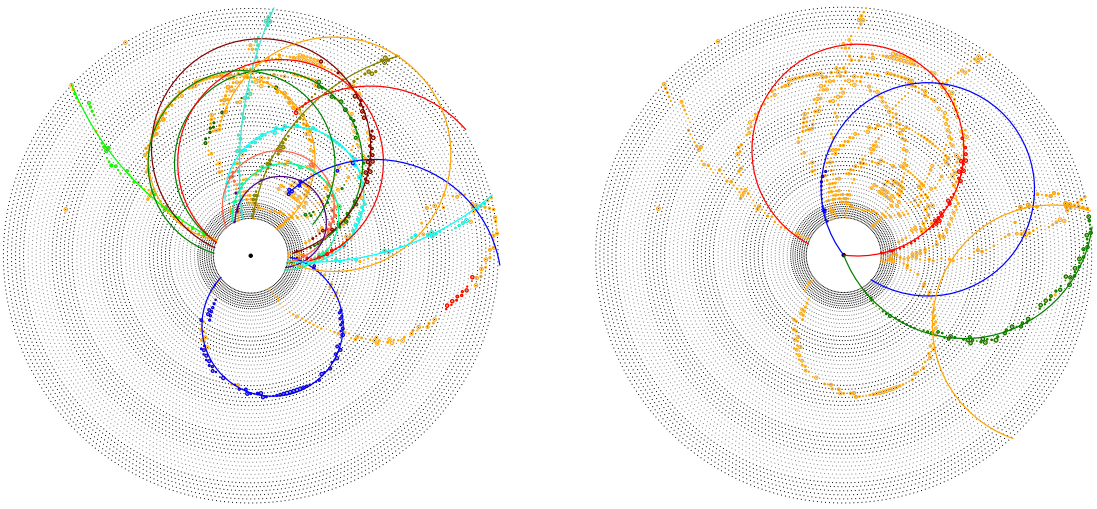

(a) Reconstructed event (b) MC tracks, marked as “missing”

Figure 7.8.: Example of missing PR tracks

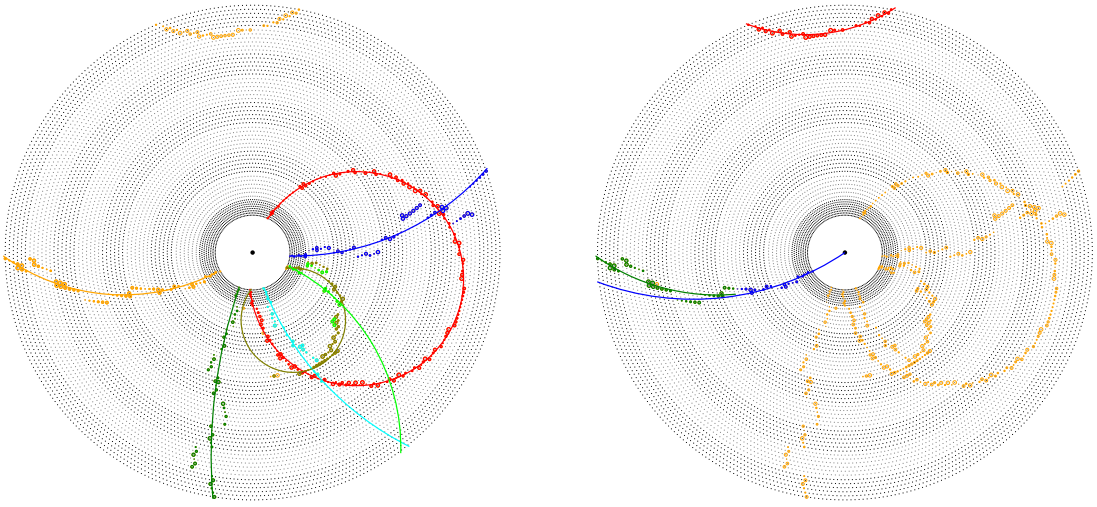

(a) Reconstructed event (b) MC tracks, marked as “missing”

Figure 7.9.: Example of missing relations between PR and MC tracks

The inefficiency of the pattern recognition mainly comes from the absence of tracks, splitting of the track into segments and merging of track into another track. An example of not found and splitted tracks is shown in Fig. 7.8. The green track in Fig. 7.8b is not reconstructed by the pattern recognition at all. Hits belonging to the blue track (Fig. 7.8b) are taken by the other tracks (hit

misassignment). The red track is splitted into few segments and merged with others, resulting in track loss.

One special case is shown in Fig. 7.9 with decayed particle, and on Monte Carlo level mother and daughter tracks are separated (Fig. 7.9b). Pattern recognition reconstructs both tracks as the same one (Fig. 7.9a), but it does not have a matchable Monte Carlo track, since it does not satisfy track hit efficiency and purity criteria.

7.3. Influence of Beam Background

Beam induced background influences the reconstruction efficiency as well as on the purity of the track sample, effectively lowering this quantities. Additional hits in the CDC result in an increased wrong hit assignment rate. This effect leads to spoiled trajectories, and the fitting based hit assignment would fail. As a result, the unused hits could be combined with the background hits, increasing the fake rate of the pattern recognition.

Background hits can be rejected before the actual pattern recognition procedure [63]. Most of the beam induced background hits are forming standalone clusters of few hits or just single standalone hits. This kind of background could not be rejected during the global pattern recognition, but it can be rejected at the earlier stages. The main idea is to perform clustering of the hits and analyze its shape. By using boosted decision tree, the algorithm can distinguish the background-like clusters from the track-like segments. The background-like clusters are masked and not considered at the later stages of the pattern recognition. As result, Legendre-based tracking can consider proper hits while the amount of the beam background hits is reduced.

Moreover, the beam background level for the Belle II experiment has been estimated [3], but the pattern recognition should be checked for the increased background level to provide assurance that events can be reconstructed even in case of larger beam induced background levels. The composition of the background in CDC is provided by the simulation package of the BASF2 framework, and added to the simulated event as additional single hits or patterns of hits. These background hits may be combined with the real tracks, lowering hit purity, as well as create fake tracks. The BASF2 framework provides a possibility to scale the background level by changing fraction of background hits in the simulation.

The performance of the Legendre based pattern recognition is compared for no background case (**no BG**), nominal background (**BG x1**) and scaled background (doubled **BG x2**, and tripled **BG x3**).

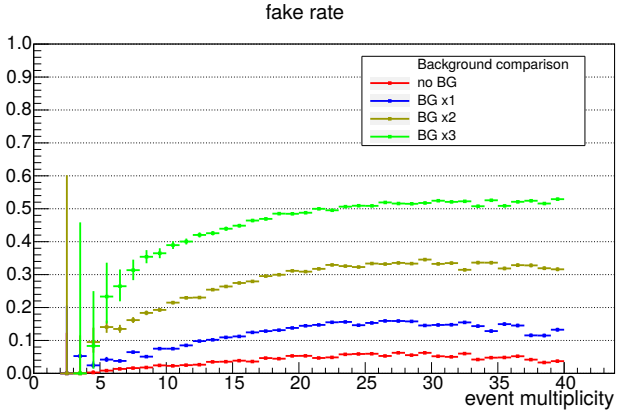

Figure 7.10.: Fake rate along the PRTrack multiplicity

7.3.1. Efficiency Dependence on p_t

The beam background mainly affects the p_t region which corresponds to the curling tracks ($p_t < 450$ MeV). As it has been shown Sec. 6, curling tracks are supposed to be constructed out of much more hits than the high-p_t tracks.

There are two kinds of background influence on the pattern recognition: creating fake tracks and distorting trajectory of good tracks. In case of a high density of hits in CDC, random hits may be combined in track-like patterns, spoiling the tracking sample with the fake tracks. This kind of effect can be observed in no background simulation for events with high track multiplicity as well as with the presence of the background (see Fig. 7.10). Distortion of trajectories occurs when correct track's hits are combined with background hits. In such case further attempts of hits assignment may fail, since background hits (after background suppression) can't be distinguished from track hits.

7.3.2. Efficiency Dependence on the Number of CDC Hits

The number of the CDC hits influences on the pattern recognition efficiency. In case of simulation without background, the reconstruction efficiency drops with increased number of CDC hits. As it was mentioned, this effect is caused by wrong combinations of hits in conditions of high hit density, as well as spoiling of event by looping tracks, which produce lots of fakes and clones.

Presence of the background effectively increase the number of CDC hits. The dependence of the reconstruction efficiency on the number of hits in an event is shown in Fig. 7.12. The no background simulation and single background simulation have their own baselines, which points to the suppressed influence of the background hits as well as effective rejection of the CDC background. Scaled background (doubled and tripled) have similar behavior and the same baseline, what could indicate for the deterioration of the background rejection.

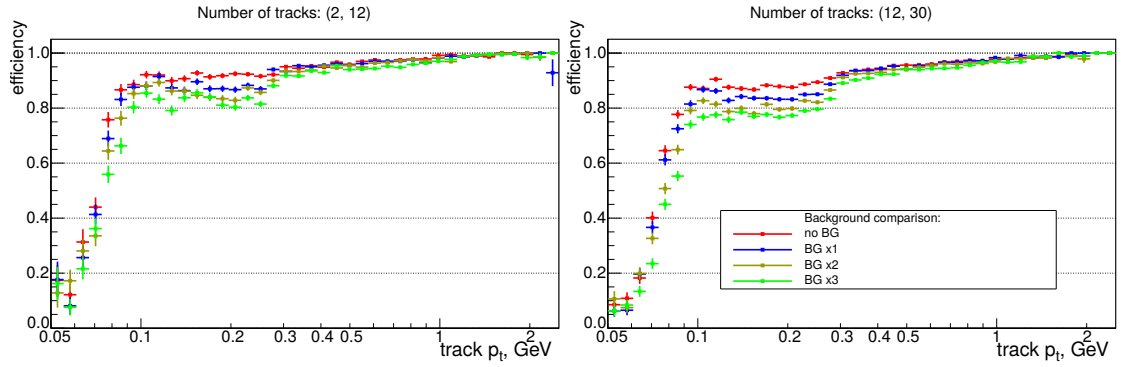

(a) Prompt track candidates

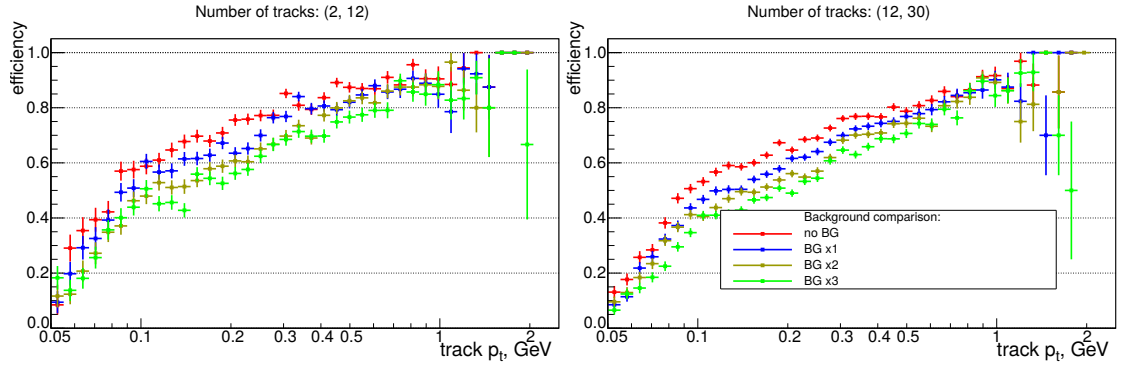

(b) Non-prompt track candidates

Figure 7.11.: Comparison of the efficiencies of the Belle II track finding chain with different beam background levels for prompt (a) and non-prompt (b) track candidates samples based on the number of generated tracks in event (event multiplicity) in bins of track p_t

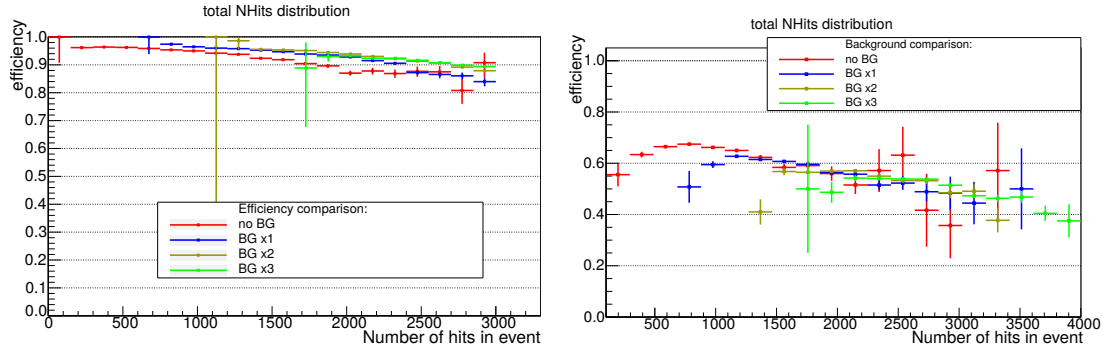

(a) Prompt track candidates (b) Non-prompt track candidates

Figure 7.12.: Comparison of the efficiencies of the Belle II track finding chain with different beam background levels for prompt (a) and non-prompt (b) track candidates samples in bins of number of CDC hits in event

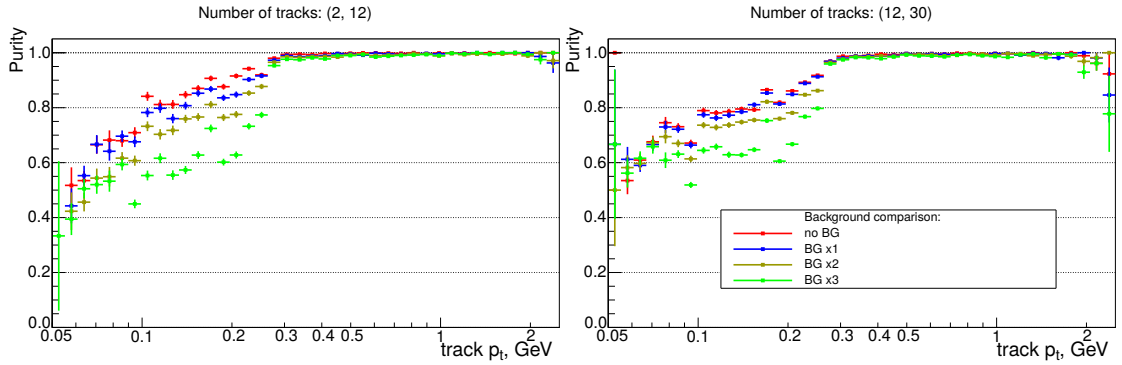

(a) Prompt track candidates

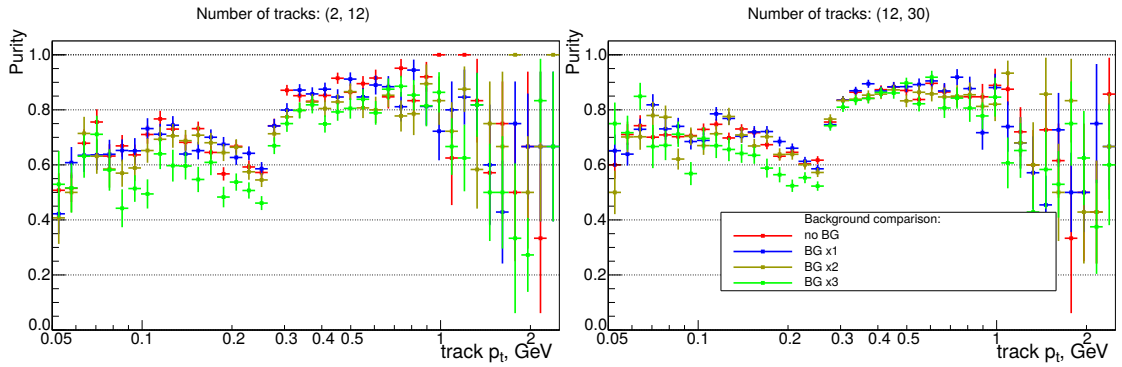

(b) Non-prompt track candidates

Figure 7.13.: Comparison of the purities of the Belle II track finding chain with different beam background levels for prompt (a) and non-prompt (b) track candidates samples based on the number of generated tracks in event (event multiplicity) in bins of track p_t

7.3.3. Purity Dependence on p_t

The purity of the tracks sample depends on the beam background level, as shown in Fig. 7.13. The most affected is the p_t region with curlers, where the probability of the random combination of additional CDC hits increases, resulting in a larger fake fake. For high-p_t prompt tracks this effect is negligible. The fake rate is shown in Fig. 7.15.

On the other hand, the clone rate decreases with the increased background level (see Fig. 7.14), but this effect is neglected by the fake rate. The clones have much less hits compared to matched tracks by definition. In case of high hit density, clones collect wrong hits and could be also classified as fakes.

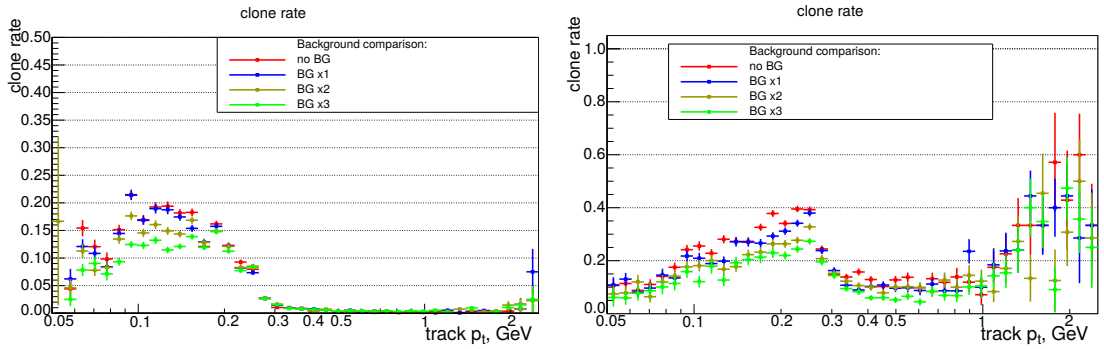

(a) Prompt track candidates (b) Non-prompt track candidates

Figure 7.14.: Comparison of the clone rates of the Belle II track finding chain with different beam background levels for prompt (a) and non-prompt (b) track candidates samples in bins of track p_t

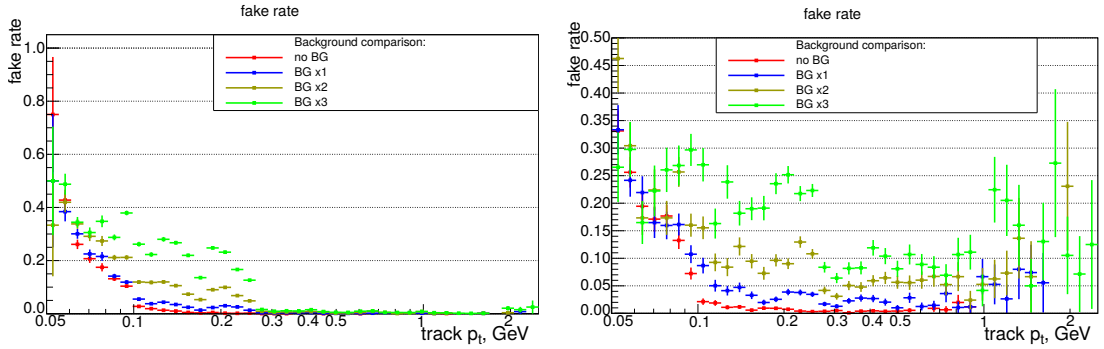

(a) Prompt track candidates (b) Non-prompt track candidates

Figure 7.15.: Comparison of the fake rates of the Belle II track finding chain with different beam background levels for prompt (a) and non-prompt (b) track candidates samples in bins of track p_t

7.3.4. Track Hit Purity and Efficiency

Track's hit efficiency and hit purity are playing an important role in understanding the performance of the track finding. This quantities describe the reconstruction accuracy and quality of the matched PRTracks.

A hit efficiency is a fraction of MCTrack hits which are present in the matched PRTrack, meaning that higher hit efficiency corresponds to a more complete track reconstruction. It also has an influence on the later stages of the event reconstruction, such as fitting, vertexing and dE/dx measurement, as missing hits or an incomplete trajectory results in larger uncertainties of the track parameters.

The second quality criteria, hit purity, is the fraction of hits in the PRTrack which are being present in the matched MCTrack. In other words, this quantity characterizes the accuracy of the hit assignment. Wrong hits may lead to the wrong determination of the track parameters as well as to the rejection of the track due to the low track quality.

The comparison of the hit efficiencies for different beam background levels for prompt and non-prompt tracks are shown in Fig. 7.17. The hit efficiency drops with the increased background level due to spending of good hits to construct fake tracks as well as due to rejection of background-like clusters of CDC hits. As the fake rate increases with the background level (see Fig. 7.15), the probability of the random exclusion of the good CDC hits by assigning them to fake tracks rises.

Prompt tracks have higher hit efficiency compared to non-prompt tracks due to the different approaches of their reconstruction. Prompt tracks are reconstructed as a dense regions in the Legendre space, and most of hits are assigned to the track. Later, proper trajectory is restored and missing hits are assigned, effectively increasing hit efficiency. On the other hand, non-prompt tracks are restored from the segments basing on the circular fit. The main difference is that segments usually contain less hits than tracks found in Legendre space, so the segment trajectories are less precise. This fact leads to less efficient hit assignment and as result lower hit efficiency. The dependence of the hit efficiency on d_0 is shown in Fig. 7.18a, indicating lower hit efficiency for the non-prompt tracks.

Curling tracks have lower hit efficiency compared to high-p_t tracks due to the material effects. As it was shown in Fig. 7.14, clone rate for curling tracks are higher and apparently leads to reduced hit efficiency.

Figure 7.17 shows hits purity for prompt and non-prompt tracks. The hit purity drops with the increased background level, and this effect is stronger for curling tracks. As it was mentioned before, curling tracks have longer paths in $\rho - \phi$ projection, and as a result, the probability of assignment of wrong hits is increased. In case of high hits density, the wrong hits in the outgoing arm of the

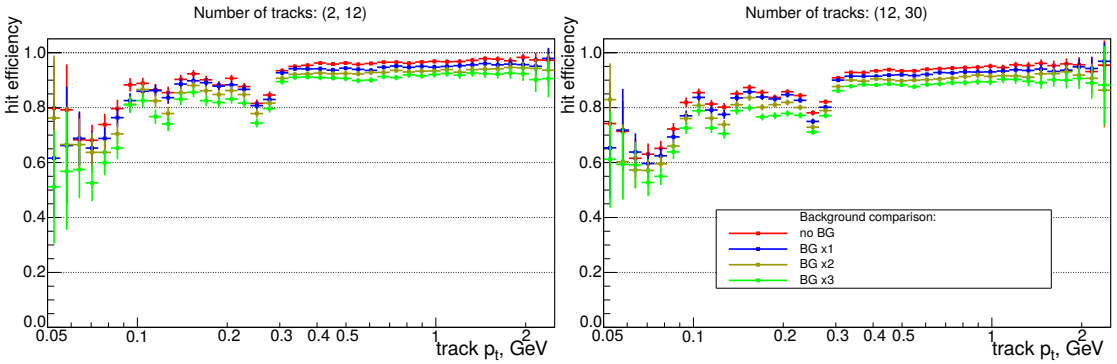

(a) Prompt track candidates

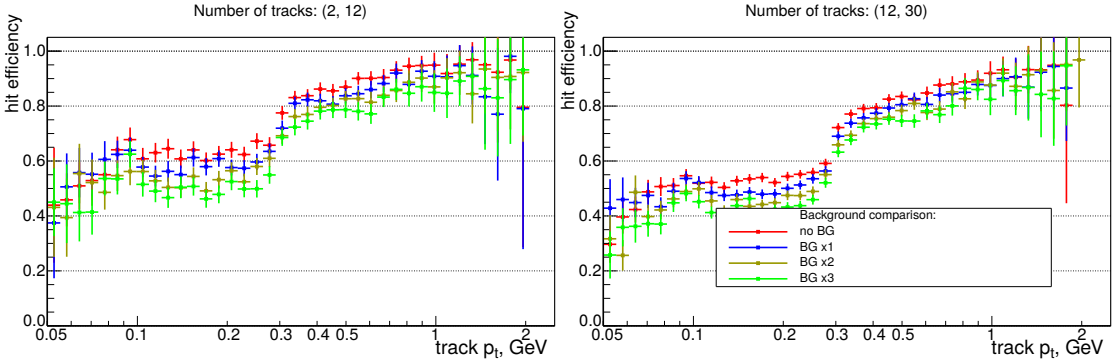

(b) Non-prompt track candidates

Figure 7.16.: Comparison of the track hit efficiencies of the Belle II track finding chain with different beam background levels for prompt (a) and non-prompt (b) track candidates samples based on the number of generated tracks in an event (event multiplicity) in bins of track p_t

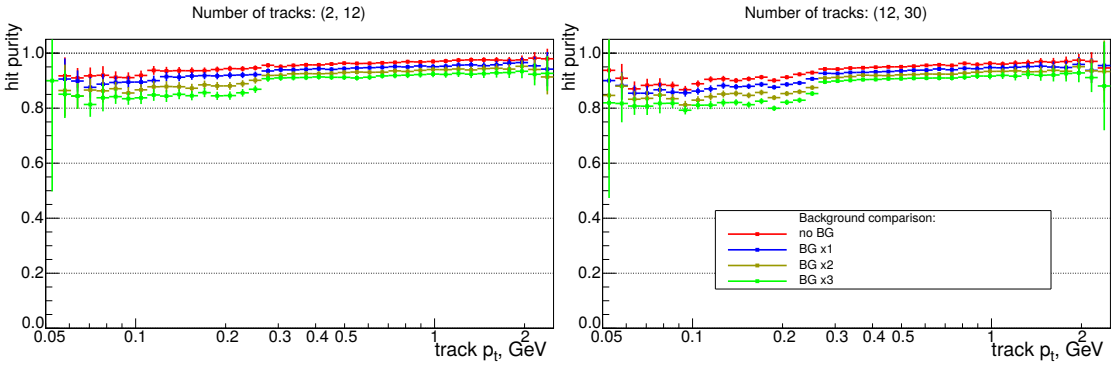

(a) Prompt track candidates

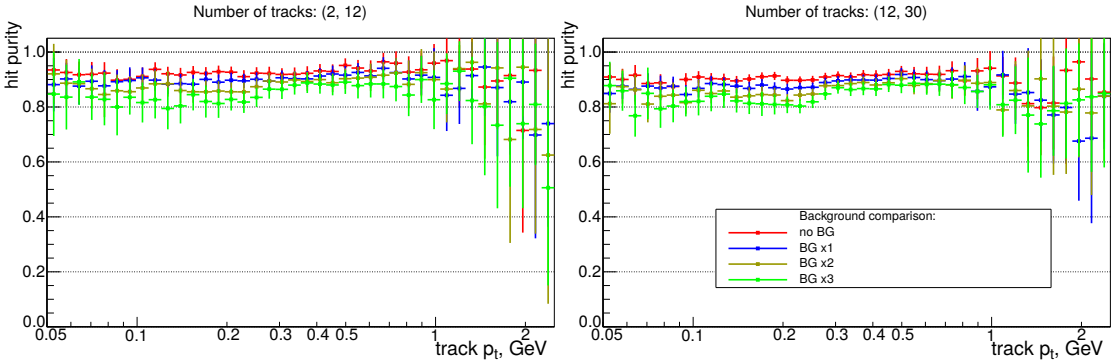

(b) Non-prompt track candidates

Figure 7.17.: Comparison of the track hit purities of the Belle II track finding chain with different beam background levels for prompt (a) and non-prompt (b) track candidates samples based on the number of generated tracks in event (event multiplicity) in bins of track's p_t

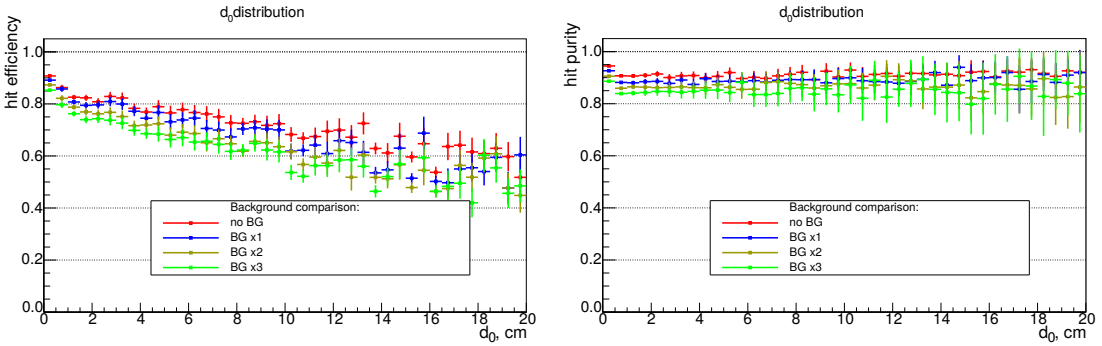

(a) Hit efficiency (b) Hit purity

Figure 7.18.: Comparison of the track hit efficiencies (a) and track hit purities (b) of the Belle II track finding chain with different beam background levels in bins of track d_0

Background level	Legendre-based axial finder	Stereohits assigner	Trasan
BG x0	104.35 ms	9.04 ms	431.25 ms
BG x1	123.22 ms	10.72 ms	624.66 ms
BG x2	161.68 ms	13.15 ms	895.20 ms
BG x3	224.11 ms	17.57 ms	1353.02 ms

Table 7.1.: Comparison of the CPU execution time.

track could be assigned. The hit purity weakly depends on the d_0 of the track (see Fig. 7.18b).

7.4. CPU Performance

The Belle II experiment expects a lot of data to collect and process with limited computational power. Thus, developed algorithm should be optimized to deliver expected pattern recognition performance within relatively low CPU time. It is one of the substantial criteria, which has been essential during development of the algorithm.

Comparison of the CPU computing time of the Legendre-based tracking with different background levels to the Trasan finder is listed in Table 7.1. The test was performed on a computer powered with Intel(R) Core(TM) i7-4790 CPU with 8 MB cache and 3.60 GHz processor base frequency. The average CPU time spent to reconstruct CDC tracks is lower for Legendre-based pattern recognition. The key features, which lead to lowered execution time are:

- QuadTree, which is used for fast candidate search in the Legendre space
- lookup table with precalculated trigonometrical functions

As it was discussed in Sec. 6.2, a QuadTree data structure allows to perform 2-dimensional binary search and to store its result in a tree. Compared to a fast Hough 2-D binary search, a QuadTree brings the possibility to use the same data object to find track candidates within multiple iterations. It means, that filled QuadTree nodes can be used in the next iterations by filtering out used hits, saving computing time. On the other hand, partial filling of the QuadTree (which is inherited feature of the fast Hough search) allows to avoid consideration of nodes which do not satisfy the search criteria and, as result, are out of interest. Thus, computing resources are used effectively without losing reconstructions efficiency.

Since QuadTree is a grid in some sense, θ values used in computing of ρ variable on the Legendre plane will be always the same. To speedup calculations, lookup table with precalculated $\sin$ and $\cos$ functions is involved. This allows to

save computing time by getting a precomputed value instead of calling trigonometrical math routines, which are CPU costly.

7.5. Discussion

The CDC pattern recognition of the Belle II experiment shows good track reconstruction performance for a wide range of transverse momenta and track origins. Compared to the Belle legacy track finder, it has its own strong points. Overall performance is on the same level, while reconstruction of low-p_t and non-prompt tracks is better for the Belle II CDC track finder.

Studies of influence of the beam induced background in CDC on the CDC pattern recognition show the stability of the track reconstruction. The scaled background level slightly decreases the performance of the track finder, what is expected and well understood. On the other hand, it has been shown that CDC pattern recognition can perform reliable track reconstruction in case of larger background levels.

8. Conclusions

This work presents the development of the tracking algorithm for the Belle II detector. The method is based on the technique developed by the ATLAS experiment [1]. It has been proved [2] that the method can be adopted to the needs of the Belle II CDC tracking and efficiently reconstruct simulated $B^+ \to \bar{D}^0(\to K^+\pi^-)\pi^+$ decays. The present work consisted in further development and implementation of features, which make the algorithm more generic in sense of track topologies as well as improving track finding performance.

The need for a reliable pattern recognition caused by the purposes of the Belle II upgrade. The wide physics program of the experiment requires the high quality event reconstruction algorithms. For example, rare processes can be studied only with a large datasets. Any inefficiency in the event reconstruction would lead to the losses of statistics and, as result, decreased accuracy of the physics analyses. The tracking part of the event reconstruction is responsible for a precise momentum measurement as well as for the trajectories definition.

The developed pattern recognition reconstructs tracks out of CDC axial hits using the method, which is based on the Legendre transformation of the conformal mapped hits. Tracks in scope of the method are considered as a set of hits, which are likely left by the same charged particle, and lying on a circular trajectory. Although the method was initially considered as a finder of a perfect tracks which originate from the interaction point, the implemented features extended the functionality of the algorithm.

The enhanced 2-dimensional binary search is used for the track candidate detection. It is implemented as a QuadTree structure, which allows to apply different quality criteria during the search. It lead to a high finding efficiency of tracks of different kinds.

The method was implemented as a part of the Belle II Analysis Software Framework as separate module. The developed module was deployed in the standard track reconstruction chain, which will be used for tracking purposes during data taking. The algorithm plays role of a global track finder, which defines most of the track patterns. In combination with other tracking algorithms, it shows high tracking performance. It was shown, that the pattern recognition is capable to operate in presence of high beam induced background.

The development was also focused on the optimization of the algorithm to reduce the execution time. It is one of the substantial requirements on par with the reconstruction efficiency. Computing resources of the experiment are lim-

ited, thus all parts of the executing code must be optimized to use computing time efficiently. Within this scope, the developed Legendre-based pattern recognition has a great improvement compared to the legacy track finder, decreasing execution time by a factor 4.

Bibliography

[1] T. Alexopoulos, M. Bachtis, E. Gazis, and G. Tsipolitis. Implementation of the legendre transform for track segment reconstruction in drift tube chambers. *Nuclear Instruments and Methods in Physics Research Section A: Accelerators, Spectrometers, Detectors and Associated Equipment*, 592(3):456 – 462, 2008.

[2] Kronenbitter, Bastian. *Measurement of the branching fraction of $B^+ \to \tau^+\nu_\tau$ decays at the Belle experiment*. PhD thesis, Karlsruher Institut für Technologie (KIT), 2014.

[3] T. Abe et al. Belle II Technical Design Report. 2010.

[4] K. Abe et al. Observation of mixing induced CP violation in the neutral B meson system. *Phys. Rev.*, D66:032007, 2002.

[5] K. Abe et al. Evidence for CP violating asymmetries $B^0 \to \pi^+\pi^-$ decays and constraints on the CKM angle ϕ_2. *Phys. Rev.*, D68:012001, 2003.

[6] K. Abe et al. Measurement of time dependent CP violating asymmetries in $B0 \to \phi K^0_s$, $K^+K^-K^0_s$, and $\eta' K^0_s$ decays. *Phys. Rev. Lett.*, 91:261602, 2003.

[7] S. K. Choi et al. Observation of a narrow charmonium - like state in exclusive $B^\pm \to K^\pm\pi^+\pi^- J/\psi$ decays. *Phys. Rev. Lett.*, 91:262001, 2003.

[8] K. Abe et al. Observation of large CP violation and evidence for direct CP violation in $B^0 \to \pi^+\pi^-$ decays. *Phys. Rev. Lett.*, 93:021601, 2004.

[9] Y. Chao et al. Evidence for direct CP violation in $B^0 \to K^+\pi^-$ decays. *Phys. Rev. Lett.*, 93:191802, 2004.

[10] S. W. Lin et al. Difference in direct charge-parity violation between charged and neutral B meson decays. *Nature*, 452:332–335, 2008.

[11] K. Abe et al. Measurement of ϕ_3 with Dalitz plot analysis of $B^\pm \to D^{(*)}K^\pm$ decay at Belle. In *3rd Conference on Flavor Physics and CP Violation (FPCP 2004) Daegu, Korea, October 4-9, 2004*, 2004.

[12] Y. Ushiroda et al. New measurement of time-dependent CP-violating asymmetry in $B^0 \to K^0_s\pi^0\gamma$ decay. *Phys. Rev. Lett.*, 94:231601, 2005.

[13] K. Ikado et al. Evidence of the Purely Leptonic Decay $B^- \to \tau^- \bar{\nu}_\tau$. *Phys. Rev. Lett.*, 97:251802, 2006.

[14] M. Staric et al. Evidence for D^0 - $\bar{D}^0$ Mixing. *Phys. Rev. Lett.*, 98:211803, 2007.

[15] J. T. Wei et al. Measurement of the Differential Branching Fraction and Forward-Backword Asymmetry for $B \to K^{(*)}\ell^+\ell^-$. *Phys. Rev. Lett.*, 103:171801, 2009.

[16] The SuperKEKB Physics Working Group. Physics at Super B Factory. 2010.

[17] Tomoyuki Konno. Status and prospects of the Belle II experiment. *Journal of Physics: Conference Series*, 627(1):012009, 2015.

[18] John R. Ellis, Junji Hisano, Martti Raidal, and Yasuhiro Shimizu. A New parametrization of the seesaw mechanism and applications in supersymmetric models. *Phys. Rev.*, D66:115013, 2002.

[19] Andrea Brignole and Anna Rossi. Anatomy and phenomenology of mu-tau lepton flavor violation in the MSSM. *Nucl. Phys.*, B701:3–53, 2004.

[20] G. H. Rees, W. T. Toner, and J. V. Trotman. Effects of Beam-Beam Forces in Large electron-Positron Storage Rings. *IEEE Trans. Nucl. Sci.*, 22:1447–1450, 1975.

[21] P. Raimondi. New developments in Super B-factories. *Conf. Proc.*, C070625:32, 2007. [IEEE Nucl. Sci. Symp. Conf. Rec.,32(2007)].

[22] T. Kuhr T. Hara and Y. Ushiroda. Belle II Coordinate System and Guideline of Belle II Numbering Scheme. 2011.

[23] C. Pulvermacher. *Analysis Software and Full Event Interpretation for the Belle II Experiment*. PhD thesis, Karlsruher Institut für Technologie (KIT), 2015.

[24] A. Moll. The Software Framework of the Belle II Experiment. *Journal of Physics: Conference Series*, 331(3):032024, 2011.

[25] R. Brun and F. Rademakers. ROOT - An Object Oriented Data Analysis Framework. Lausanne, 1996. Proceedings AIHENP'96 Workshop.

[26] S. Agostinelli et al. Geant4-a simulation toolkit. *Nuclear Instruments and Methods in Physics Research Section A: Accelerators, Spectrometers, Detectors and Associated Equipment*, 506(3):250 – 303, 2003.

[27] Google Test Framework Repository. `https://github.com/google/googletest`.

[28] D. J. Lange. The EvtGen particle decay simulation package. *Nucl. Instrum. Meth.*, A462:152–155, 2001.

[29] Torbjorn Sjostrand, Stephen Mrenna, and Peter Z. Skands. A Brief Introduction to PYTHIA 8.1. *Comput. Phys. Commun.*, 178:852–867, 2008.

[30] Piotr Golonka and Zbigniew Was. PHOTOS Monte Carlo: A Precision tool for QED corrections in Z and W decays. *Eur. Phys. J.*, C45:97–107, 2006.

[31] O. Shekhovtsova, I. M. Nugent, T. Przedzinski, P. Roig, and Z. Was. MC generator TAUOLA: implementation of Resonance Chiral Theory for two and three meson modes. Comparison with experiment. *AIP Conf. Proc.*, 1492:62–66, 2012.

[32] German Rodrigo, Henryk Czyz, and Johann H. Kuhn. Radiative return at NLO: The Phokhara Monte Carlo generator. In *Proceedings, 37th Rencontres de Moriond on Electroweak Interactions and Unified Theories*, pages 233–234, 2002.

[33] M. Feindt and U. Kerzel. The NeuroBayes neural network package. *Nucl. Instrum. Meth.*, A559:190–194, 2006.

[34] Wolfgang Waltenberger. RAVE: A detector-independent toolkit to reconstruct vertices. *IEEE Trans. Nucl. Sci.*, 58:434–444, 2011.

[35] Millepede II Homepage. `http://www.wiki.terascale.de/index.php/Millepede_II`.

[36] ISO/IEC. Information technology – Programming languages – C++. ISO International Standard ISO/IEC 14882:2011, International Organization for Standardization, Geneva, Switzerland, 2011.

[37] SCons: A software construction tool. `http://www.scons.org/`.

[38] Apache™ Subversion®. `https://subversion.apache.org/`.

[39] Git Web Homepage. `https://git-scm.com/`.

[40] BASF2 Validation. Belle II TWiki page. `https://belle2.cc.kek.jp/~twiki/bin/view/Software/ValidationPlots`.

[41] Thomas Kuhr. Computing at belle ii. *Journal of Physics: Conference Series*, 331(7):072021, 2011.

[42] E. Laure et al. Programming the grid with glite. *Computational Methods in Science and Technology*, 12(1):33–45, 2006.

[43] Tom Fifield, Ana Carmona, AdriÃąn CasajÃžs, Ricardo Graciani, and Martin Sevior. Integration of cloud, grid and local cluster resources with dirac. *Journal of Physics: Conference Series*, 331(6):062009, 2011.

[44] Jakob Lettenbichler. Tracking in the Belle II Vertex Detector. Connecting The Dots Workshop, Vienna, 2016.

[45] C. Pulvermacher. dE/dx Particle Identification and Pixel Detector Data Reduction for the Bell II Experiment. Diploma thesis, Karlsruher Institut für Technologie (KIT), 2012.

[46] Mattias Ohlsson, Carsten Peterson, and Alan L. Yuille. Track finding with deformable templates âĂŤ the elastic arms approach. *Computer Physics Communications*, 71(1):77 – 98, 1992.

[47] R. Mankel. Pattern recognition and event reconstruction in particle physics experiments. *Reports on Progress in Physics*, 67(4):553, 2004.

[48] J. J. Hopfield. Neural networks and physical systems with emergent collective computational abilities. *Proc. National Academy of Science, USA*, 79:2554–2558, 1982.

[49] Bruce H. Denby. Neural Networks and Cellular Automata in Experimental High-energy Physics. *Comput. Phys. Commun.*, 49:429–448, 1988.

[50] Carsten Peterson. Track finding with neural networks. *Nuclear Instruments and Methods in Physics Research Section A: Accelerators, Spectrometers, Detectors and Associated Equipment*, 279(3):537 – 545, 1989.

[51] I. Abt, I. Kisel, S. Masciocchi, and D. Emelyanov. CATS: A cellular automaton for tracking in silicon for the HERA-B vertex detector. *Nucl. Instrum. Meth.*, A489:389–405, 2002.

[52] F. Laplanche I. Kisel, V. Kovalenko. Cellular automaton and elastic net for event reconstruction in the nemo-2 experiment. *Nuclear Instruments and Methods in Physics Research Section A: Accelerators, Spectrometers, Detectors and Associated Equipment*, 387(3):433 – 442, 1997.

[53] N. Margolus T. Toffoli. Cellular automata machines: A new environment for modelling (4th ed.). *MIT Press, Cambridge*, 1987.

[54] O. Frost. A Local Tracking Algorithm for the Central Drift Chamber of Belle II. Diploma thesis, Karlsruher Institut für Technologie (KIT), 2013.

[55] H.D. Schulz and H.J. Stuckenberg. A trigger processor for argus. In *Topical Conference on the Application of Microprocessors to High-Energ Pyphysics Experiments*, CERN, Geneva, Switzerland, 1981.

[56] P.V.C. Hough. Methods and means for recognizing complex patterns. U.S. Patent 3069654, 1962.

[57] Hungwen Li, Mark A Lavin, and Ronald J Le Master. Fast hough transform: A hierarchical approach. *Computer Vision, Graphics, and Image Processing*, 36(2):139 – 161, 1986.

[58] V. Karimäki. Effective circle fitting for particle trajectories. *Nuclear Instruments and Methods in Physics Research Section A: Accelerators, Spectrometers, Detectors and Associated Equipment*, 305(1):187 – 191, 1991.

[59] A. Strandlie, J. Wroldsen, R. Frühwirth, and B. Lillekjendlie. Particle tracks fitted on the riemann sphere. *Computer Physics Communications*, 131(1âĂŞ2):95 – 108, 2000.

[60] R. Frühwirth. Application of kalman filtering to track and vertex fitting. *Nuclear Instruments and Methods in Physics Research Section A: Accelerators, Spectrometers, Detectors and Associated Equipment*, 262(2):444 – 450, 1987.

[61] New electronics tested for Belle II central drift chamber. Feature Story, KEK, Japan. `http://www2.kek.jp/proffice/archives/feature/2010/BelleIICDCDesign.html`.

[62] XT Relation. Belle II TWiki page. `https://belle2.cc.kek.jp/~twiki/bin/view/Detector/CDC/XT-Relation`.

[63] N. Braun. Momentum Estimation of Slow Pions and Improvements on the Track Finding in the Central Drift Chamber for the Belle II Experiment. Master thesis, Karlsruher Institut für Technologie (KIT), 2015.

[64] M. Hansroul. Fast Circle Fit with the Conformal Mapping Method . *Nucl. Instrum. Meth.*, A270:498–501, 1988.

[65] Hans Schwerdtfeger. *Geometry of Complex Numbers*. Courier Corporation.

[66] O. Frost, Helix gymnastics. F2F Meeting - Karlsruhe 2015.

Appendix

A. Additional Purity Plots

The Fig. A.1 shows the comparison of the clone rates of the CDC track finder to Trasan track finder. It can be seen that overall clone rate is the same, despite Trasan has higher clones contribution in low-p_t region.

The Fig. A.2 shows the fake rate comparison. It can be seen that Legendre-based track finder has a higher fake rate in low-p_t region.

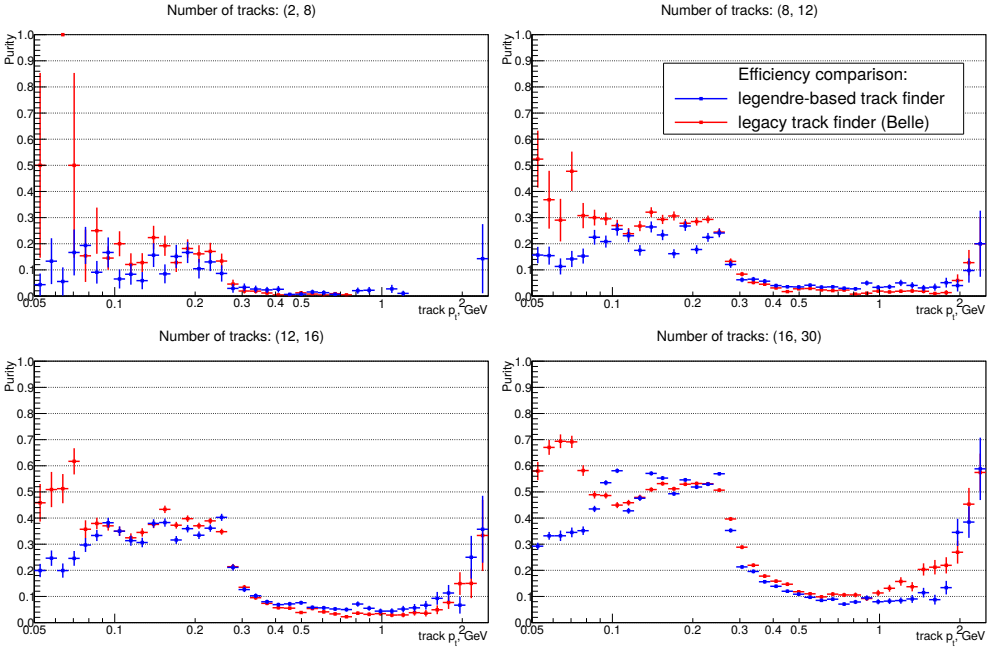

Figure A.1.: Comparison of the clone rates of Belle II track finding chain to legacy track finder (the Belle experiment) based on the number of generated tracks in event (event multiplicity) in bins of track's p_t

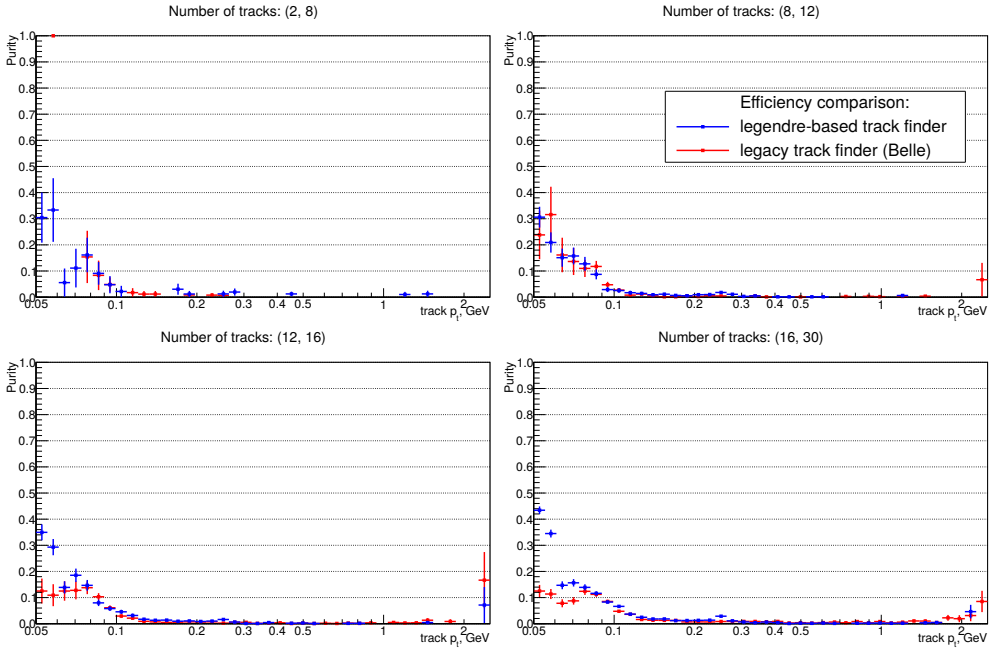

Figure A.2.: Comparison of the fake rates of Belle II track finding chain to legacy track finder (the Belle experiment) based on the number of generated tracks in event (event multiplicity) in bins of track's p_t

List of Figures

List of Tables

Acknowledgements

I want to thank Prof. Dr. Michael Feindt for giving me an opportunity to perform this development, and for making this work possible. Thanks to PD Dr. Andreas Meyer for acting as a co-referee, and for the help in the improvement of the thesis.

This work wouldn't be possible without Dr. Martin Heck, who gave me a guidance and supervised my work from the very beginning to the end. My work, as well as the work of the whole tracking group, was successful due to his leadership abilities. I want to thank Dr. Thomas Hauth for giving me valuable advices. With his support I made a big step forward in the algorithm development. I am thankful to the Belle II tracking group for productive discussions.

Many thanks to my colleagues at KIT. I am grateful to the B-group of the IEKP, and I am proud to be part of it. I have learned a lot and spent a wonderful time. Many thanks to my officemates, Nils Braun, Markus Prim and Christian Pulvermacher, for great moments and for a pleasant atmosphere.

I want to say thank you to all my friends, who supported me the whole time. Special thanks to Viktoria, who gave me strength when it was most needed.

Last but not the least, I would like to thank my family. All the work which I have done so far was made possible by their support and wise counsel.